MASTER THESIS

Monitoring and Electrolytic Removal of Nickel from Bismuth and the Lead-bismuth Eutectic

Das Überwachen und elektrolytische Entfernen von Nickel aus Bismut und dem Blei-Bismut-Eutektikum

Guido Alexander Zaunrith, BSc

Date(21/08/2017)

Chair of Mining Engineering and Mineral Economics
Department Mineral Resources Engineering
Montanuniversitaet Leoben

A-8700 LEOBEN, Franz Josef Straße 18
Phone: +43 3842-402-2001
Fax: +43 3842-402-2002
bergbau@unileoben.ac.at

Declaration of Authorship

„I declare in lieu of oath that this thesis is entirely my own work except where otherwise indicated. The presence of quoted or paraphrased material has been clearly signaled and all sources have been referred. The thesis has not been submitted for a degree at any other institution and has not been published yet. Two additional copies of this work have been submitted; one at the École Nationale Supérieure des Mines de Paris (Paris – France) and one at the Studiecentrum voor Kernenergie (Mol – Belgium)”

Acknowledgement

I would first like to thank my thesis advisor Jun Lim, PhD, of the Studiecentrum voor Kernenergie at Mol – Belgium. The door to Lim´s office was always open whenever I ran into a trouble spot or had a question about my research or writing. He consistently allowed this paper to be my own work, but steered me in the right the direction whenever he thought I needed it.

I would also like to acknowledge Christophe Coquelet, PhD, of the Centre Thermodynamique des Procédés at the École Nationale Supérieure des Mines de Paris (Mines ParisTech) – France, as the second reader of this thesis, and I am gratefully indebted to his for his very valuable comments on this thesis.

I would also like to thank the European Commission for supporting my research project through the GENTLE Student Research Experience founding.

Finally, I must express my very profound gratitude to my family for providing me with unfailing support and continuous encouragement throughout my years of study and through the process of researching and writing this thesis. This accomplishment would not have been possible without them. Thank you.

Guido A. Zaunrith

Abstract

To face climate change and the continuously increasing energy demand, nuclear power is an inevitable technology. Irrespective of the chosen forecast scenario, globally the number of plants will augment and therefore the demand on fuel will increase. As, at the current level of exploration, uranium is a limited resource occurring rarely in the big consumer countries, shortages cannot be ruled out. Solution to this can be the developing of new reactors able to burn other types of nuclear fuel. This concept has already been proven applicable by the application of mixed oxide fuels and could reach a new dimension by turning towards fast reactors.

Depending on the nuclear plant´s age, state and geographical location as well as the political and public context, further safety and security improvements are inevitable. This already led to important adaptations for the III Generation coming up at the moment. But developing a safer generation of nuclear fission power plants, based on new physical concepts (as for example subcritical accelerator driven systems), might be the better and easier saleable solution.

Also, there is the nuclear waste, a legacy of past and present power plants. Parts of this waste are highly radioactive and will stay it for hundreds of thousands of years. To decrease its dangerousness is one of the main challenges of our time. And again, fast reactors seem to be the most promising solution. In fact, feeding them with minor actinide enriched fuel, leads to their transmutation and reduces the time span for the waste to come back to a natural level of radiotoxicity to some centuries.

At SCK•CEN, the Belgian nuclear research center, scientists are working on these tasks through the MYRRHA Project. MYRRHA stands for Multi-purpose hYbride Research Reactor for High-tech Applications and is based on an experimental accelerator driven system. This means that through a particle accelerator, protons will be shot on a so-called spallation target, liberating the required amount of neutrons necessary for nuclear fission. Next to a huge portfolio of other scientific experiments and medical isotope production, MYRRHA enables with its external supply of neutrons a subcritical operation of the reactor, increasing the reactor safety significantly. In the same time, the controlled proton beam, hand in hand with the subcritical driving mode, allows the insertion of fuel highly enriched with transuranic elements and activation products. Or in other words; Through transmutation MYRRHA will allow to test a new technology for treating nuclear waste in a way to reduce its radiotoxic lifetime to some hundreds of years. Moreover, MYRRHA will be operated in the fast neutron spectrum.

The necessity of a spallation target and of a coolant preserving the neutrons in their fast spectrum led the scientist to the use of the lead-bismuth eutectic (LBE).

As indicated in its name, the LBE is the eutectic mixture of lead (45 at.%) and bismuth (55 at.%). Its biggest advantages are: the low melting temperature

(125.5 °C), the high boiling temperature (around 1670 °C) and its low reactivity. Due to the big temperature span between freezing and boiling the reactor can be driven at ambient pressure and thanks to its low reactivity intrusion of other substances will be less grave than in other reactor types.

Nonetheless the LBE corrodes the surrounding steels. The dissolution of impurities in the coolant has two main disadvantages. First, it might lead to a weakening of the structural materials. Second, it changes the chemical composition of the coolant and that could lead to a different neutronic behavior of the reactor.

To solve this problem two approaches are checked. One is the installation of a cold trap, where the LBE is cooled down to a temperature at which the solubility of the metallic impurities is low enough to have them precipitating. By means of a filter these impurities would then be filtered out. The other one is the electrochemical extraction. This solution consists in inducing an electromotive force so that the ionized metallic atoms migrate to and depose on an immersed anode. This solution approach could have the advantage of enabling the electrochemical concentration measurement of the concerned impurities.

Since nickel is one of the metallic impurities in LBE caused by the corrosion of stainless steel, the aim of this work would have consisted in a first step to develop a sensor and in a second step to test its extraction. The therefor designed electrochemical cell is displayed on the right.

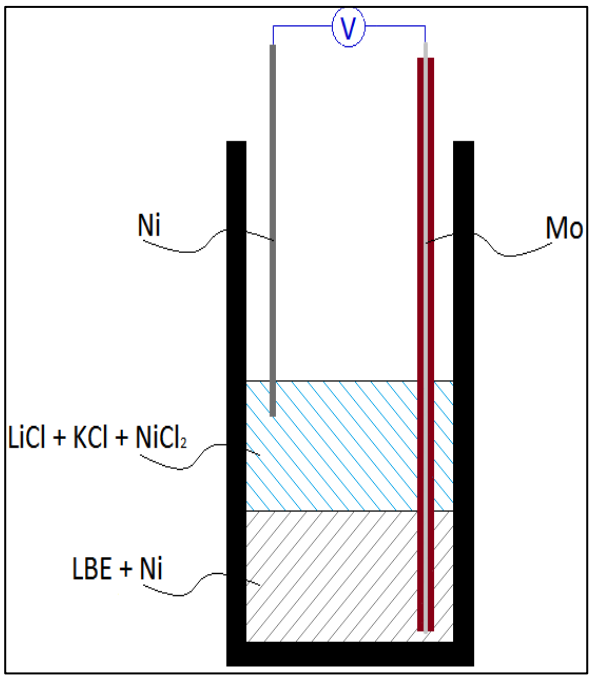

Sketch: Set-up from experiment 1

In an argon atmosphere, the LBE was introduced in a test tube. Then a eutectic salt mixture consisting of potassium chloride (40.5 mole%) and lithium chloride (59.5 mole%) was added as ion conductor. The argon atmosphere was necessary to prevent any oxygen contamination and so the formation of bismuth- or lead oxide.

Thanks to the significant density difference (about 10 g/cm³ for LBE and about 2 g/cm³ for the salt) the salt remains swimming on top of the LBE. Metallic nickel (about 8.9 g/cm³), added in small amounts over several steps, directly sank to and dissolved in the LBE. Further nickel chloride was added as electrolyte. In comparison to other experiments described in literature, the amount of admixed nickel chloride was set to be around 3-5 wt.% of the eutectic salt mixture.

Then a molybdenum wire, inserted in an aluminum oxide tube, was immerged to the ground of the test tube. The purpose of the alumina tube was to physically separate the molybdenum wire from the salt and the nickel wire. Then a nickel wire

was inserted in the salt, acting as an electrode. The other electrode of the cell is the LBE itself.

Once the cell has been prepared and brought to the desired temperature (400-550 °C), as it is needed to be above the salt mixture's melting point, the potential was measured.

Following the Nernst equation, the potential is a function of ideal gas constant R (8.3145 $J \cdot K^{-1} \cdot mol^{-1}$), the temperature T in Kelvin, the number of exchanged electrons in the reaction n (2 in case of the nickel ion), the Faraday constant F (96485.34 $C \cdot mol^{-1}$) and the ratio between the activity of the element of interest (nickel) at the reference electrode side $a_{Ni,ref}$ and the activity of the in the LBE dissolved element $a_{Ni,LBE}$:

$$E = E^0 - \frac{RT}{nF} * ln\left({a_{Ni,ref}}/{a_{Ni,LBE}}\right)$$

where E^0 is the standard electrode potential. (0 in this case.) Apart from this, working with a nickel wire of high purity allows setting $a_{Ni,ref}$ equal to 1. The activity of nickel in LBE is a function of its concentration $C_{Ni,LBE}$ and solubility S and can be given as:

$$a_{Ni,LBE} = \frac{C_{Ni,LBE}}{S}$$

The solubility is determined by recommended formulas from Gossé (2014):

$$S = 10^{\left(5.2 - \frac{3500}{T}\right)} \qquad \text{between 623-688 K}$$

or

$$S = 10^{\left(1.7 - \frac{1009}{T}\right)} \qquad \text{between 688-1173 K}$$

Based on the theoretical calculations and a couple of preliminary tests, it was demonstrated that the cell as designed is not stable. In fact, comparing the stability of different possible molecules showed that the used nickel chloride is less stable than the lead chloride. So, lead chloride is forming and liberated nickel dissolving in the LBE. The alternative use of a different salt was checked for fluorides and rejected. The experiments with the LBE were stopped at that point. Despite that, the thermoelectric potential was determined empirically.

In general, the idea of the potentiometric concentration determination is still good and could be applied for an iron or manganese sensor.

To prove the principle in itself, in a second part, the nickel concentration determination in bismuth was tested. Based on the gained experience an improved cell was designed (see the following sketch).

The major adaptations have been an increase of the cell´s size and the direct immersion of the thermocouple into it.

The thermoelectric potential for this cell was determined empirically too.

To calculate the expected potentials, the formulas must be adapted to:

$$E = E^0 - \frac{RT}{nF} * ln\left({a_{Ni,ref}}/{a_{Ni,Bi}}\right)$$

and according to Gossé (2014):

$S = 10^{\left(3.81-\frac{2429}{T}\right)}$ between 543-738 K

or

$S = 10^{\left(2.05-\frac{1131}{T}\right)}$ between 738-918 K

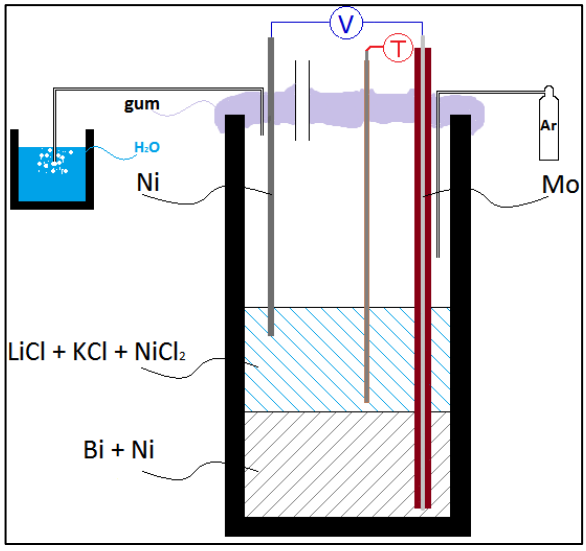

Sketch: Set-up from experiment 2

The conclusion of these last experiments (see also the graph below) is that the potentiometric concentration determination of metallic impurities is possible. A new solubility limit of nickel in bismuth, that nearly corresponds to the measured one, has been calculated. Nevertheless, at the reached stage, there remain some important knowledge gaps about the specimen´s true behavior.

Especially the exact solubility should be rechecked during further tests. With remaining uncertainties about it, the formation of a Bi_3Ni precipitation cannot be excluded and it is yet not proven that this precipitation is not influencing the nickel activity in the LBE.

Furthermore, the post experimental inspection of the used equipment showed strange deposits on the sections of the protection tubes that have been above the salt surface. The origin of these deposits could be organic impurities in the used chemicals.

As for the moment, the focus is primary on the sensor, the nickel extraction has been postponed.

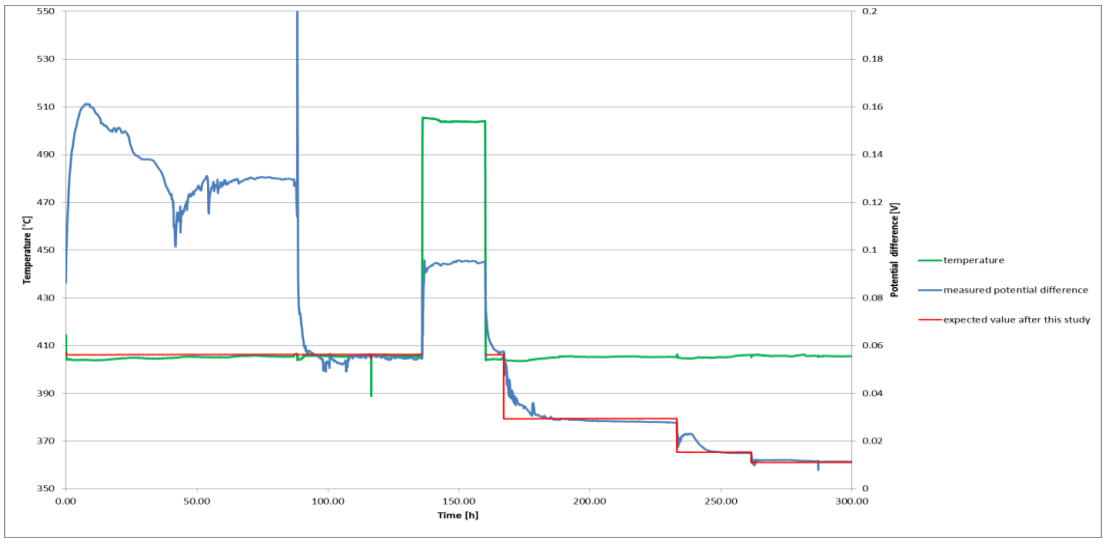

Graph: Measured and expected potentials from experiment 2

Zusammenfassung

Die Kernenergie ist eine unvermeidbare Technologie, um dem Klimawandel und dem stetig steigenden Energiebedarf entgegen treten zu können. Unabhängig vom ausgewählten Vorhersageszenario wird die globale Anzahl an Kernkraftwerken steigen und damit auch die Nachfrage an Brennstoff. Da, zum gegenwärtigen Explorationsstand, Uran ein begrenzter Rohstoff ist, der nur selten in den Ländern der großen Verbraucher vorkommt, können Engpässe nicht ausgeschlossen werden. Eine Lösung hierfür wäre die Entwicklung neuer Reaktoren, die zur Verbrennung anderer Kernbrennstoffe fähig sind. Die Vertretbarkeit dieses Konzepts wurde bereits durch die Anwendung von Mischoxiduranbrennstoffen bewiesen und könnte dank der Schnellen Brüter eine neue Dimension erreichen.

Abhängig von dem Alter, dem Zustand und der geographischen Lage eines Kernkraftwerks, sowie dem politischen und öffentlichen Kontext, sind weitere Verbesserungen im Bereich der Sicherheit unvermeidbar. Dies führte bereits zu bedeutenden Anpassungen an der derzeit aufkommenden III. Generation. Allerdings wäre die Entwicklung einer sichereren Generation von Fissionsreaktoren, basierend auf neuen physikalischen Konzepten (wie zum Beispiel unterkritischen beschleunigerbetriebenen Systemen), vielleicht die bessere und leichter vertretbarere Lösung.

Des Weiteren ist da noch der Atommüll als Altlast der früheren und jetzigen Kraftwerke. Teile dieses Abfalls sind hochradioaktiv und werden es auch noch für hunderttausende von Jahre bleiben. Die Verringerung der davon ausgehenden Gefahr ist eine der wesentlichen Herausforderungen unserer Zeit. Und abermals scheinen Schnelle Brüter hierfür die vielversprechendste Lösung zu sein. Tatsächlich führt deren Beladung mit an Transuraniden angereichertem Brennstoff zu deren Transmutation und somit auch zu einer Reduktion der Zeitspanne, bis die Radioaktivität des Mülles ein natürliches Niveau erreicht hat, auf ein paar Jahrhunderte.

Über das MYRRAH-Projekt am SCK-CEN, dem belgischen Studienzentrum für Kernenergie, arbeiten Wissenschaftler an diesen Aufgaben. MYRRHA steht für “Multi-purpose hYbride Research Reactor for High-tech Applications” und basiert auf einem experimentellen beschleunigerbetriebenen System. Dies bedeutet, dass durch einen Teilchenbeschleuniger Protonen auf ein sogenanntes (Spallations-) Target geschossen werden, wodurch die für die Kernspaltung notwendige Menge an Neutronen freigesetzt wird. Neben einem bedeutenden Portfolio an weiteren wissenschaftlichen Experimenten und der Herstellung medizinischer Isotope ermöglicht MYRRHA, dank der externen Neutronenversorgung, eine unterkritische Betriebsweise des Reaktors und bringt somit einen bedeutenden Sicherheitsgewinn mit sich. Zugleich erlaubt der kontrollierte Protonenstrahl kombiniert mit der unterkritischen Fahrweise die Beladung mit an Transuraniden hochangereichertem Brennstoff. Oder in anderen Worten; Mittels der Transmutation kann in MYRRHA eine neue Technologie zur Behandlung von radioaktivem Abfall getestet werden,

die dessen radiotoxische Zeitspanne auf ein paar Jahrhunderte reduziert. Des Weiteren wird MYRRHA im Spektrum der schnellen Neutronen betrieben.

Die Notwendigkeit eines (Spallations-) Targets als auch eines Kühlmittels, welches die Neutronen in ihrem schnellen Spektrum belässt, führte die Wissenschaftler zur Nutzung des Blei-Bismut-Eutektikums (LBE).

Wie durch den Namen angedeutet ist das LBE eine eutektische Mischung aus Blei (45 At.-%) und Bismut (55 At.-%). Seine größten Vorteile sind: die niedrige Schmelztemperatur (125,5 °C), die hohe Siedetemperatur (circa 1670 °C) and seine geringe Reaktivität. Dank der großen Temperaturspanne zwischen der Erstarrung und dem Sieden kann der Reaktor unter Umgebungsdruck betrieben werden und dank der geringen Reaktivität ist das Eindringen andere Stoffe weniger gravierend als in anderen Reaktortypen.

Nichtsdestotrotz korrodiert das LBE die umgebenden Stähle. Das Lösen von Verunreinigungen in die Kühlflüssigkeit hat zwei wesentliche Nachteile. Erstens kann es zu einer Schwächung der Strukturmaterialien führen. Zweitens verändert es die chemische Zusammensetzung des Kühlmittels und dies könnte zu einem anderen Neutronenverhalten des Reaktors führen.

Um dieses Problem zu lösen werden zwei Ansätze verfolgt. Einer ist der Einbau einer Kühlfalle, in der das LBE auf eine Temperatur abgekühlt wird, bei der die Löslichkeit der metallischen Unreinheiten niedrig genug ist, um sie auszufällen. Durch einen Filter würden diese Unreinheiten dann herausgefiltert. Der andere ist die elektrochemische Extraktion. Dieser Ansatz umfasst das Induzieren einer elektromotorischen Kraft, sodass die ionisierten Metallatome zu einer eingetauchten Anode wandern und sich dort absetzen. Dieser Lösungsweg hätte den Vorteil, dass eine elektrochemische Konzentrationsbestimmung der betroffenen Verunreinigungen ermöglicht würde.

Da Nickel eine dieser metallischen Verunreinigungen ist, die mit der Korrosion von Edelstahl einhergehen, war das Ziel dieser Arbeit in einem ersten Schritt einen Nickelsensor zu entwickeln und in einem zweiten Schritt seine Extraktion zu testen. Die hierfür entwickelte elektrochemische Zelle ist rechts abgebildet.

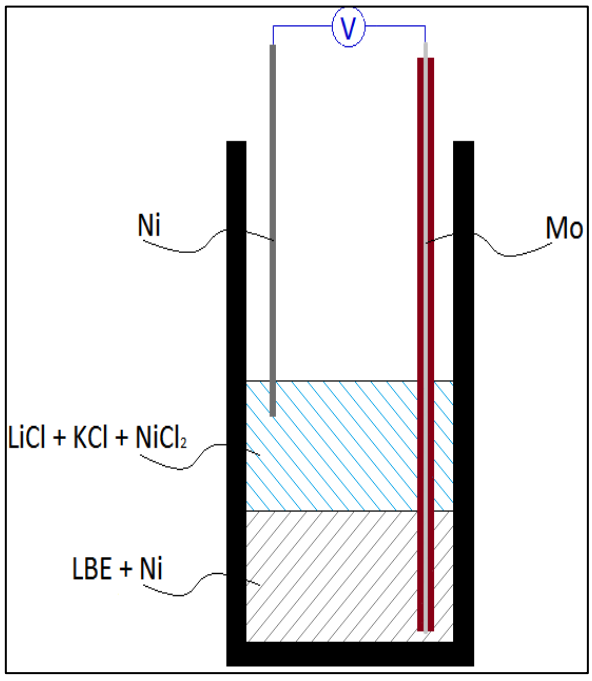

Skizze: Versuchsaufbau des 1. Experiments

Unter einer Argonatmosphäre wurde das LBE in ein Teströhrchen gefüllt. Dann wurde eine eutektische Salzmischung aus Kaliumchlorid (40,5 Mol-%) und Lithiumchlorid (59,5 Mol-%) als Ionenleiter hinzugefügt.

Die Argonatmosphäre war notwendig um jeglicher Kontamination durch Sauerstoff und so der Bildung von Bismut- oder Bleioxiden vorzubeugen.

Dank des bedeutenden Dichteunterschieds (circa 10 g/cm³ für das LBE und circa 2 g/cm³ für das Salz) schwimmt das Salz auf dem LBE. Metallisches Nickel (circa 8,9 g/cm³), beigemengt in kleinen Mengen über mehrere Schritte, sank unmittelbar in Richtung LBE und löste sich in diesem. Weiters wurde Nickelchlorid als Elektrolyt beigemengt. Angelehnt an andere Experimente, die in der Literatur beschrieben werden, wurde der Anteil des beizumengenden Nickelchlorids auf 3-5 Gew.-% des eutektischen Salzgemischs festgelegt.

Dann wurde ein durch ein Aluminiumoxidröhrchen gezogener Molybdändraht bis auf den Grund des Teströhrchens eingetaucht. Der Zweck des Aluminiumoxidröhrchens war es den Molybdändraht physisch von dem Salz und dem Nickeldraht zu trennen. Danach wurde der als Elektrode fungierende Nickeldraht in das Salz getaucht. Die andere Elektrode der Zelle ist das LBE selbst.

Sobald die Zelle fertiggestellt und auf die gewünschte Temperatur (400-500 °C) gebracht wurde, die notwendig ist um den Schmelzpunkt des Salzegemischs zu überschreiten, wurde das Potenzial gemessen.

Entsprechend der Nernst-Gleichung ist das Potenzial eine Funktion der universellen Gaskonstante R (8,3145 $J \cdot K^{-1} \cdot mol^{-1}$), der Temperatur T in Kelvin, der Anzahl der in der Reaktion übertragenen Elektronen n (2 im Fall des Nickelions), der Faraday-Konstante F (96485,34 $C \cdot mol^{-1}$) und dem Verhältnis der Aktivität des relevanten Elements (Nickel) an der Referenzelektrodenseite $a_{Ni,ref}$ zu der Aktivität des im LBE gelösten Elements $a_{Ni,LBE}$:

$$E = E^0 - \frac{RT}{nF} * ln\left({a_{Ni,ref}}/{a_{Ni,LBE}}\right)$$

Wobei E^0 das Standardelektrodenpotenzial ist. (0 in diesem Fall.) Da des Weiteren mit einem hochreinen Nickeldraht gearbeitet wurde, kann $a_{Ni,ref}$ gleich 1 gesetzt werden. Die Aktivität des Nickels im LBE ist eine Funktion seiner Konzentration $C_{Ni,LBE}$ und seiner Löslichkeit S und ist gegeben durch:

$$a_{Ni,LBE} = \frac{C_{Ni,LBE}}{S}$$

Die Löslichkeit wird mit den von Gossé (2014) empfohlenen Formeln berechnet:

$$S = 10^{\left(5.2 - \frac{3500}{T}\right)} \qquad \text{zwischen 623-688 K}$$

oder

$$S = 10^{\left(1.7 - \frac{1009}{T}\right)} \qquad \text{zwischen 688-1173 K}$$

Anhand von theoretischen Berechnungen und einer Reihe vorbereitender Tests wurde bewiesen, dass die Zelle, so wie sie designt wurde, nicht stabil ist. Und zwar zeigt der Stabilitätsvergleich verschiedener möglicher Moleküle, dass das verwendete Nickelchlorid weniger stabil ist als das Bleichlorid. Daher bildet sich Bleichlorid

und das freigesetzte Nickel löst sich im LBE. Die alternative Nutzung eines anderen Salzes wurde für Fluoride überprüft und verworfen. Die Experimente mit LBE wurden an diesem Punkt eingestellt. Das thermoelektrische Potenzial wurde ungeachtet dessen noch empirisch bestimmt.

Allgemein ist die Idee der potenziometrischen Konzentrationsbestimmung immer noch gut und könnte bei einem Eisen- oder Mangansensor Anwendung finden.

Um das Prinzip selbst zu beweisen wurde in einem zweiten Teil die Konzentrationsbestimmung von Nickel in Bismut getestet. Anhand der im Vorfeld gemachten Erfahrungen wurde eine verbesserte Zelle konzipiert (siehe nachfolgende Skizze).

Die wichtigsten Anpassungen waren eine Größenzunahme der Zelle und das direkte Eintauchen des Thermoelements in diese.

Das thermoelektrische Potenzial dieser Zelle wurde ebenfalls empirisch bestimmt.

Um die zu erwartenden Potenziale berechnen zu können, müssen die Formeln wie folgt angepasst werden:

$$E = E^0 - \frac{RT}{nF} * ln\left({a_{Ni,ref}}/{a_{Ni,Bi}}\right)$$

und nach Gossé (2014):

$S = 10^{\left(3.81-\frac{2429}{T}\right)}$ zwischen 543-738 K

oder

$S = 10^{\left(2.05-\frac{1131}{T}\right)}$ zwischen 738-918 K

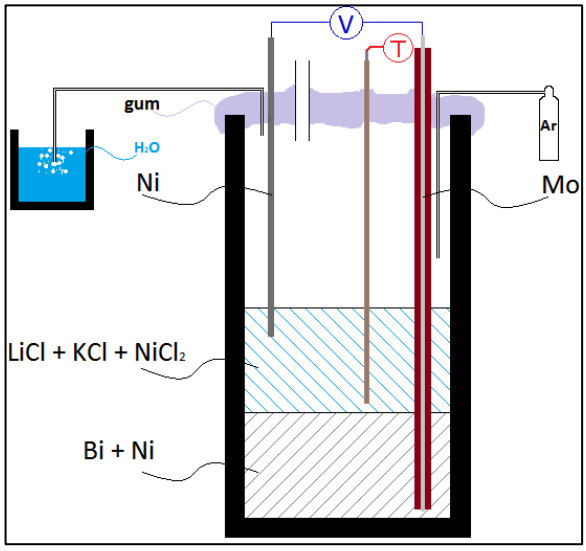

Skizze: Versuchsaufbau des 2. Experiments

Das Fazit dieser letzten Experimente (siehe auch nachstehende Graphik) ist, dass die potenziometrische Konzentrationsbestimmung von metallischen Verunreinigungen möglich ist. Eine neue Löslichkeit von Nickel in Bismut, die weitestgehend der gemessenen entspricht, wurde berechnet. Nichtsdestotrotz verbleiben zum jetzigen Stand noch Wissenslücken in Bezug auf das genaue Verhalten des Präparats.

Insbesondere sollte während weitere Tests die exakte Löslichkeit nochmals überprüft werden. Ohne Klarheit diesbezüglich kann die Bildung einer Bi_3Ni Präzipitation nicht ausgeschlossen werden und es ist momentan noch nicht bewiesen, dass diese Fällung keinen Einfluss auf die Nickelaktivität im LBE hätte.

Des Weiteren zeigten die postexperimentellen Untersuchungen der verwendeten Utensilien ungewöhnliche Ablagerungen an Stellen der Schutzröhrchen, die oberhalb der Salzoberfläche lagen. Diese Ablagerungen könnten von organischen Unreinheiten in den verwendeten Chemikalien stammen.

Da der Fokus zurzeit primär auf dem Sensor liegt, wurde die Nickelextraktion vertagt.

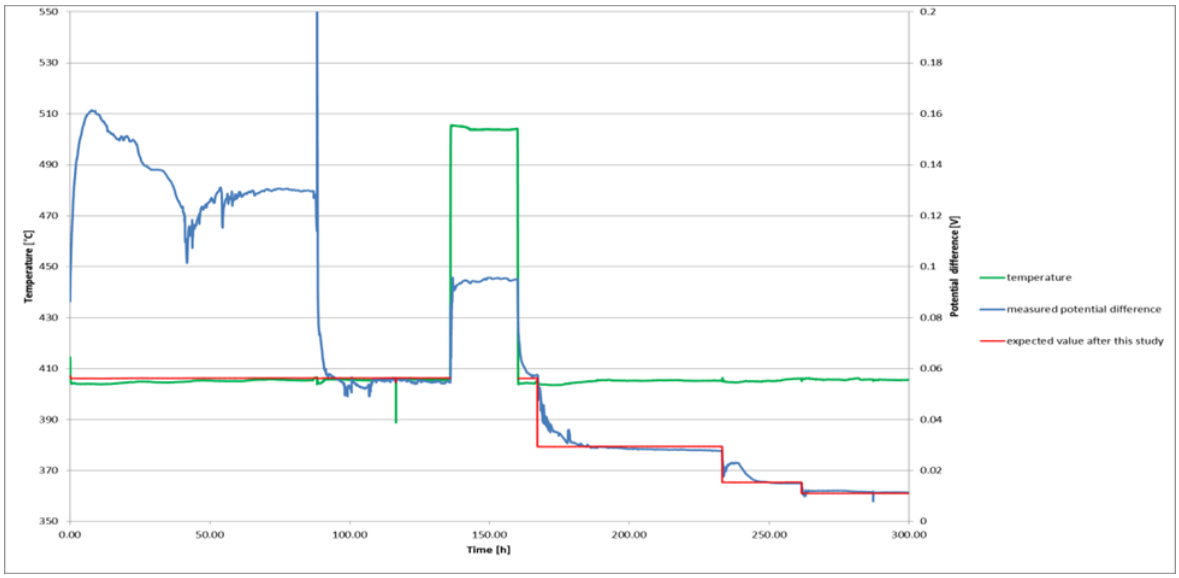

Graphik: Gemessene und erwartete Potentiale aus dem 2. Experiment

Table of Contents

1 Introduction

1.1 Global Outlook

The last decade has certainly been an eventful period for the nuclear energy sector. After the 21st Conference of Parties (COP 21) in Paris, it is clear that the climate change can only be stopped, or rather be limited, through a “decarburization” of our technologies. And that must happen worldwide. Concerning the electricity production, the civil use of nuclear power seems to be a reasonable choice along with the renewables and maybe some other future solutions. Therefore, one would expect an increase in the number of plants. And in fact, if one looks at the map showing the status of the nuclear programs at the end of 2013 (Figure 1), it is clearly visible that globally the interest in maintaining and building new nuclear plants prevails. Nuclear phase-out programs are progressing only in central Europe.

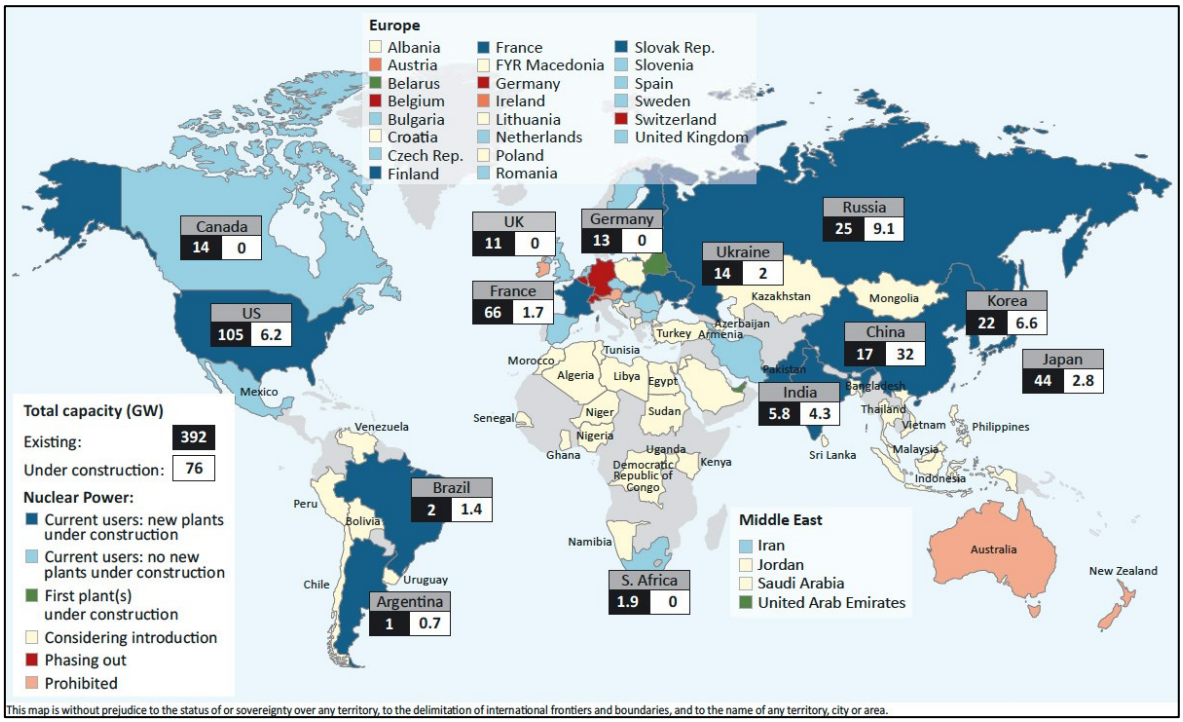

Figure 1: Status of the nuclear power programs, end 2013 (IEA, 2014, p. 357)

Also, the overall demand of energy will certainly not decrease in the decades to come. On the contrary, according to the Intended Nationally Determined Contribution (INDC) Scenario the primary energy demand will increase by 20% until 2030. (IEA, 2015).

Especially Russia, South Korea and China will strongly enlarge their nuclear capacities. Altogether, following the 2-degree scenario the installed capacity shall

more than double until 2050. A forecast of this evolution is given in figure 2. (OECD/IEA – OECD/NEA, 2015)
(All capacities are given in gross capacities.)

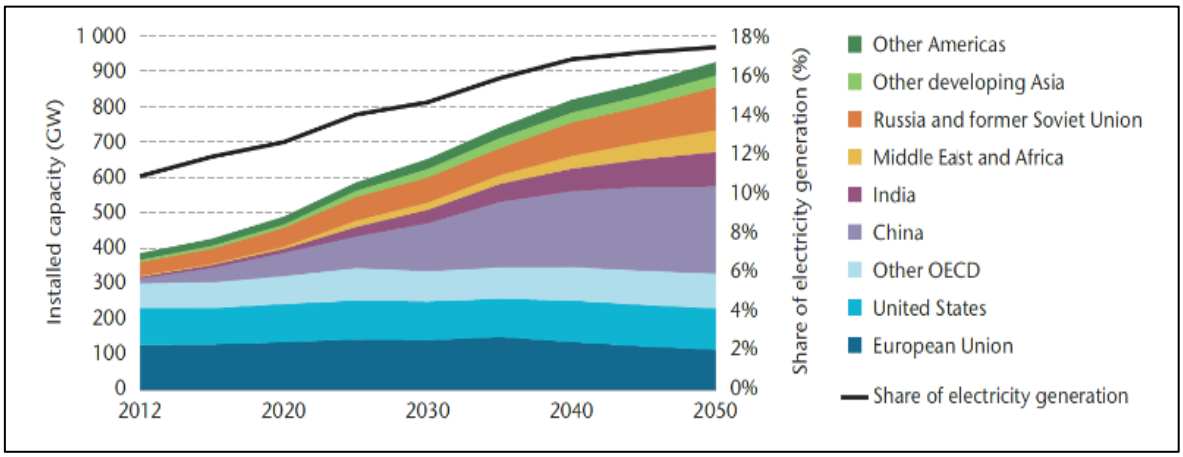

Figure 2: Forecast of the installed nuclear capacities in the 2 °C-Scenario (OECD/IEA and OECD/NEA, 2015, p. 22)

1.2 A Turn

In the same time, we witness the propagation of a new generation. Heralded with the implementation of the Advanced Boiling Water Reactor (ABWR) in Japan and with a couple of European Pressurized Reactors (EPR) in construction in Europe and China, the III Generation brings basically upgrades in power capacities, fuel utilization and safety precautions. In particular the safety upgrades are of great significance with regard to the current security threats and the last catastrophe at Fukushima Daiichi.

This accident was for sure the most striking nuclear event in the last years. Following an earthquake of magnitude 9.0 (M_W), on the 11th March 2011 a tsunami wave hit the plant site and affected some of the cooling systems. As a result, yet not exactly assessable meltdowns followed in three of the six rectors. Furthermore, hydrogen explosions occurred, destroying the outer confinement and liberating radioactive material. All in all, it became, after Chernobyl, the second accident rated 7 on the International Nuclear and Radiological Event Scale (INES) and proved that even the most unlikely events may happen. Taking this into account is clearly the duty of any future reactor designing, irrespective of whether it is the EPR NM, AP1000, Hualong One, CANDU 6, VVER-1200 or any other type.

Based on these events, nuclear energy using countries re-evaluated their nuclear program. Some of them decided to adapt or upgrade their facilities, others, like Germany or Switzerland, to shut them down gradually and still others, like Belgium, to decide about the thematic in a close future.

Anyway, in the next years a lot of facilities, especially in Europe, will reach the end of their service life. An exact number cannot be given as some countries or operators are thinking about extending the official life expectancies of their plants.

But whether one considers the increasing number of operating facilities or the increasing number of facilities that are going to be decommissioned (see also figure 31 (annex A-6)), in both cases, the overall amount of nuclear waste accruing will rise, bringing up again the question of how to handle it.

1.3 Nuclear Waste

Radioactive waste is for sure one of the most important and polemic topics regarding the use of civil nuclear energy. And yet, today a lot of countries have not defined their final solution of what to do with it. Shortly described, radioactive waste is any type of waste containing radioactive material and therefore emitting radiation above a certain (nationally defined) clearance level.

In relation to this, it is advantageous to have a feeling for the natural radiation level humans are exposed to in their normal daily life. Therefor a list of the main natural and artificial sources is given in table 5 (annex A-1) including the doses and ranges of individual doses of ionizing radiation, varying from 1-13 mSv per year. (UNSCEAR, 2008)

In case of the nuclear energy production the waste is a result of operating and/or dismantling the plants. Altogether, it can be estimated that a typical 1000 MW_e light water reactor generates 200-350 m³ of low and intermediate-level waste per year and 27 m³ of used fuel per year, equaling 75 m³ of disposal volume after direct encapsulation or 28 m³ of disposal volume if processed and vitrified. (WNA[1], 2015)

According to the International Atomic Energy Agency (IAEA) the waste can be rated in following six classes:

- **Exempt waste** *"contains such small concentrations of radionuclides that it does not require provisions for radiation protection, irrespective of whether the waste is disposed of in conventional landfills or recycled."*
- **Very short lived waste** *"contains only radionuclides of very short half-life with activity concentrations above the clearance levels. Such waste can be stored until the activity has fallen beneath the levels for clearance, allowing for the cleared waste to be managed as conventional waste. […] The main criteria for the classification of waste as […]"* very short lived waste *"are the half-lives of the predominant radionuclides and the acceptability of the amounts of longer half-life radionuclides. […] However, in general, the management option of storage for decay is applied for waste containing radionuclides with half-lives of the order of 100 days or less."*
- **Very low level waste** is *"waste that does not necessarily meet the criteria of […]"* exempt waste, *"but that does not need high level of containment and*

isolation and, therefore, is suitable for disposal in near surface landfill type facilities with limited regulatory control. […] Nevertheless, it is expected that with a moderate level of engineering and controls, a landfill facility can safely accommodate waste containing artificial radionuclides with levels of activity concentrations one or two orders of magnitude above the levels for exempt waste, for waste containing short lived radionuclides and with limited total activity."

- **Low level waste** is *"waste that is above clearance levels, but with limited amounts of long lived radionuclides. Such waste requires robust isolation and containment for periods of up to a few hundred years and is suitable for disposal in engineered near surface facilities. This class covers a very broad range of waste. […]"* Low level waste *"may include short lived radionuclides at higher levels of activity concentration, and also long lived radionuclide, but only at relatively low levels of activity concentrations. […] In many States it is assumed that institutional controls can be relied upon for a period of up to around 300 years. Under this assumption, bounding values for low level waste in terms of activity concentration levels can be derived by estimating doses to exposed individuals after this period of institutional control."*
- **Intermediate level waste** is *"waste that, because of its content, particularly of long lived radionuclides, requires a greater degree of containment and isolation than that provided by near surface disposal."* In fact, *"a precise boundary between"* low level waste *"and intermediate level waste […] cannot be provided, as limits on the acceptable level of activity concentrations will differ between individual radionuclides or groups of radionuclides."* Anyway, intermediate level waste *"needs no provision, or only limited provision, for heat dissipation during its storage and disposal. […]"* It *"may contain long lived radionuclides, in particular, alpha emitting radionuclides that will not decay to a level of activity concentration acceptable for near surface disposal during the time for which institutional controls can be relied upon. Therefore, waste in this class requires disposal at greater depths, of the order of tens of meters to a few hundred meters."*
- **High level waste** is *"waste with levels of activity concentrations high enough to generate significant quantities of heat by the radioactive decay process or waste with large amount of long lived radionuclides that need to be considered in the design of a disposal facility for such waste. Disposal in deep, stable geological formations usually several hundred meters or more below the surface is the generally recognized option for disposal […]."* High level waste *"typically has levels of activity concentrations in the range of 104-106 TBq/m³ (e.g. for fresh spent fuel from power reactors, which some States consider radioactive waste)."* (IAEA, 2009)

To get a better impression on how to proceed for classification, it is advised to take a look on the illustration and examples in figure 27 (annex A-2) and figure 28 (annex A-3).

In figure 3 are shown the different activity evolutions of some transuranic elements and activation products in high level waste.

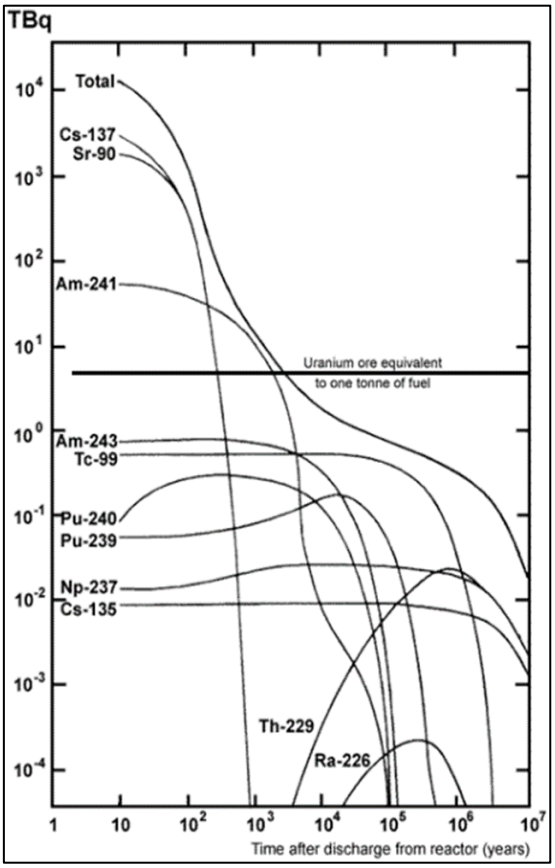

Figure 3: Activity of high level waste from one tone of spent fuel (in WNA[2], 2014, from IAEA, 1992 - radioactive waste management)

In a thermal reactor, transuranic elements are mainly the result of the neutron capture by uranium-238 atoms, transforming them to uranium-239. This one, not being stable, quickly emits β-radiation and becomes neptunium-239 and further plutonium-239. Some of these might then capture neurons too and create plutonium-240 and plutonium-241. Also through β-decay this last one can transform into americium-241 and so on. Three of the main radioactive decay series including their half-lives are given in figure 29 (annex A-4).

The most important activation products, relating to reactor activities, might be tritium, carbon-14, cobalt-60, iron-55 and nickel-63. They are the result of neutrons impacting on materials surrounding the fuel. (WNA[2], 2014)

But next to all those information about nuclear waste and the mostly not solved problem of the final treatment (except of Finland that decided to bury it once for all), there remains another question; the one of the fuel supply security.

1.4 Security of Fuel Supply

As nuclear power is considered to be an important part of the future worldwide energy mix and as the total amount of plants is increasing, it is inevitable to take into consideration the fuel supply when talking about new technologies. In this regard, two questions arise: Is there enough fuel for future developments? And is the access to the fuel granted?

Figure 4 shows a comparison between the reactor requirements of uranium (U) and its production. A-II stand for the *"production capability of existing and committed centers supported by RAR"* (reasonably assured resources) *"and inferred resources recoverable at <USD 130/kgU"* and B-II for *"production of existing, committed,*

planned and prospective centers supported by RAR and inferred resources recoverable at <USD 130/kgU." The low case scenario corresponds to an increase of installed nuclear capacity up to about 400 GW_e net and the high case scenario to an increase up to 678 GW_e net.

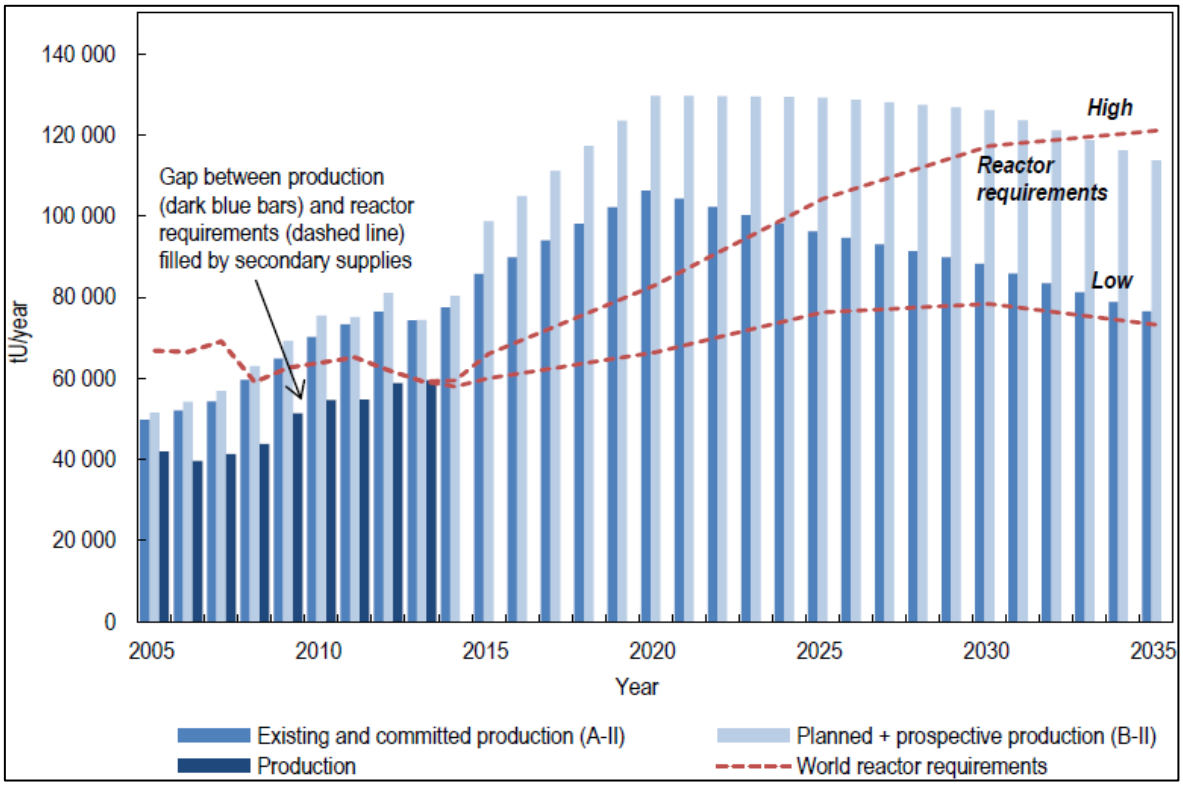

Figure 4:Projected annual world uranium production capability to 2035 with projected world reactor requirements (OECD/IAEA and OECD/NEA, 2014, p. 125)

Pertaining to the first question, it is visible that nowadays the mine production is smaller than the requirements. This is possible through complementing primary sources by secondary ones. Secondary sources include: *"stocks and inventories of natural enriched uranium; both civilian and military in origin; nuclear fuel produced by reprocessing spent reactor fuels and from surplus military plutonium; uranium produced by the re-enrichment of depleted uranium tails."* (OECD/IAEA and OECD/NEA, 2014, p. 107) They can be expected to continue to be a source of supply but might decline in availability in the future. (For example, the Russian-US blend down program of highly enriched uranium ended in 2013.) However, the access to information about those supplies is so limited, that a precise prediction of their disposability is not possible.

Moreover, one can see that if all existing and committed mines produce at or near stated production capability, the high case demand might exceed production around 2023. By including the planned and perspective production the demand could exceed production around 2032. As the real mine production is rarely above 85% of its capability, the meeting of those two could happen earlier. For the scenario with the low case requirement, production is projected to be sufficient at any time.

At that point, it is important to remind that in any case exploring and mining activities are strongly dependent from the resource's value. Indeed, it can be assumed that with an increasing price, prospection activities will augment and new sites will open.

Today's identified resources including all cost categories of all RAR and inferred resources consist of about 7 635 200 t of uranium up to a price of 130 US$/kg U, what would be sufficient for over 120 years of consumption considering the 2012 requirements of 61 600 t U. (OECD/IAEA and OECD/NEA, 2014)

RAR-uranium is *"uranium that occurs in known mineral deposits of such size, grade, and configuration that it could be recovered within the given production cost ranges, with currently proven mining and processing technology. Estimates of tonnage and grade are based on specific sample data and measurements of the deposits and on knowledge of deposit characteristics"*. (EIA, 2016)

Thus, on a short-term perspective, it can be asserted that a shortage of fuel is quite unlikely. Whereas on a long-term perspective, it could be possible that, in case of a very prosper evolution of the nuclear sector and a low uranium price impeding the mine development, shortages in fuel will occur.

To answer the second question, one should compare the uranium producing countries with the uranium consuming countries. Referring to figure 5, one can notice that, in exception of Canada and South Africa, none of the consumers can satisfy its own demand without importing. (OECD/IAEA and OECD/NEA, 2014)

Regardless of its geological availability, this and the strong dependence of some countries on nuclear energy make uranium to a strategic resource of high political interest. And wherever there is a strong political interest, there is a possibility that economy and market are not functioning "naturally". The evolution of the oil price and its consequences in 2015-2016 could serve as an example.

A map showing the distribution of identified resources up to a price of 130 USD/kg U is given in figure 30 (annex A-5). A striking point is that there are no significant resources in Europe and that in Russia, the United States and China there are respectively 9%, 4% and 3% of the identified resources. Yet these four are the four biggest consumers and those with the highest growth forecast. (OECD/IAEA, 2014)

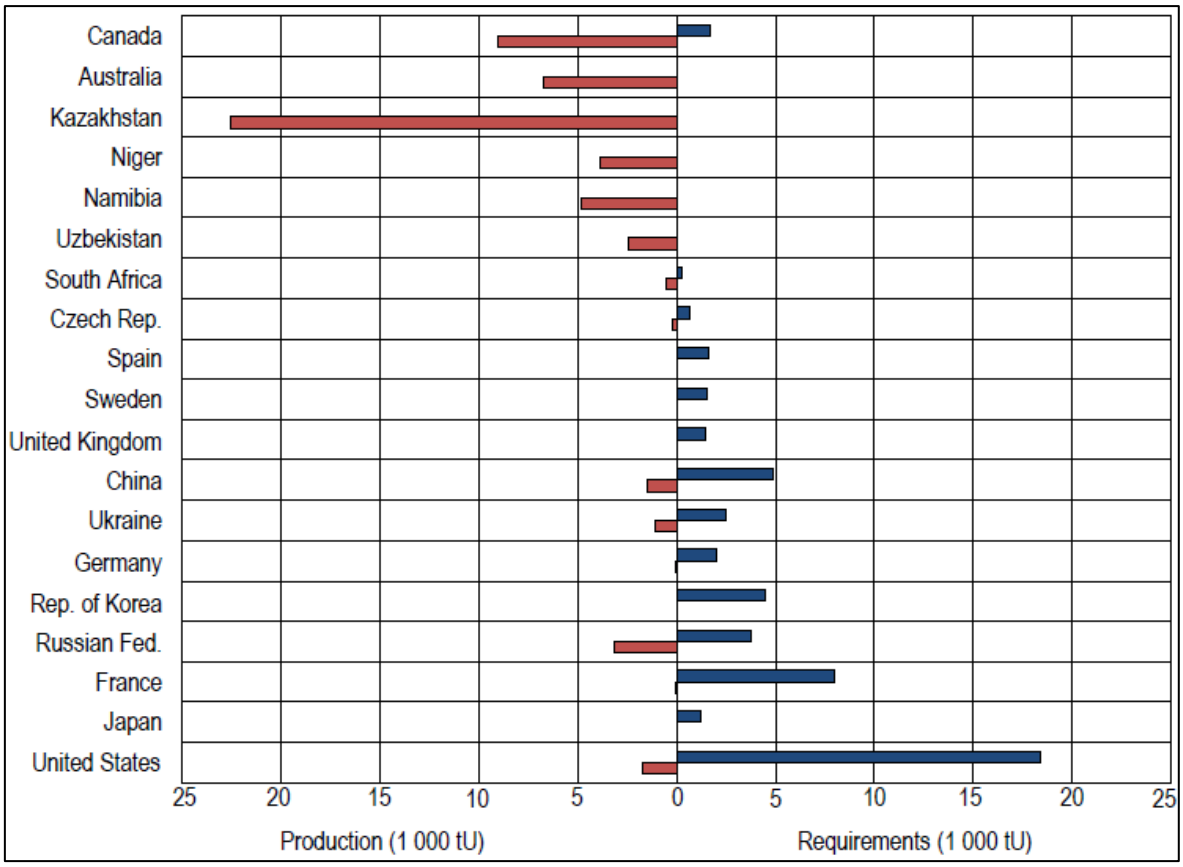

Figure 5: Estimated (in 2013) uranium production and reactor related requirements for major producing and consuming countries (OECD/IAEA and OECD/NEA, 2014, p. 108)

Finally, whether it may be for security or for safety reasons, whether it may be for fuel supply guaranty or for waste treatment and disposal, the research for innovative, efficient and applicable nuclear technologies is essential for the future of the sector and for its part in the energy transition. The international community being aware of this, hence focused their efforts on six basic concepts for the fourth generation: the sodium-cooled fast reactor, the very-high-temperature reactor, the supercritical-water-cooled reactor, the gas-cooled fast reactor, the molten salt reactor and the lead-bismuth cooled fast reactor. This last one being one of the more promising ones, especially in terms of radioactive waste treatment, is materializing through the MYRRHA-project.

2 MYRRHA

MYRRHA stands for Multi-purpose hYbride Research Reactor for High-tech Applications and is an experimental accelerator driven system (ADS). It is currently developed by the Belgian SCK•CEN and is conceived as a flexible fast-spectrum irradiation facility. It is able to run in both subcritical and critical mode. The reactor cooling will be done by means of a lead-bismuth eutectic (LBE). Therefore, MYRRHA will be not only a facility for material science, fundamental research, fuel development, radioisotope and dropped silicon production, but also a demonstrator for the ADS concept, the lead-bismuth cooled fast reactor technology, and a way for high level waste transmutation.

2.1 ADS

In an ADS, one combines a proton accelerator with a spallation target and a subcritical core. Due to the subcritical operating mode, the chain reaction is not self-sustaining and therefore the entire system can be exploited in a safe and controllable way at all circumstances, including the case in which the core is loaded with an important amount of minor actinides. This makes the ADS system to one of the most interesting options for further treatment of highly radioactive waste.

2.1.1 The Proton Accelerator

The accelerator provides high energy protons that are then headed on a spallation target. *"The needed final energy of the particles is many times higher than what can be obtained from a single acceleration passage. This is why the acceleration has to take place repeatedly in time, and this is why the applied accelerating fields must have an oscillating nature. The frequency of these oscillations is typically in the so-called radiofrequency (RF) domain, say 50 MHz to 1 GHz, and therefore the particle acceleration takes place in RF cavities."*

In general, there are three possibilities for delivering the particle beam on the target. Categorized according to the time structure there are: the direct current beam delivery, the continuous wave beam delivery and the pulse beam delivery. The first type can be obtained by a direct current accelerator, the second by an isochronous cyclotron and the third by a continuous wave linear accelerator. This last one, being a steady state machine, could also be operated in a continuous wave compatible way. (SCK•CEN[1])

The favored solution for MYRRHA is a linear accelerator, which is supposed to deliver a continuous wave proton beam of up to 3.2 mA at an energy of 600 MeV. To allow the necessary measurements and monitoring of the reactor's sub-criticality, the beam will be shut off for 200 µs once per second. (Abderrahim H. A., 2011)

2.1.2 The Spallation Target

"The spallation target is a neutron source providing primary neutrons that are multiplied by the surrounding sub-critical core. The primary neutrons are produced by the spallation reaction of heavy-metal target nuclei, bombarded by high-energy protons generated by the accelerator." (SCK•CEN[2])
To visualize the difference between spallation and fission figure 6 is given below:

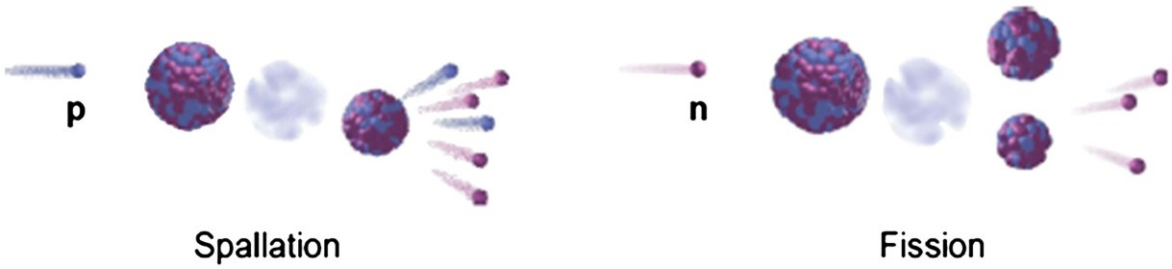

Figure 6: Spallation versus fission (Abderrahim, 2011, p. 3)

In fact, during spallation fragments of the nucleus (protons and neutrons) are ejected, while during fission the nucleus gets split.

The spallation process can be divided into two steps. In a first one, named intranuclear cascade, the incoming protons interact with the target nucleons what leads to the emission of very high energetic secondary particles (mainly protons, neutrons, alpha-particles, etc.). In the second one, the target nucleons are lifted to a very high excitation state to then de-excite through evaporation of a large quantity of neutrons at the lower energy (some MeV). If nuclear fissile material is present, at lower energy both steps can be accompanied by nuclear fission processes. In figure 7 is shown schematically how the incoming protons hit the target material and the hereby produced secondary particles spread out through the core.

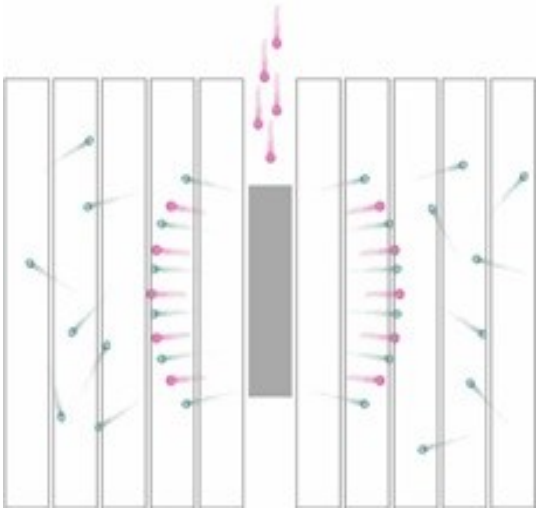

Figure 7: Schematic representation of the spallation process (SCK•CEN[2])

Depending on the initial energy of the incident particles and the atomic number of the target nuclei a large amount of spallation neutrons can be produced. *"For example, a lead target bombarded with 1 GeV protons can yield about 25 neutrons per incident proton, at 600 MeV one expects about 13 neutrons per incident proton (from the spallation reaction alone)."* (SCK•CEN[2])

A recapitulative process scheme is given in figure 32 (annex A-7).

2.1.3 The Subcritical Core

As mentioned previously the core will be operating sub-critically. For inherent safety reasons, the sub-criticality level will be set around 0.95. Moreover, the core combines a fast spectrum zone for structural material research, minor actinide transmutation studies and ADS fuel studies with a thermal spectrum island for isotope production, long lived fission product transmutation research, and light water reactor fuel safety studies. (SCK•CEN[4])

The fuel will be a mixed plutonium-uranium oxide fuel (MOX) with an envisaged enrichment of 30 to 35% of plutonium. Furthermore, for the first core of MYRRHA the *"well-known ASS of 15-15 Ti class (such as AIM1 in France, DIN 1.4970 in Germany, D9 in the USA) will be used for the fuel cladding. Advanced ferritic-martensitic steel (FMS) T91 is chosen as the candidate material for future fuel loadings, once qualification will be completed."* (SCK•CEN[5])

2.2 The Mechanical Design

MYRRHA is designed as a pool-type ADS. Accordingly, all the primary systems are housed in the reactor vessel. Thanks to the reactor pit there is no more need of an outer vessel. Inside the vessel is a diaphragm separating the hotter LBE plenum at lower pressure from the cold LBE plenums at higher pressure. Additionally, the diaphragm supports the in-vessel fuel storage. Together a core barrel and a core support plate form the core supporting structure. The core itself consists of MOX fuel pins surrounding a central hexagon, housing a window beam tube-type spallation target. There are all in all thirty-seven positions that can be occupied by in-pile test sections, the spallation target or control and shutdown rods.

The use of LBE as a coolant allows temperatures at the core inlet down to 270 °C, increasing that way the ΔT for nominal conditions to 140 °C. The coolant's velocity is 2 m/s. Moreover, the primary cooling system consists of two pumps and four heat exchangers. They have been designed to evacuate a maximum thermal power of 110 MW; thus 10 MW more than the nominal core power is.

The instrumentation will be located directly above the core. This requests a fuel handling from underneath the core. In fact, there will be two fuel-handling machines manipulating the fuel assemblies kept by buoyancy under the core support plate. A section of the latest design – the MYRRHA-FASTEF reactor – is given in figure 8 and a cut of its core is given in figure 33 (annex A-8). (Abderrahim, 2015)

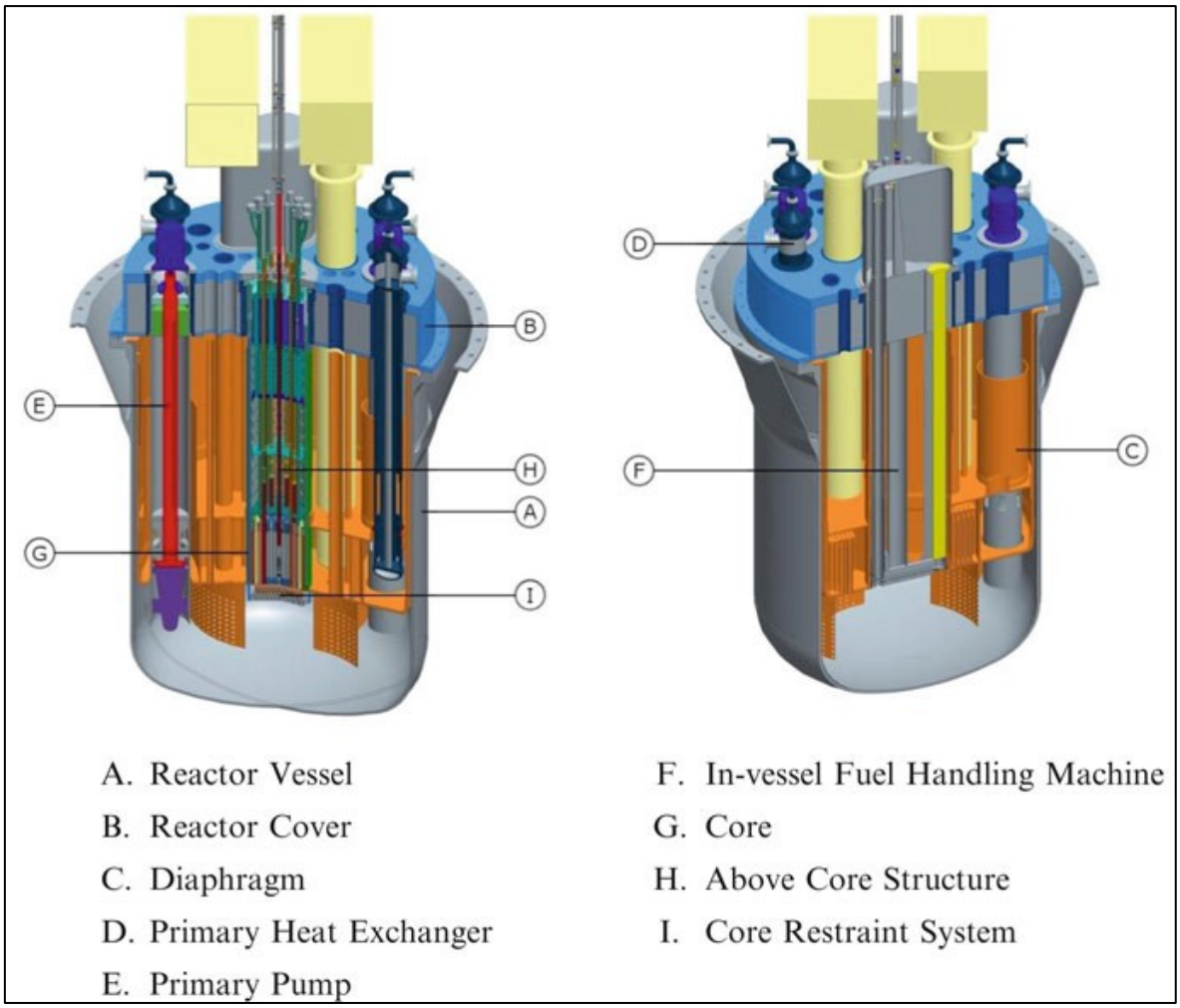

Figure 8: Section of the MYRRHA-FASTEF reactor (Abderrahim, 2015, p. 65)

2.3 Fast Neutrons and Transmutation

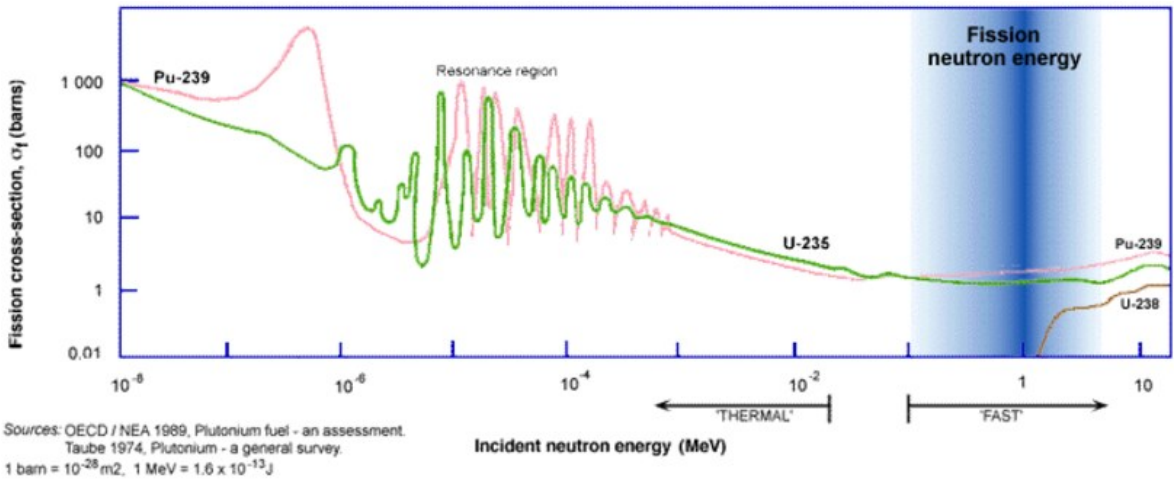

Figure 9: Neutron cross section for fission of uranium and plutonium (WNA[2], out of: OECD/NEA, 1989, p. 22)

As one can see in figure 9 that there are two neutron energy domains usable for fission. There is the one called “thermal” with particle energies about 0.025 eV and the one called “fast” with particle energies above about 1 keV.

Most of the nuclear reactors of the II & III Generation are operating with thermal neutrons; one of the main reasons being the comparatively high cross section for ^{235}U in this domain. But as natural uranium contains only about 0.72% of ^{235}U (and 99.27% of ^{238}U), it needs first to be enriched before it becomes usable for the power production. When MOX is used, ^{239}Pu is added to the fuel. On the contrary, some types of the IV Generation reactors (and also MYRRHA) will be working within the fast neutron spectrum. One of the most important reasons for it being that in this domain ^{238}U has a relevant fission cross section.

From the fuel security point of view, the usability of ^{238}U, so the usability of 99.27% of the mined uranium, would solve any fuel supply problem.

Another important reason and central intention of working with fast neurons in MYRRHA is the possibility of transmutation. As spent nuclear fuel from light water reactors contains a mixture of uranium, plutonium, fission products and minor actinides, it is highly radioactive on the short as on the long term. Eliminating the minor actinides from the waste would decrease its radiotoxicity and heat load significantly and therefore notably ease the long-term storage.

To achieve that, there are two possibilities of partitioning and transmutation: the single stratum approach and the double strata approach. In the first one, minor actinides are burned in Generation IV fast neutron reactors (FNR). Therefor they can be mixed homogeneously to the fuel or be loaded in dedicated targets. In both cases reactor safety is the limiting factor. Hence only small amounts of actinides can be loaded. (e.g.: Mixed fuel cannot contain more than 4-5% of minor actinides.) In the

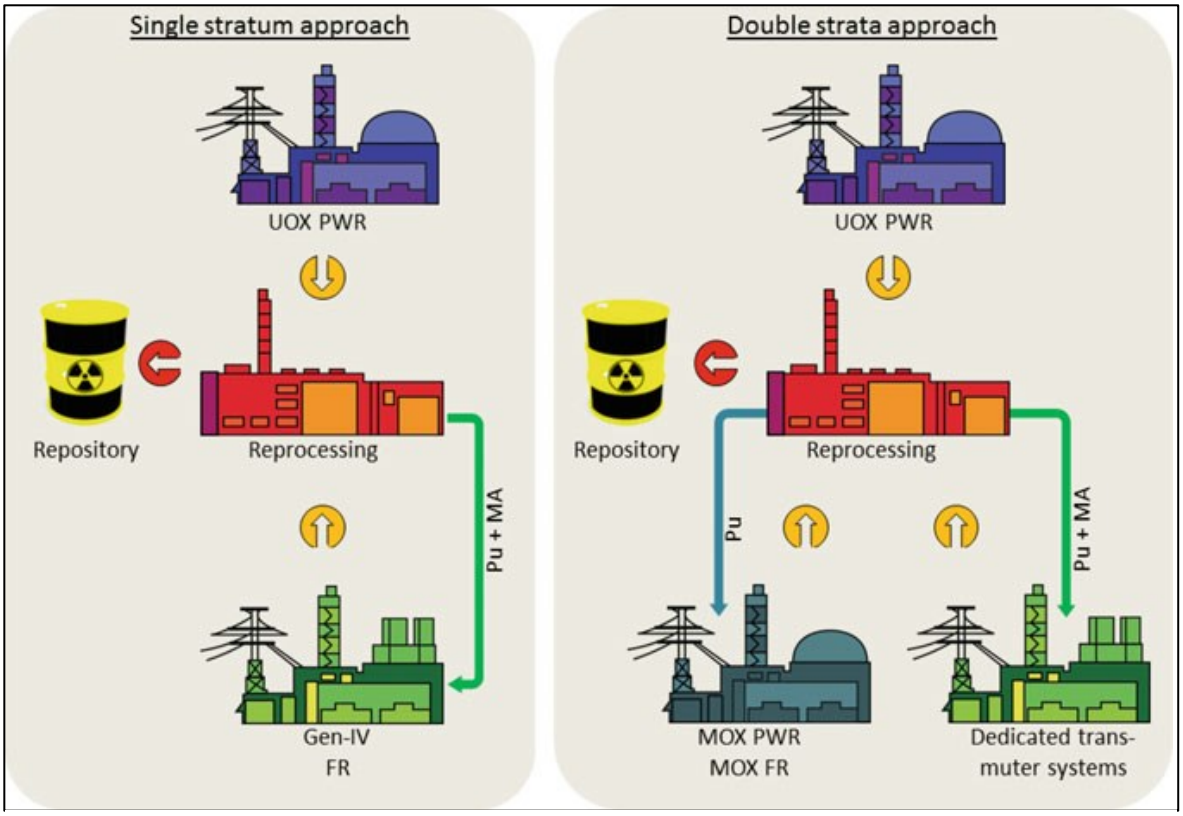

Figure 10: Single stratum versus double strata approach (Abderrahim, 2012, p. 68)

double strata approach plutonium is separately burned in light water reactors and fast rectors, while the actinides are burned in dedicated ADS facilities. As those facilities can run sub-critically, very high minor actinide containing fuel can be burned which has the advantage that, with them built close to fuel reprocessing and transmuter fuel fabrication sites, the transportation time and distances of hazardous waste are shorted importantly. A rough comparison scheme of the two approaches is given in figure 10.

To illustrate the expected benefits of the partitioning and transmutation processes figure 12 is given below.

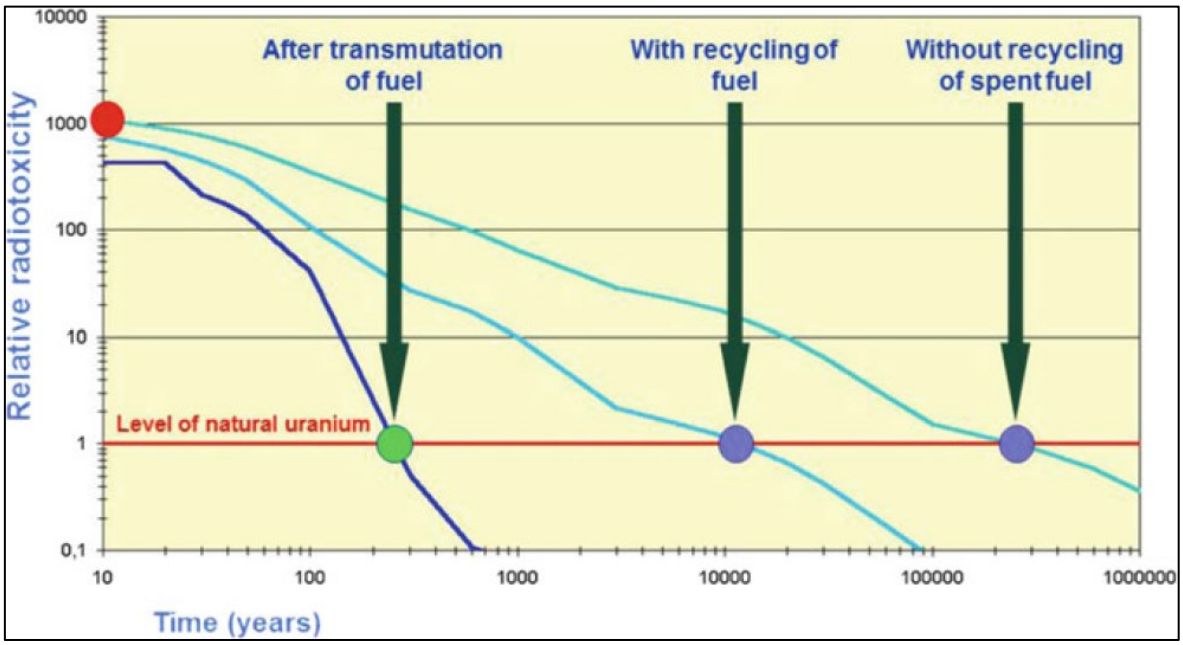

Figure 11: Radiotoxicity of radioactive waste (Abderrahim, 2015, p. 61, out of: Lecomte, 2008, p. 153)

It is visible that the reprocessing of the spent fuel diminishes the time for the waste's radioactivity to reach the one of natural uranium by a factor of one twentieth to one thirtieth and then through transmutation again by a factor of one fiftieth to one ninetieth. So finally, instead of having a heightened radiotoxicity for over hundreds of thousands of years, the waste reaches a natural level after hundreds of years. (Abderrahim, 2015)

And this period of time is considered to be short enough to be manageable.

To sum up, MYRRHA is a nuclear reactor working with fast neutrons. That is why the coolant should preferably consist of heavy stable atoms so that the colliding neutrons keep their kinetic energy. Beside these neutronic reasons, the coolant has also to act as the spallation target for the incoming protons.

The high heat deposition due to the proton beam and the limited space conditions ask for a forced convection heat removal by a liquid metal. (SCK•CEN[2])

In the same time, the coolant must stay liquid at any moment which is why the lead-bismuth eutectic has been chosen.

3 The Lead-bismuth Eutectic

As indicated before, potential coolants must be able to remove the produced heat and to act as spallation targets too. At present, heavy liquid metals, lead and the lead-bismuth eutectic are considered as applicable solutions. The main disadvantage of these coolants is their high corrosivity at temperatures above about 500 °C. Given that the melting point of the LBE is at about 125 °C, the system can be operated at lower temperatures so that the corrosion rate is diminished and maintenance simplified. Hence it became the favored option for MYRRHA. Other, yet not explored, solutions might be the lead-lithium eutectic and the lead-magnesium eutectic. (OECD/NEA, 2015)

3.1 Properties

Depending on the source one can find different values for the LBE's characteristics. In this chapter will be given the values recommended by the LBE handbook.

Melting point at atmospheric pressure:

- *"For bismuth (Bi):* *271.442 °C* *(554.592 K)*
- *For lead (Pb):* *327.502 °C* *(600.652 K)*
- ***For LBE at 45.0 at.% Pb:*** ***125.5 °C*** ***(398.65 K)***
- *For the peritectic point at 71 at.% Pb:* *187 °C* *(460.15 K)*
- *The lower limits of the elements solubility in the solid state: 0.5 atomic percent (at.%) Pb in Bi and 22 at.% Bi in Pb."* (OECD/NEA, 2015)

In weight percent (wt.%) the composition of LBE is 44.5 wt.% of Pb and 55.5 wt.% of Bi. (Gokcen's phase diagram is given in figure 12.) The recommended value for the LBE melting heat is given at atmospheric pressure with:

$$Q_{M,0(LBE)} = 8.04 \pm 0.06\ kJ\ mol^{-1} = 38.6 \pm 0.3\ kJ\ kg^{-1} \tag{3.1}$$

The boiling point shall be given, as it is the upper limit for the temperature range of operation of the LBE as coolant:

$$T_{B,0(LBE)} = 1927 \pm 16\ K \tag{3.2}$$

The density of molten LBE (obtained through a linear regression of literature data) is:

$$\rho_{LBE} = 11065 - 1293 * T \tag{3.3}$$

with ρ_{LBE} in [kg·m^{-3}] and T in Kelvin within a temperature range of 400-1273 K. Furthermore, it can be expressed by:

$$\rho_{LBE} = \frac{\mu_{LBE}}{\left(x_{\mu(Pb)} * \sqrt[3]{\frac{\mu_{Pb}}{\rho_{Pb}}} + \left(1 - x_{\mu(Pb)}\right) * \sqrt[3]{\frac{\mu_{Bi}}{\rho_{Bi}}}\right)^3} \tag{3.4}$$

with μ_{Pb}, μ_{Bi} and μ_{LBE} being respectively the molar masses of Pb, Bi and LBE and $x_{\mu(Pb)}$ and $x_{\mu(Bi)}$ being the molar fractions. A graph where the density is plotted versus the temperature is given in figure 34 (annex A-9).

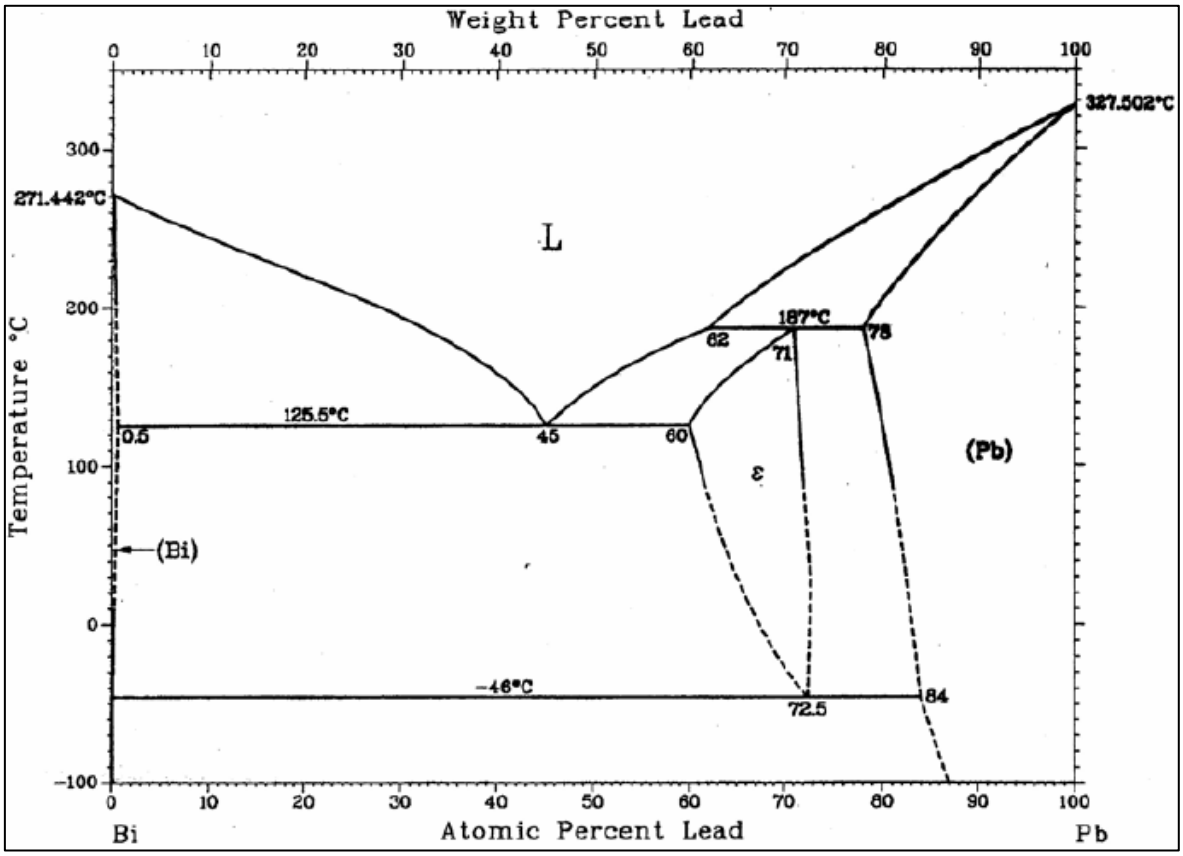

Figure 12: Phase diagram of the Pb-Bi system (OECD/NEA, 2015, p. 30, out of: Gokcen 1992)

The electric resistivity in [Ωm] (obtained through a liner interpolation correlation of literature data) is given by:

$$r_{LBE} = (90.9 + 0.048 * T) * 10^{-8} \tag{3.5}$$

with T in Kelvin. See also figure 36 (annex A-9).
And the recommended correlation for the liquid LBE thermal conductivity in [$W \cdot m^{-1} \cdot K^{-1}$] is:

$$\lambda_{LBE} = 3.284 + 1.617 * 10^{-2} * T - 2.305 * 10^{-6} * T^2 \tag{3.6}$$

with T in Kelvin. See also figure 35 (annex A-9).
The thermal diffusivity a_p, as function of the thermal conductivity λ, the density ρ and the specific heat c_p is given by:

$$a_p = \frac{\lambda}{\rho * c_p} \tag{3.7}$$

and represented in figure 38 (annex A-9). (OECD/NEA, 2015)

Next to the low melting point, the low reactivity and vapor pressure, and the high boiling point – about 1670 °C (OECD/NEA, 2015) – are pros for the application as coolant.

3.2 Purity Requirements

If impurities find their way into the LBE, its chemical composition is changed. This can then influence or change the entire nuclear system. For example, the circuits and components can be contaminated by radioactive elements formed through irradiation and physical parameters of the reactor might be influenced. Or, at a high level of impurity of some elements, the coolant chemistry control and the corrosion resistance could be affected. Moreover, chemical reactions can occur changing thermal and hydraulic characteristics of the reactor and inducing precipitations or even flow blockage.

Those impurities can be the result of technological limits during the refining and casting processes or they can be corrosion and erosion products accruing because of the interaction from LBE with different structural materials. Other sources can be the coolant interaction with gases in the circuit, the spallation process, the release of fission products due to clad rupture or the adding of impurities on purpose. (OECD/NEA, 2015)

The solubility of some metallic elements – mostly silver, cadmium, chromium, copper, iron, indium, nickel and tin – in liquid LBE can be described by a formula of the shape:

$$\log S = A * B/T \tag{3.8}$$

with T in Kelvin and S in wt.%.
The recommended values for A and B for nickel in LBE are given in the table 1 below:

Reference	Temperature [K]	A	B
(Martinelli, 2010)	603-712	5.2	3500
(Martinelli, 2010)	712-1173	1.7	1009
(Gossé, 2014)	528-742	4.32	2933
(Gossé, 2014)	742-1173	1.74	1006

Table 1: Factors A and B for the solubility law of nickel in LBE (OECD/NEA, 2015, p. 151)

Nickel impurities may come from the fuel or fuel cladding (^{59}Ni) with the consequence of coolant activation, or they are corrosion products which leads to deposits and maybe plugging. (OECD/NEA, 2015)

As parts of MYRRHA will be made of austenitic steel, nickel impurities are expected to a certain extend. It is therefore necessary to find a way to first measure its concentration in the LBE coolant and second to find a way to remove it.

4 The Theoretical Background for a Nickel Sensor

In the previous chapter we have seen that the coolant's chemistry and therefore its thermodynamic behavior and flow properties can be modified by impurities. Furthermore, they may change the reactor physics. Nickel impurities can occur, mainly due to corrosion of the structural materials, and lead to deposits and plugging. Because of this, it is necessary to find a way to measure even low concentrations of nickel in the LBE and to remove it from the coolant. As the actual measurements by laser-induced breakdown spectroscopy are expensive and not precise enough, a new, electrochemical way shall be tested in this work.

The principle of potentiometric sensors is based on the measurement of electrical potential differences (E) arising between a reference and a counter electrode physically separated by an electrolyte. An ideal reference electrode should have a stable and well-known electrochemical potential. The electrolyte should be an ion conducting material. In our study, the working electrode is the liquid LBE.

The link between the measured potential difference E and the activity a of the dissolved substances in LBE is the Nernst equation (see (4.1)). In fact, at equilibrium condition, E is a function of the ideal gas constant R (8.3145 J·K^{-1}·mol^{-1}), the temperature T in Kelvin, the number of exchanged electrons in the reaction n (2 in case of the nickel ion), the Faraday constant F (96485.34 C·mol^{-1}), and the ratio between the activity of the element of interest at the reference electrode side $a_{x,ref}$ and the activity of the dissolved element in LBE $a_{x,LBE}$.

Nernst equation:

$$E = E^0 - \frac{RT}{nF} * ln\left({a_{x,ref}}/{a_{x,LBE}}\right) \quad [V] = \frac{[JK^{-1}mol^{-1}]*[K]}{[1]*[Cmol^{-1}]} * ln\left(\frac{[1]}{[1]}\right) \qquad (4.1)$$

As no nickel sensor has been built or tested yet, its theoretical basis shall be compared to the ones of the oxygen sensor.

4.1 A Potentiometric Oxygen Sensor

4.1.1 The Working Electrode; LBE

Assumption: The oxygen dissolves in LBE as oxygen atom species and it follows Henry's law (see (4.2)) up to the solubility limit. (In the following part, all temperatures T are given in Klevin.)

$$K_H = \frac{a_{O,LBE}}{c_O} \qquad (4.2)$$

with $a_{O,LBE}$ the activity of oxygen in LBE, C_O the actual concentration of oxygen in LBE in weight percent and K_H Henry's constant. The relation between K_H and the excess molar free energy of dissolution of oxygen into LBE $G^{EX}_{O(LBE)}$ is given by:

$$G^{EX}_{O(LBE)} = RT * \ln(K_H) \tag{4.3}$$

with $G^{EX}_{O(LBE)}$ in [J·mol^{-1}].
Now, one can calculate the activity $a_{O,LBE}$ by combining the equations (4.2) and (4.3) resulting in:

$$a_{O,LBE} = C_O * K_H = C_O * exp\left(\frac{G^{EX}_{O(LBE)}}{RT}\right) \tag{4.4}$$

The required excess molar free energy is a function of the temperature:

$$G^{EX}_{O,LBE} = -127398 + 27.238 * T \quad (\pm 717)\ Jmol^{-1} \tag{4.5}$$

in a temperature range from 812 K to 1012 K.
Combining (4.4) and (4.5) results in:

$$a_{O,LBE} = C_O * exp\left(\frac{-127398+27.238*T}{RT}\right) \tag{4.6}$$

4.1.2 The Reference Electrode; Bi/Bi$_2$O$_3$

When considering a metal-metal oxide reference electrode such as Bi/Bi$_2$O$_3$, the chemical equation that has to be considered is:

$$2Bi_{(l)} + 3O \rightleftarrows Bi_2O_{3(s)}$$

so that the equilibrium condition is:

$$\Delta G = G^0_{Bi_2O_3} + RT * ln\left(K_{Bi \rightleftarrows Bi_2O_3}\right) = 0 \tag{4.7}$$

where $K_{Bi \rightleftarrows Bi_2O_3}$ stands for the equilibrium constant which is related to the chemical activities of the different elements through:

$$K_{Bi \rightleftarrows Bi_2O_3} = \frac{[a_{(Bi_2O_3)}]}{[a_{(Bi)}]^2 * [a_{O,ref}]^3} \tag{4.8}$$

In the case we are considering pure bismuth and pure bismuth oxide, their activities are equal to 1 (see Noggle, 1996, p. 361). By combining equations (4.6) and (4.7) we come to:

$$a_{O,ref} = exp\left(\frac{G^0_{Bi \rightleftarrows Bi_2O_3}}{3RT}\right) \tag{4.9}$$

This free molar energy (for α-Bi$_2$O$_3$) can be obtained by:

$$G^0_{Bi_2O_3} = -583400 + 293.8 * T \tag{4.10}$$

in a temperature range from 572 K to 988 K.

So, we can finally reformulate the Nernst equation as follows:

$$E = E^0 - \frac{RT}{2F} * \left(\frac{G^0_{Bi,Bi_2O_3}}{3RT} - \frac{G^{EX}_{O(LBE)}}{RT} - ln(C_O) \right) \quad (4.11)$$

NB: *During the calibration test, the LBE is kept under saturated conditions (as the surface of the liquid metal is open to air).*

The solubility limit (in wt.%) for the temperature range 673-733 K is expressed using the correlation derived by Lim:

$$log(C_{O,sat}) = 2.64 - \frac{4426}{T} \quad (4.12)$$

in the temperature range from 673 K to 733 K.

4.2 A Potentiometric Nickel Sensor

Like the potentiometric oxygen sensor, a potentiometric nickel sensor shall be conceived and tested. Therefor the theoretical concept is given below.

4.2.1 The Working Electrode; LBE

Assumption: In analogy to the oxygen case, nickel is suspected to dissolve in LBE as nickel atom species. Its activity $a_{Ni,LBE}$ is supposed to be a function of the nickel concentration $C_{Ni,LBE}$ in LBE and the nickel solubility S (both in wt.%):

$$a_{Ni,LBE} = \frac{C_{Ni,LBE}}{S} \quad (4.13)$$

The nickel solubility in wt.% of the LBE varies upon the temperature. Different equations are given in literature, based on different temperature ranges:

- for 623 K<T<688 K, the correlation is:

$$log_{10}(S) = 5.2 \pm 0.12 - \frac{3500}{T} \quad (4.14)$$

- for 688 K<T<1173 K, the correlation is:

$$log_{10}(S) = 1.7 \pm 0.08 - \frac{1009}{T} \quad (4.15)$$

The first formula (4.14) is the result of tests performed by Martinelli (2010), while the second one (4.15) is a linear regression based on the overall experimental points available in literature and quoted in Martinelli (2010).

Combining respectively (4.13) and (4.14) or (4.13) and (4.15), the activity can be expressed:

- for 623 K<T<688 K as: $a_{Ni,LBE} = {C_{Ni,LBE}}\Big/{10^{\left(5.2-\frac{3500}{T}\right)}}$ (4.16)

- for 688 K<T<1173 K as: $a_{Ni,LBE} = {C_{Ni,LBE}}\Big/{10^{\left(1.7-\frac{1009}{T}\right)}}$ (4.17)

4.2.2 The Reference Electrode; Nickel

As the nickel electrode is made of nickel with a purity higher than 99.98%, the chemical reaction occurring is supposed to be:

$$Ni^{2+} + 2e^{-} \rightleftarrows Ni$$

and its activity $a_{Ni,ref}$ is assumed to be equal to 1.

Taking for example the temperature field of (4.16), the Nernst equation results in:

$$E = E^0 - \frac{RT}{2F} * ln\left(\frac{1}{C_{Ni,LBE} \Big/ 10^{\left(5.2-\frac{3500}{T}\right)}}\right) \tag{4.18}$$

The standard electrode potential E^0 is zero because there is only nickel reacting.

4.3 The Thermoelectric Potential Between the nickel- and molybdenum-wire in LBE

Once the solubility limit is reached, $a_{Ni,LBE}$ is assumed equal to 1. This means that the remaining measurable potential is the thermoelectric potential between the two electrodes in LBE.

The thermoelectric potential E^{th} of the nickel and molybdenum wires was experimentally measured by immerging a nickel wire in a pot with molten LBE at known temperature. The measured values are given in figure 14:

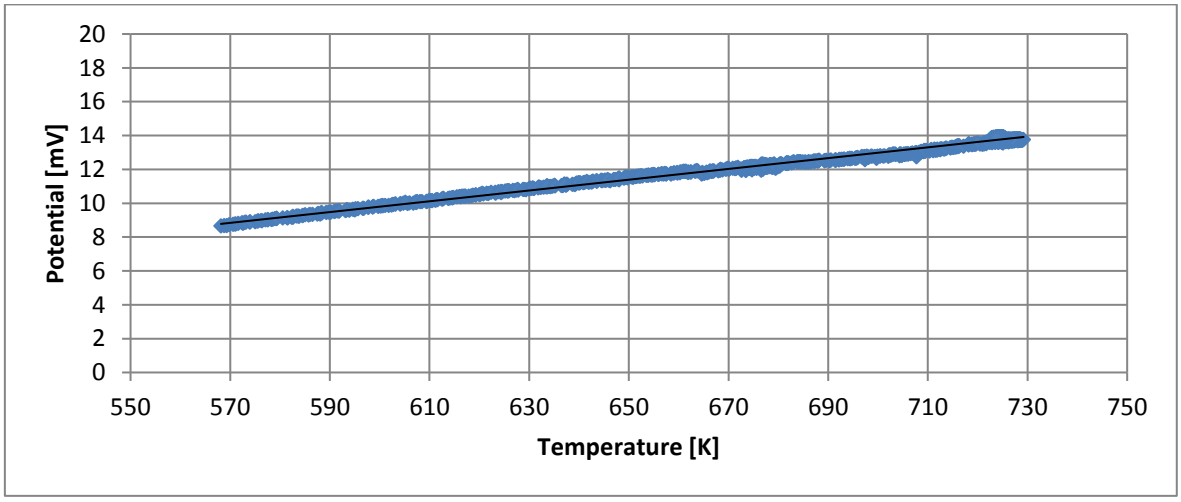

Figure 13: Nickel-molybdenum thermoelectric potential in dependence of the temperature in LBE

A linear regression of the thermoelectric potential over the temperature gives following relation:

$$E^{th} = -9.329 * 10^{-3} + 3.188 * 10^{-5} T \tag{4.19}$$

in the temperature range from 573 to 723 K (with R^2=0.9932).

5 The Nickel Sensor

5.1 Theoretical Values

The potentials, that are expected to be measured for a given concentrations are represented in figure 14. The dashed lines give the calculated potential, and the full lines give the potential once E^{th} has been taken into consideration.

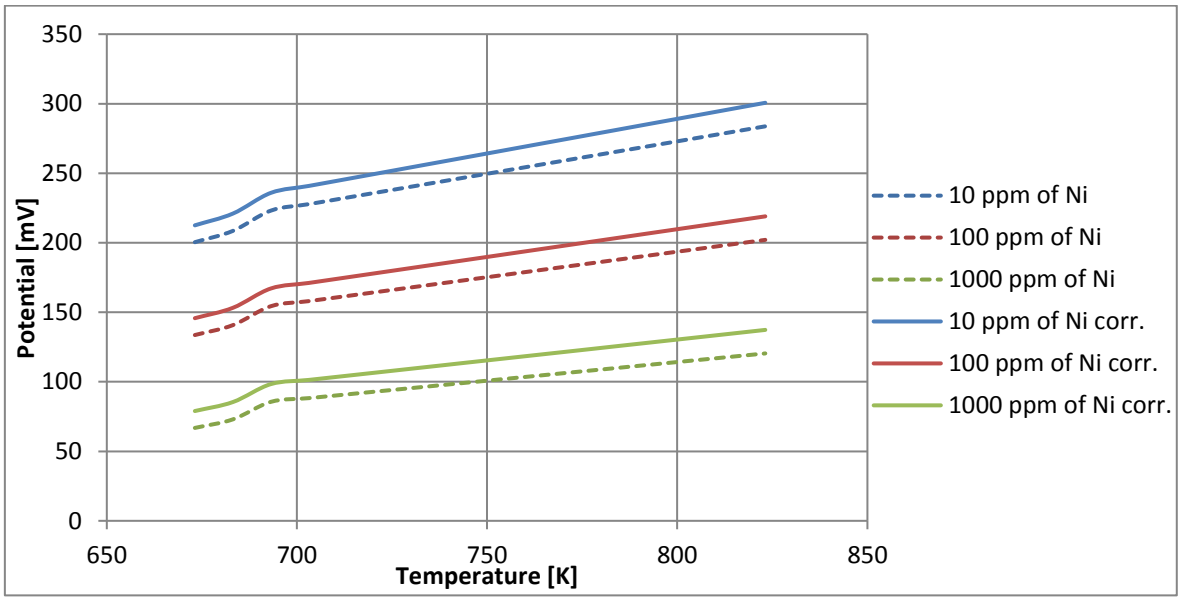

Figure 14: Expected potential as function of the temperature and the concentration

5.2 The Set-up

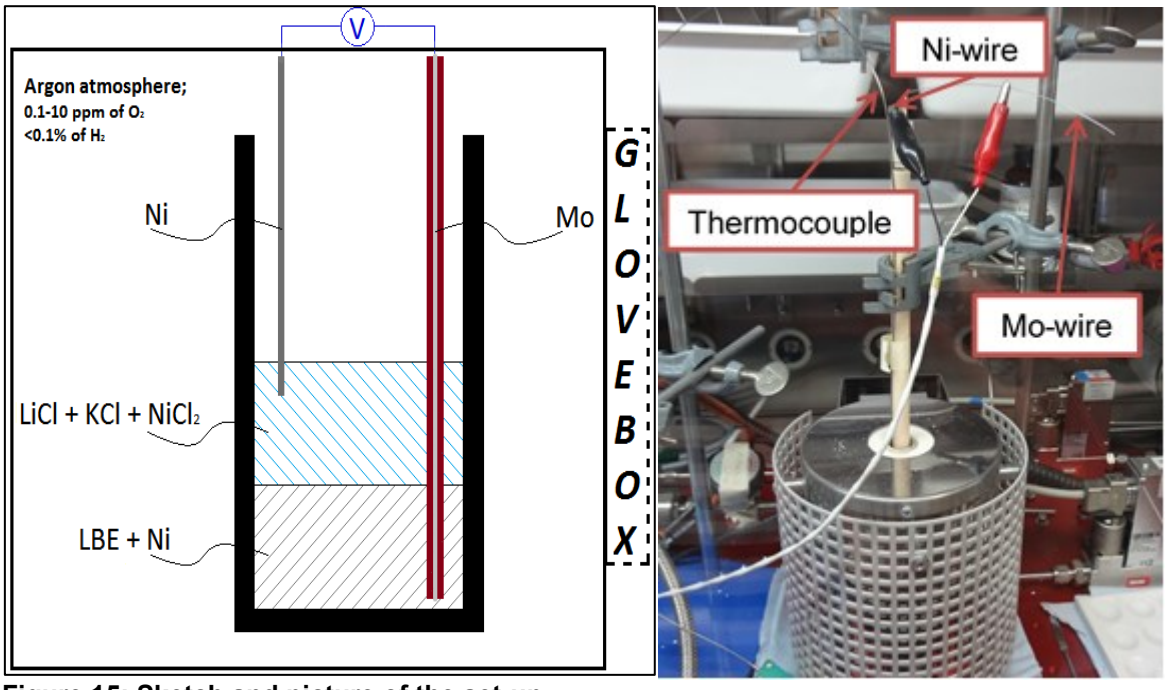

Figure 15: Sketch and picture of the set-up

N.B.: The purpose of the LiCl-KCl eutectic as salt is to lower the salt's melting temperature to 357 °C.

5.3 Limits of Feasibility

5.3.1 The Temperature Deviation

One of the most important factors for any kind of measurement is to know the sample's temperature. For this reason, a temperature distribution test has been done in the furnaces (in- and outside of the glove box). Figure 16 shows the considerable temperature difference between the one indicated on the furnace and the one measured with a thermocouple introduced inside the furnace.

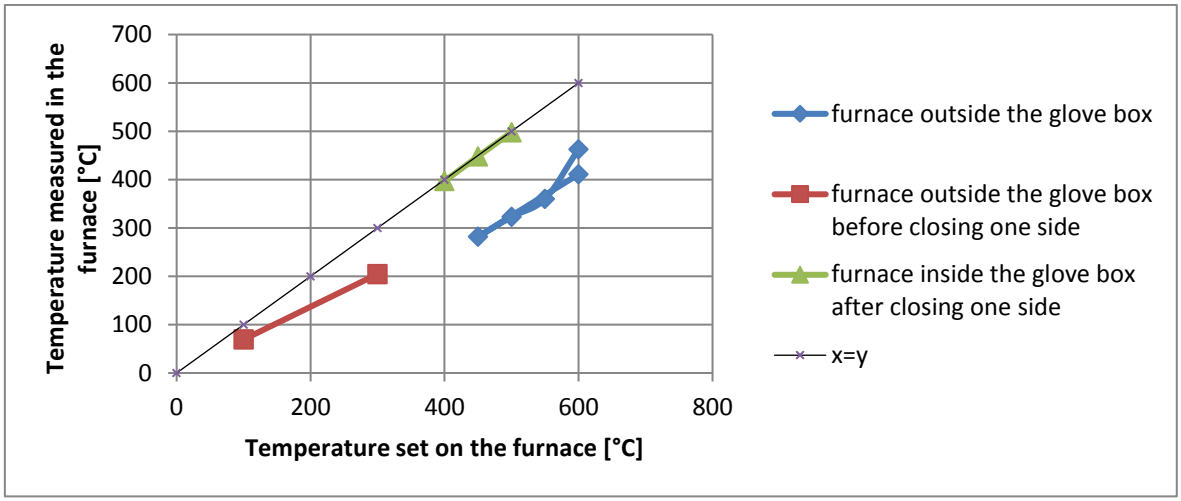

Figure 16: Furnace temperature deviation

Closing the opening on the lower side of the furnace reduced the natural convection and therefore the deviation significantly. However, a deviation remained. Figure 17 shows the deviation in dependence of the penetration depth.

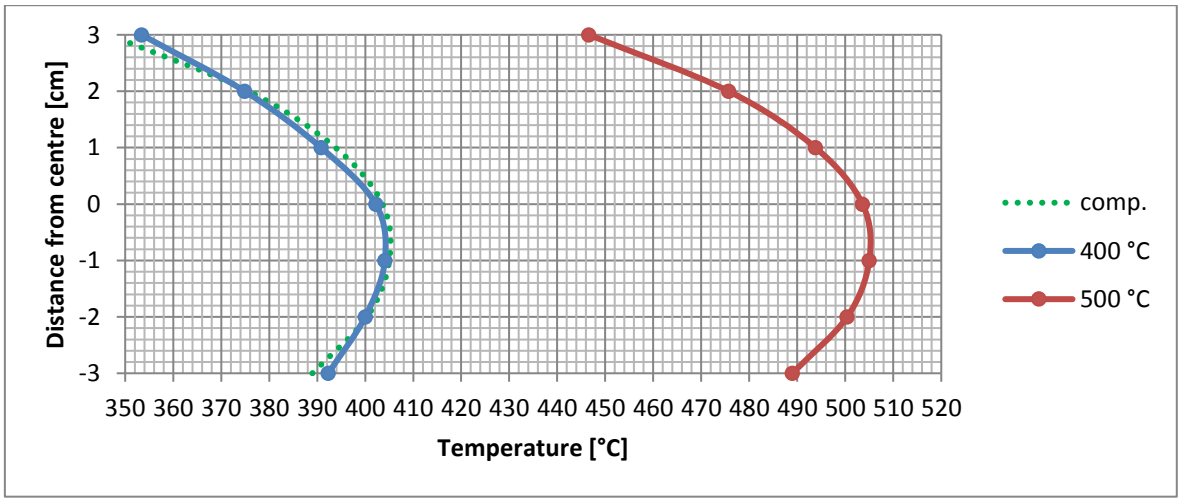

Figure 17: Temperature deviation in function of the distance to the furnace´s central heating point

The dotted green line corresponds to the 500 °C line shifted to the left so that a comparison it to the 400 °C line is simplified. One can see that the trend is quite similar. Due to the increasing deviation with the distance to the center, it seems favorable to introduce the sample tube so that the tube's end is 2 cm below the furnace center and to have a sample height of 2 cm (1 cm LBE and 1 cm salt).

5.3.2 The Required Precision

One of this work's aims is to develop a sensor able to measure impurities down to a few ppm. The recipient containing the sample is a test tube with a diameter of 0.6 cm. The sample preparation has been done in a glove box. But as we have seen in the previous part, temperature deviation from the set temperature becomes more then significant even after closing the bottom side of the furnace.

Therefore, work is possible only in a zone of 1-2 cm from the furnace's central heating point. This results in LBE and salt masses of 2.8 g, and 0.57 g respectively. 10 ppm of this LBE mass correspond to a nickel mass of 28 µg and 0.3 wt.% (from the salt) correspond to 1.71 mg of $NiCl_2$. These masses are too small to be weighed manually with the given instruments and without a significant accuracy loss.

A solution for this problem is to work with bigger masses, whereas therefor one needs a bigger furnace than the one in the glove box.

5.4 Stability of the Components

To see if the used components stay stable once they are mixed together, one can draw an Ellingham diagram as given in figure 18. To trace this graph, Gibbs free energy change data from Barin (1995) has been used and adapted by basing it on the single Cl^- in a way so that it became comparable.

Given the different Gibbs free energy changes, one can conclude that $PbCl_2$ is more stable than $NiCl_2$. This means, that when the $NiCl_2$ is added to the salt, it reacts with the LBE forming $PbCl_2$ and liberating Ni in the LBE. So, the concentration in the LBE is falsified. This became also visible through some preliminary test, where the measured voltage was coincident with the expected one for the first few seconds but then continuously dropped, indicating an increase of the nickel concentration in the LBE.

The conclusion at this state is, that a Ni-sensor for LBE based on a cell using chlorides as electrolyte is not feasible. Using fluorides is not an option neither, as one can read out of the Ellingham diagram given in figure 38 (annex A-10).

Nonetheless it seems to be a promising technology for measuring manganese impurities (with $MnCl_2$ or MnF_2 as electrolyte) and iron impurities (with $FeCl_2$ or FeF_2 as electrolyte).

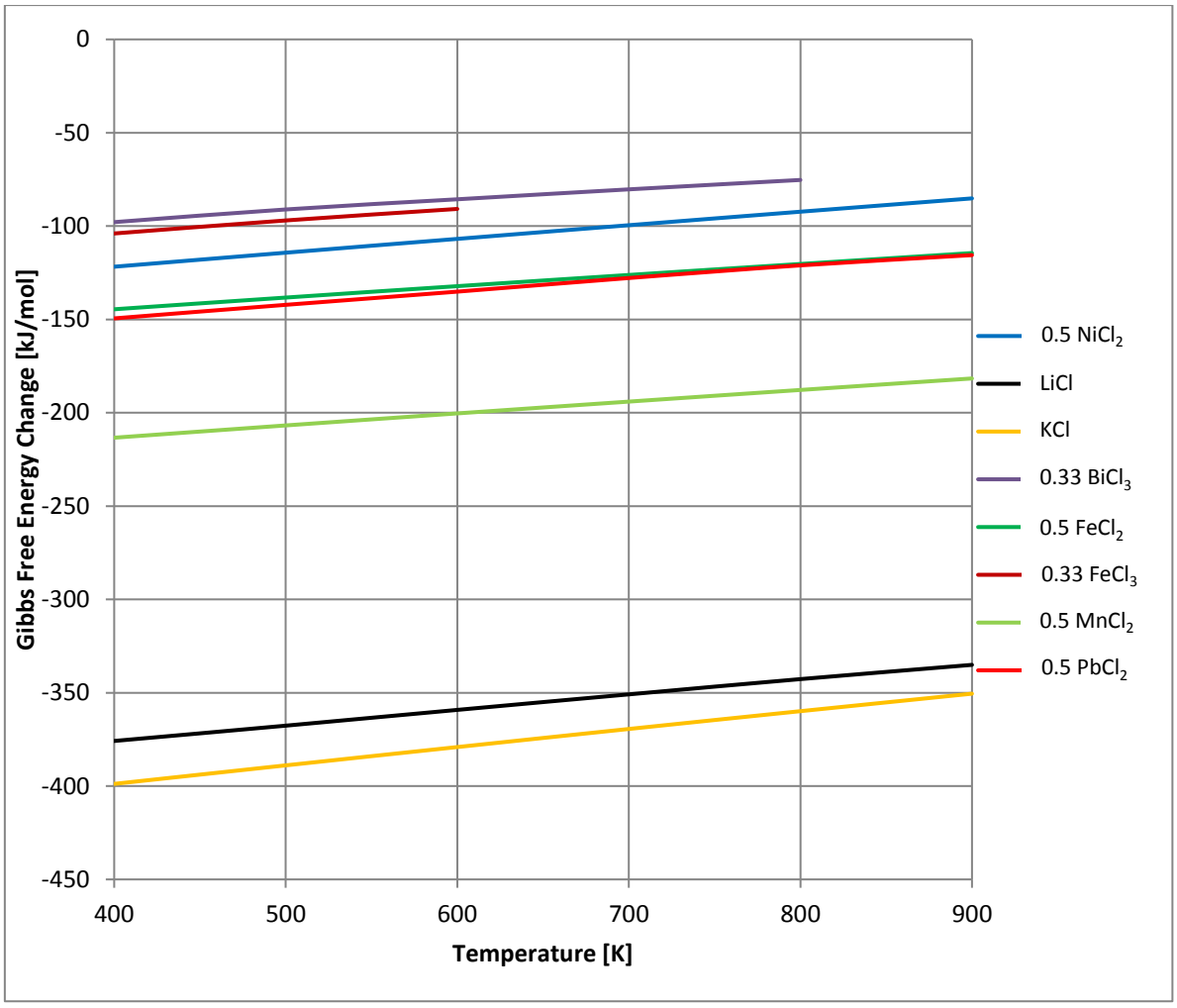

Figure 18: Ellingham diagram of chlorides

6 Nickel in Bismuth

To validate the idea of the potentiometric concentration determination of metals, nickel detection has been tested in bismuth. According to the Ellingham diagram (figure 18) the $BiCl_3$ is less stable than the $NiCl_2$. Hence no problems should occur from this side.

6.1 Theoretical Background

In analogy to nickel in the lead-bismuth eutectic, the same principles are valid for nickel in pure bismuth.

6.1.1 Nickel Solubility

For the nickel solubility (in wt.% of bismuth) different data are available in literature:

- Between 543-738 K the solubility is: $log_{10}S = 3.81 - \frac{2429}{T}$ (6.1)
- Between 738-918 K the solubility is: $log_{10}S = 2.05 - \frac{1131}{T}$ (6.2)
- Between 918-1173 K the solubility is: $log_{10}S = 1.35 - \frac{484}{T}$ (6.3)

or

- Between 723-903 K the solubility is: $log_{10}S = 2.61 - \frac{1538}{T}$ (6.4)

Thus, the activity can be expressed:

- for 543 K<T<738 K as: $a_{Ni,Bi} = {C_{Ni,Bi}}/{10^{\left(3.81-\frac{2429}{T}\right)}}$ (6.5)
- for 738 K<T<918 K as: $a_{Ni,Bi} = {C_{Ni,Bi}}/{10^{\left(2.05-\frac{1131}{T}\right)}}$ (6.6)

6.1.2 The Thermoelectric Potential Between the Ni- and Mo-wire in Bismuth

As it has been the case for the nickel activity in LBE, it is the same for its activity in bismuth: Once the solubility limit is reached $a_{Ni,Bi}$ is assumed to be equal to 1.

The thermoelectric potential E^{th} of the nickel and molybdenum wires was experimentally measured by immerging a nickel wire in a test tube with molten bismuth at known temperature. The measured values are given in figure 19:

A linear regression of the thermoelectric potential over the temperature gives following relation:

$$E^{th} = -1.335 * 10^{-2} + 3.591 * 10^{-5} T \quad (6.7)$$

in the temperature range from 573 K to 873 K (with R^2= 0.9986). (See figure 19)

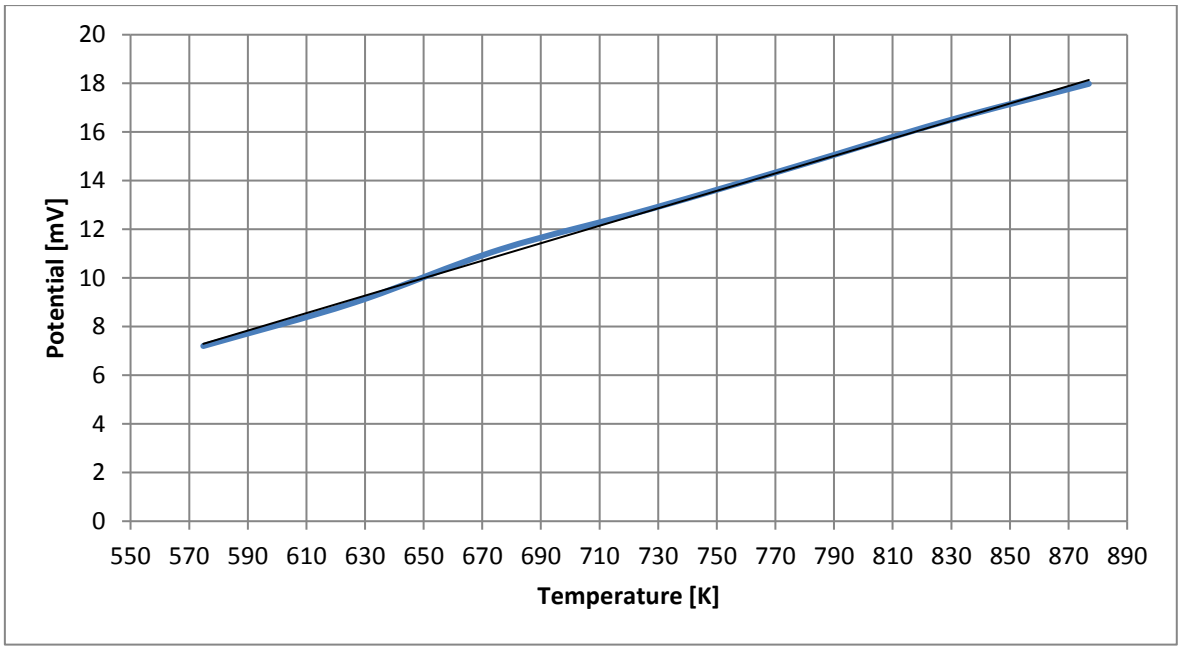

Figure 19: Nickel-molybdenum thermoelectric potential in dependence of the temperature in bismuth

6.1.3 The Nickel-Bismuth Phase Diagram

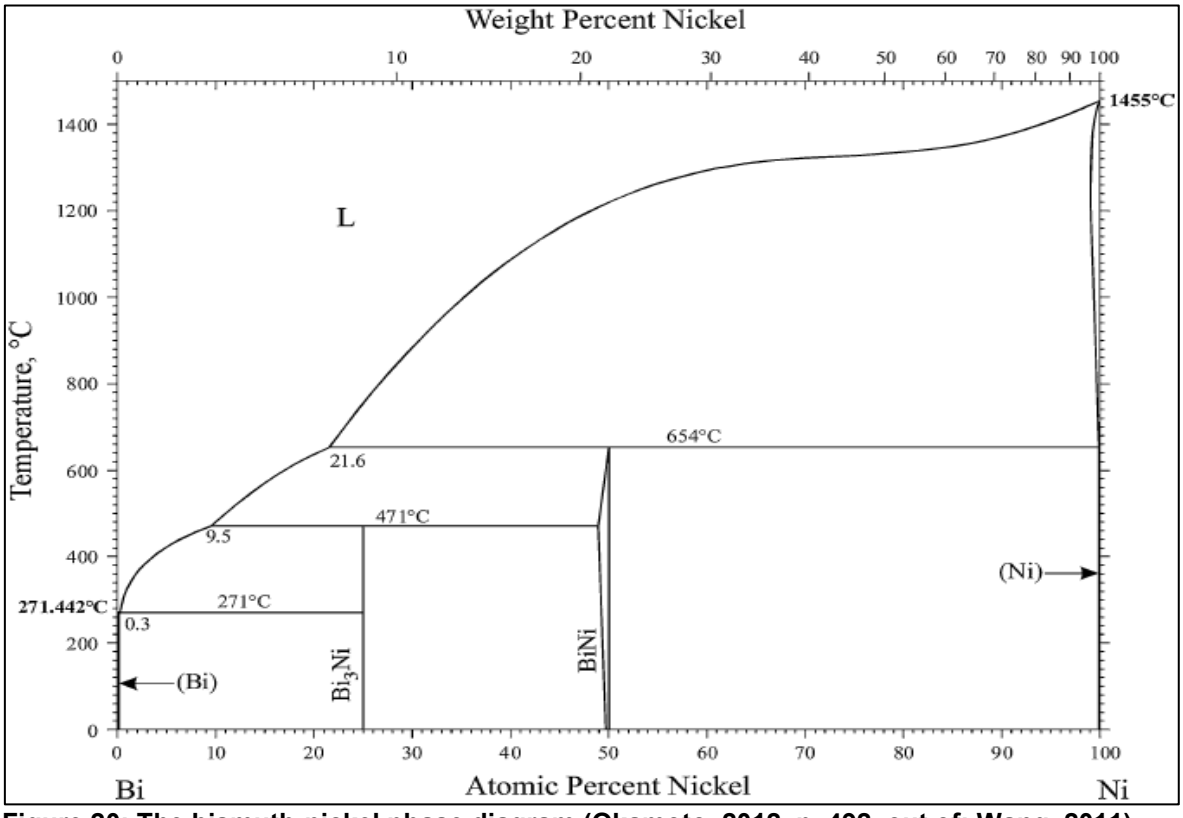

Figure 20: The bismuth-nickel phase diagram (Okamoto, 2012, p. 492, out of: Wang, 2011)

According to the formula of Gossé (2014) the solubility limit of nickel in bismuth in the temperature range from 400 °C to 550 °C lies between 1.59 wt.% and 4.47 wt.%. As recommended by the LBE handbook, Gossé's formulas were used in this work. Nevertheless, once his values are plotted in the diagram (green line in

figure 39 (annex A-11), they lie in a zone where Bi_3Ni is formed. This shall indicate the variety of proposed formulas and therefore the difficulty of a proper potential prediction as well as the incapacity of giving a reasonable accuracy for the measurements at this stage.

6.2 Implementation

6.2.1 The Set-up

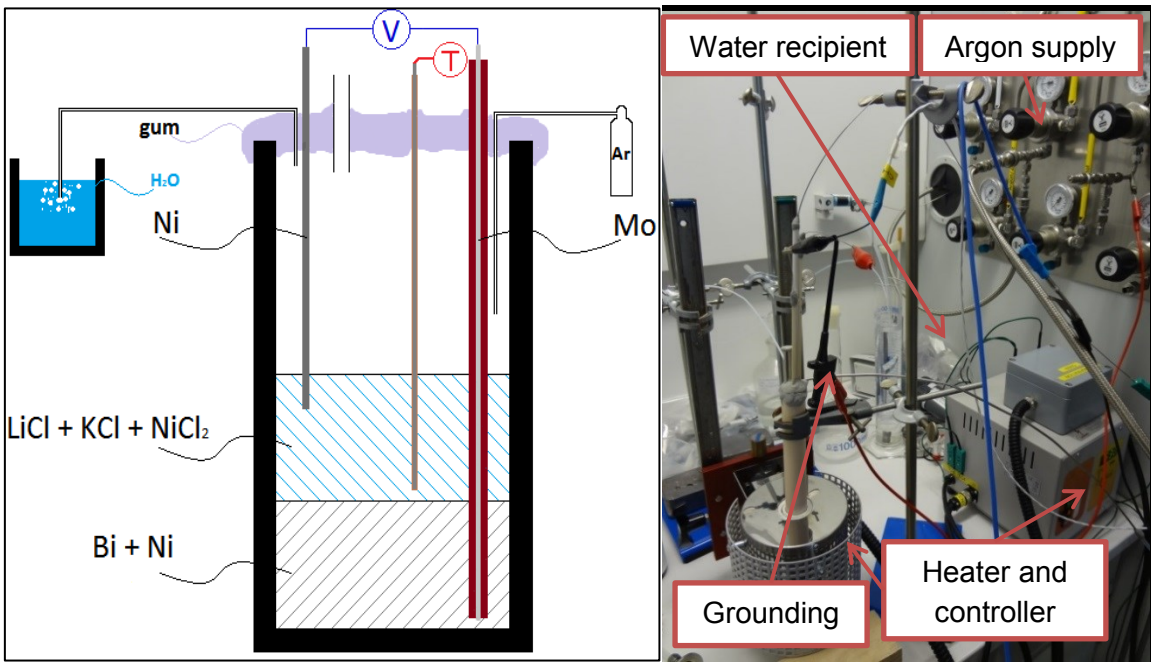

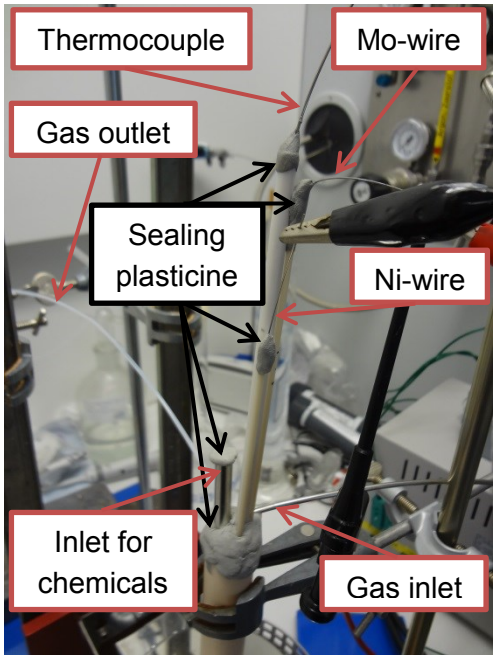

Figure 21: Sketch and two pictures of the set-up

As mentioned before, increasing the size of the sample will help to increase the working precision. That is why the nickel in bismuth sample have been prepared in a bigger test tube and therefore in the furnace outside of the glove box.

To preserve the argon atmosphere the tube was sealed on the top with some type of gum/plasticine. A small tube serving as inlet for the chemicals was put in place, the same as gas in- and outlets. The gas outlet tube was inserted in a recipient filled with water to prove the gas flow through bubble generation. Beside the settings described in annex A-12 a grounding wire has been attached to the molybdenum wire. A list of the used instruments and compounds is given in annex A-

12 too. To get the most precise measurement possible, the thermocouple (protected by an alumina tube) was directly dipped in the salt.

Following the example of a similar experiment (Kumar, 2016) the quantity of $NiCl_2$ to be added as electrolyte was chosen to be 3 wt.% of the salt's mass.

6.2.2 Results of the First Experiment

In the following graph of the first long term experiment are given the measured potential (in blue) as well as the measured temperature (in green). The, on basis of Gossé´s formulas, calculated expected potentials are shown through the dotted red line. Considering E^{th}gives the corrected values (full red line).

In this experiment, the effects of adding molybdenum and copper were tested too. While the molybdenum did not provoke any change, the copper led to a voltage drop. This is caused by the formation of copper chloride and the following liberation of nickel from the nickel chloride. The exact quantity of copper chloride formed cannot be given. But assuming that all copper has reacted, the amount of released nickel can be deduced. The orange dotted line shows the expected and corrected potentials for the case that all copper would have reacted.

Every potential drop goes hand in hand with the admixing of nickel.

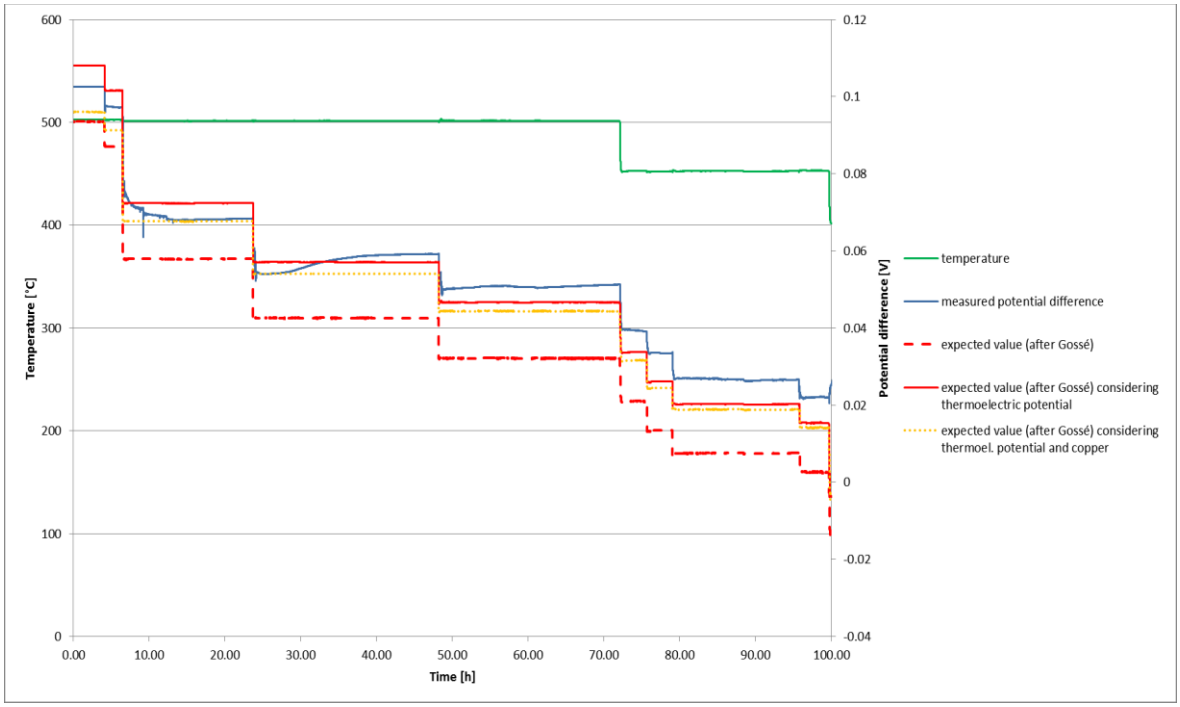

Figure 22: Measured and calculated potentials from experiment 1

One can see in figure 22 that in the first two experimental phases the measured potential lies between the corrected Gossé line and the line considering the copper. Hence it can be assumed that not all the copper has reacted to copper chloride. Along with the increase of the nickel concentration the importance of the copper becomes less and less. Nevertheless, it shall be mentioned that the measured po-

tential in phase three overlaps with the calculated copper considering line. In addition, in phase four another, yet unknown, reaction occurred resulting in the fact that from thereon the measured potential will stay below the expected ones. Is there a $Bi_3Ni_{(s)}$ formation? (Exact data about the nickel masses added, its concentration and the temperature changes are given in annex A-13/Experiment 1.)

The standard deviation of the measured values from the copper corrected line within the 30 minutes before a change was made are:

plateau	1	2	3	4	5	6	7	8	9
σ [mV]	6.62	5.88	0.57	5.17	6.94	7.85	8.98	7.75	7.97

Table 2: Standard deviation; experiment 1

6.2.3 Conclusions of the First Experiment

This experiment confirmed the principles of the potentiometric concentration measurement. But it showed also that the system is very sensitive to other impurities and their interaction with the electrolyte. Furthermore, the system reacts immediately to composition and temperature modifications but needs then several hours (up to days) to come back to an equilibrium.

To be sure that no bismuth is reacting with $NiCl_2$ the equilibrium concentration shall be calculated in a next step.

6.2.4 $NiCl_2$/$BiCl_3$-Equilibrium Calculation

For this calculation, thermochemical data from Barin (1995) has been used. After a linear regression of that data, the formulas to calculate the Gibb´s free energy change are:

- For $\Delta G_{f,NiCl_2}$ in [J/mol]: $-301090 + 145.49 * T$ (with R^2=0,9999) (6.8)
- For $\Delta G_{f,BiCl_3}$ in [J/mol]: $-351469 + 157.29 * T$ (with R^2=0,9998) (6.9)

In general:

$$\Delta G_{\left(\frac{1}{2}NiC_2\right)} = \Delta_f G^0_{\left(\frac{1}{2}NiCl_2\right)} + RTln\left(\frac{a_{NiCl_2}{}^{\frac{1}{2}}}{a_{Ni}{}^{\frac{1}{2}} * a_{Cl}}\right) \quad (6.10)$$

and

$$\Delta G_{\left(\frac{1}{3}BiCl_3\right)} = \Delta_f G^0_{\left(\frac{1}{3}BiCl_3\right)} + RTln\left(\frac{a_{BiCl_3}{}^{\frac{1}{3}}}{a_{Bi}{}^{\frac{1}{3}} * a_{Cl}}\right) \quad (6.11)$$

where a_{BiCl_3} and a_{NiCl_2} are equal to 1, as they are solids, and a_{Bi} and a_{Cl} are equal to 1, as they are elemental. At equilibrium $\Delta G_{\left(\frac{1}{2}NiC_2\right)}$ and $\Delta G_{\left(\frac{1}{3}BiCl_3\right)}$ are equal to zero so that:

$$\Delta_f G^0_{\left(\frac{1}{3}BiCl_3\right)} = \Delta_f G^0_{\left(\frac{1}{2}NiCl_2\right)} + RTln\left(\frac{1}{a_{Ni}^{\frac{1}{2}}}\right) \tag{6.12}$$

The concentration can be calculated by introducing (6.5) or (6.6) in (6.12) and reformulating it to:

$$C_{Ni,eq.} = e^{\left(\frac{2*\left(\frac{\Delta G_{f,NiCl_2}}{2} - \frac{\Delta G_{f,BiCl_3}}{3}\right)}{RT}\right)} * 10^{\left(3{,}81 - \frac{2429}{T}\right)} \tag{6.13}$$

for the temperature range from 543 K to 738 K or:

$$C_{Ni,eq.} = e^{\left(\frac{2*\left(\frac{\Delta G_{f,NiCl_2}}{2} - \frac{\Delta G_{f,BiCl_3}}{3}\right)}{RT}\right)} * 10^{\left(2{,}05 - \frac{1131}{T}\right)} \tag{6.14}$$

for the temperature range from 738 K to 918 K.

As one can see in figure 23, the equilibrium concentration in the temperature range of interest (400-550 °C) is below 0.04 wt.% and therefore negligible in the experiments where the added nickel masses were about 0.4 wt.% (thus more than ten times higher).

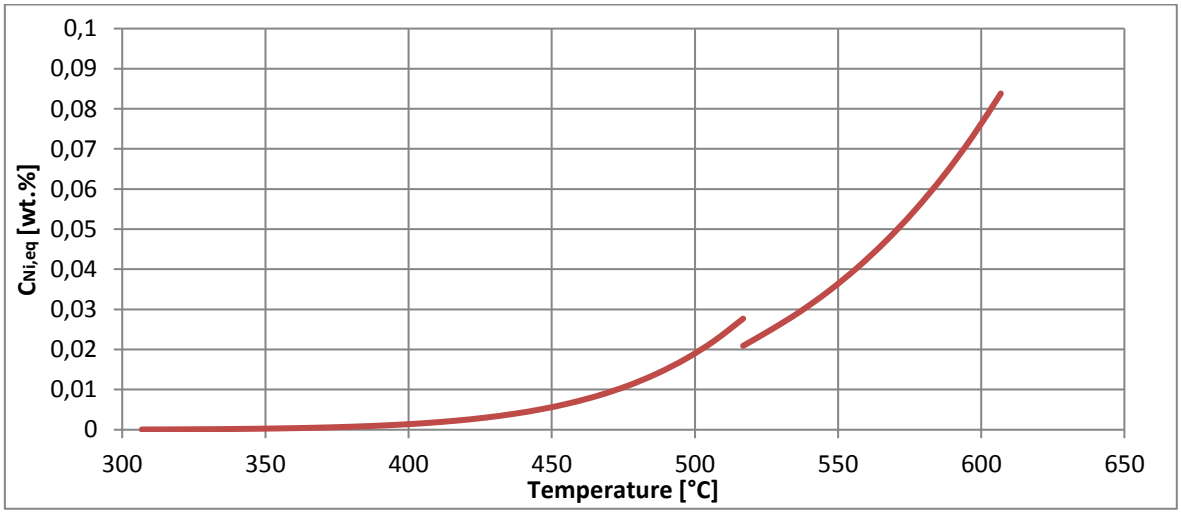

Figure 23: Nickel equilibrium concentration

6.2.5 Results of the Second Experiment

In the former parts, we saw that the used solubility limits calculated by Gossé (2014) lie in a zone in which, according to other´s data, the formation of Bi_3Ni is already possible. In case this would happen, the assumption of having $a_{Ni,Bi} = 1$ once saturation is reached, could become invalid. To test this, the sample was saturated with nickel. If then the measured E^{th} corresponds still to the expected one, the formation of significant amounts of Bi_3Ni could be excluded. Figure 24 shows the measured potential (in blue) and the calculated one according to Gossé (dotted

thinner red line) and its corrected version (full red line) in dependence of the temperature (green line).

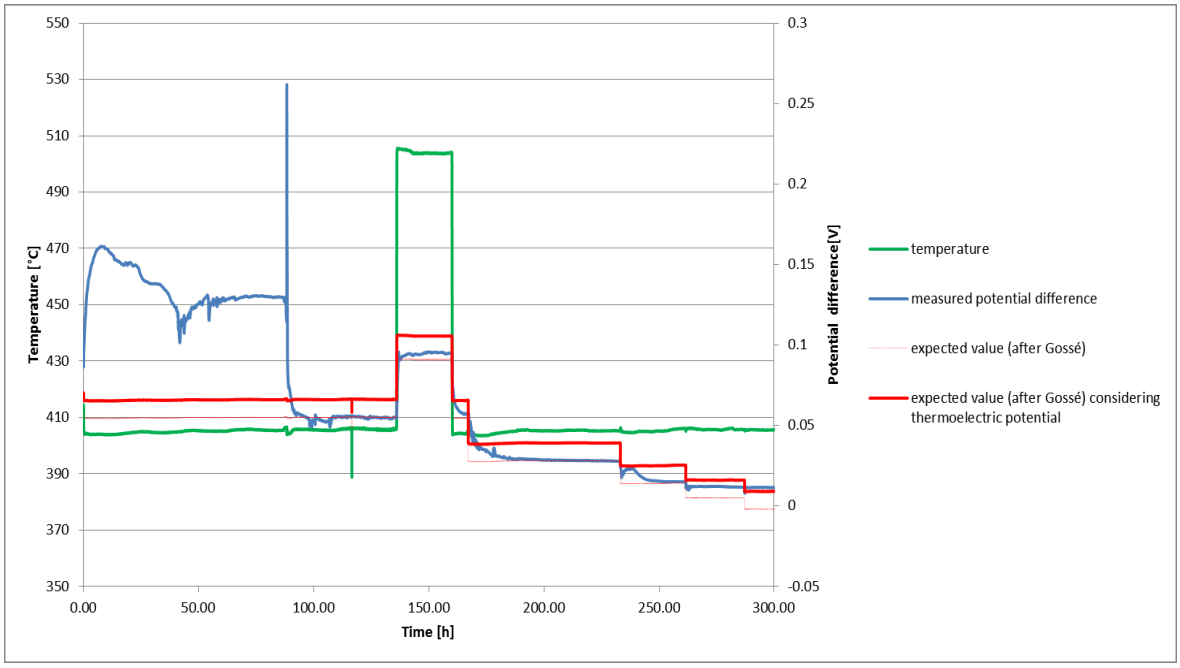

Figure 24: Measured and expected potentials from experiment 2

In this experiment, the nickel chloride has been added only at hour 88 (visible through the peak). This proves that without its use the measured potential is not stable and does not reflect the nickel concentration. After the addition, the measured potential is close to the expected one at both tested temperatures. After adding two more times a known amount of nickel (plateaus 4 & 5), the measured potential deviates slightly from the expected one. Whatever happened in the cell remains unexplained for the moment. (Exact data about the nickel masses added, its concentration and the temperature changes are given in annex A13/Experiment 2.)

The standard deviation between the measured values and the calculated and corrected ones within the 30 minutes before a change was made are:

plateau	1	2	3	4	5	6	7
σ [mV]	1.46	4.81	not considered	5.31	6.57	1.59	(4.61)

Table 3: Standard deviation; experiment 2

Between the plateaus 6 & 7 the solubility has been exceeded. Therefore, the theoretical value is not correct anymore. As visible in the close-up in figure 25, the potential stays nearly unchanged after the addition of nickel at hour 287.

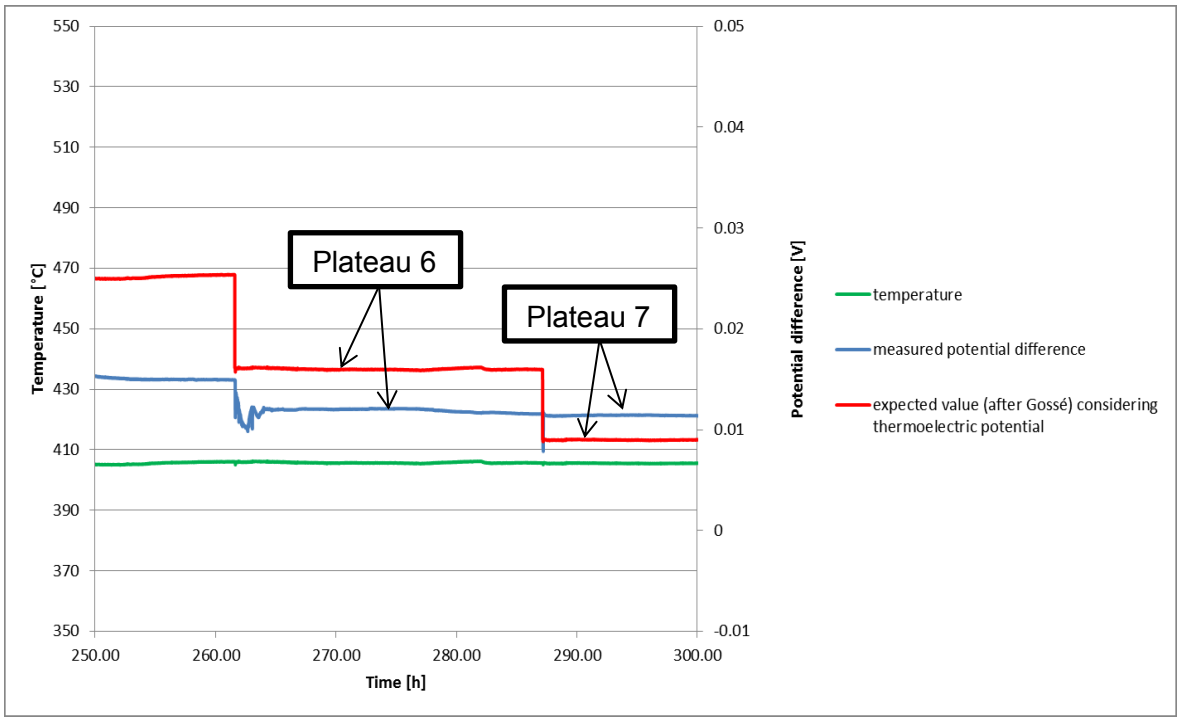

Figure 25: Close-up of figure 24

As there have been uncertainties about the solubility data used, the one extractable from the gained data shall be calculated. As described before:

$$E = \frac{-RT}{2F} * \ln\left(\frac{1}{a_{Ni,Bi}}\right) \tag{6.15}$$

With two measured potentials we have:

$$E_1 = \frac{-RT}{2F} * \ln(A * C_1) \quad \text{and} \quad E_2 = \frac{-RT}{2F} * \ln(A * C_2) \tag{6.16 \& 6.17}$$

with K being the activity coefficient and C the nickel concentration. Furthermore:

$$\Delta E = E_2 - E_1 = \frac{RT}{2F} * \ln\left(\frac{AC_1}{AC_2}\right) \quad \text{and} \quad \Delta C = C_2 - C_1 \tag{6.18 \& 6.19}$$

Combining (6.18) and (6.19) gives:

$$\Delta E = \frac{RT}{2F} * \ln\left(\frac{C_2 - \Delta C}{C_2}\right) \quad \text{or} \quad \Delta E = \frac{RT}{2F} * \ln\left(\frac{C_1}{\Delta C - C_1}\right) \tag{6.20 \& 6.21}$$

As ΔC and ΔE are known, C_1 and C_2 can be calculated by:

$$C_1 = \frac{\Delta C * e^{\left(\frac{2F\Delta E}{RT}\right)}}{\left(1 - e^{\left(\frac{2F\Delta E}{RT}\right)}\right)} \quad \text{or} \quad C_2 = \frac{\Delta C}{\left(1 - e^{\left(\frac{2F\Delta E}{RT}\right)}\right)} \tag{6.22 \& 6.23}$$

Then the activity coefficient can be calculated through:

$$A = \frac{E^{\frac{-2FE}{RT}}}{C} \tag{6.24}$$

and finally, the solubility:

$$S = \frac{C_{solub.}}{A} = \frac{1}{A} \tag{6.25}$$

This has been done for two different phases of the experiment. The found and averaged activity coefficient and solubility are (for 404 °C):

$$A_{Ni,Bi} = 0.8230 \qquad \text{and} \qquad S_{Ni,Bi} = 1.2185$$

One can see that the solubility at this temperature differs quite a lot from the one of Gossé (1.67 wt.%).

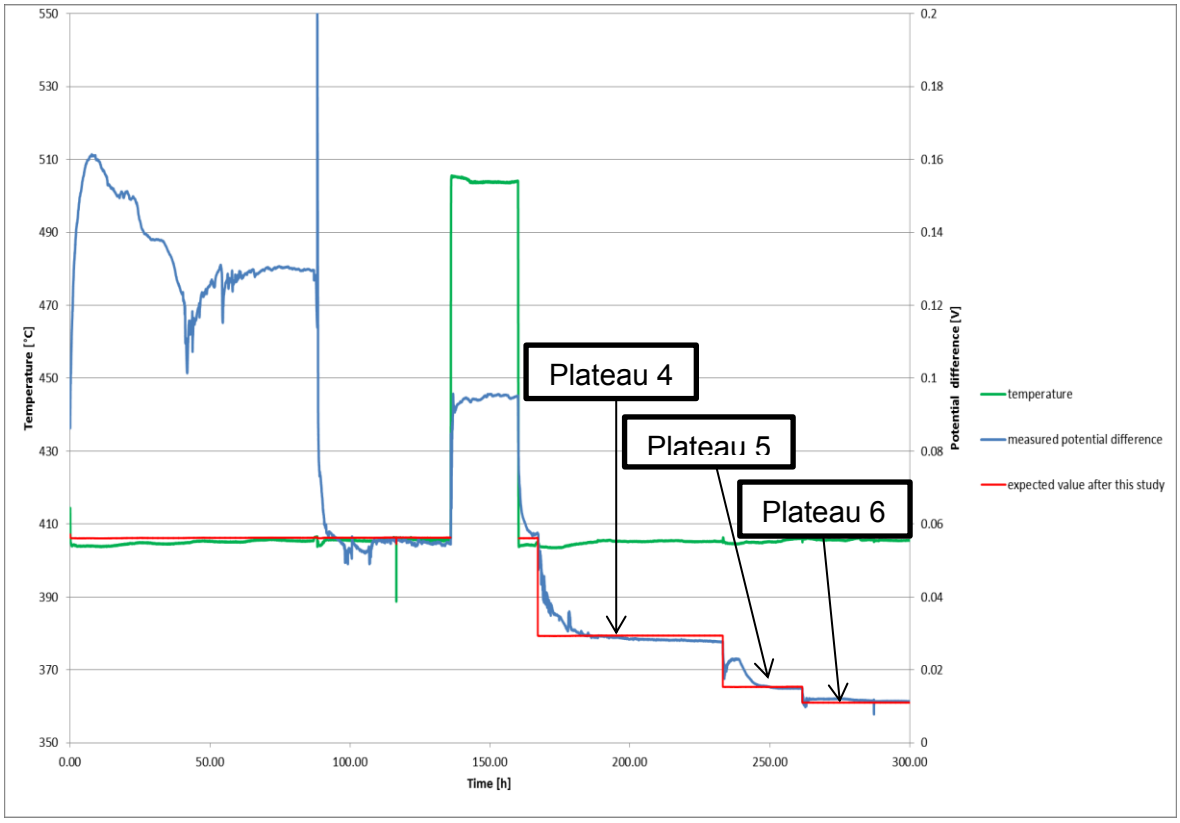

Figure 26: Measured and expected potentials with Gossé´s solubility and the one calculated in this work; experiment 2

The solubility from this study has been calculated using values from the plateaus 4 & 5 and 5 & 6 (see figure 26). As according to my values the solubility was reached between phase 4 and 5, the potential was set 0 so that only the thermoelectric potential remained measurable. In addition the unknown initial concentration was calculated to be 0.065 wt.%. The standard deviation between the values of this study and the measured ones are given in the table below.

plateau	1	2	3	4	5	6	7
σ [mV]	1.71	wrong temperature	not considered	1.48	0.38	0.53	0.37

Table 4: Standard deviation between this work´s predicted values and those from experiment 2

So, if the solubility defined in this study is used, one obtains much more accurate values than if one uses Gossé's solubility. Though this solubility is only known for 404 °C and has yet not been proven reproducible. Tests at other temperatures have to be done.

6.2.6 Conclusions of the Second Experiment

There are three main conclusions to gain from this second experiment. First, that the principle of the potentiometric concentration determination has been proven applicable a second time. Then, that the use of nickel chloride as electrolyte is compulsory. Third, that the thermoelectric potential of the two wires is of importance and that the calculated linear regression is working. But as the values gained during two different experiments (wires in LBE and wires in bismuth) are not exactly the same, this potential should be reassessed during another experiment in a gas atmosphere. (The difference could be explained by the fact, that the nickel wire was dissolving during the experiment.)

Once the exact thermoelectric potential is known and the measured potential stagnates at this value (after reaching the solubility limit), it could be postulated that the nickel activity remains equal to 1 whenever the solubility is reached. But as a slight decreasing of potential is notable in figure 25, the possible Bi_3Ni formation can yet not be excluded.

For the sake of completeness, it shall be recalled that the usage of pure bismuth as a coolant for MYRRAH is rejected because of its relatively high melting point (271.4 °C)

7 The "Nickel Pump"

The advantage of the electrochemical extraction of impurities compared to the other two options (the deep bed filtration and the cake filtration (OECD/NEA, 2015)) would be that no cold trap is needed to trigger the precipitation. That way the energy necessary for the cooling process is economized.

For the moment, the priority lies more on the development of a nickel sensor than the development of the "nickel pump". This seems logical, as a precise extraction of nickel from the LBE in MYRRHA is only making sense if its concentration in LBE can be monitored too. Therefore, the "nickel pump" will not be discussed in this work, especially as no experimentation has been done.

8 Conclusions and Outlook

Through this work the feasibility of an electrochemical metal impurity concentration monitoring has been confirmed. Nevertheless, some deviations remain between the theoretical values and the ones measured in the laboratory.

This can partially be explained by the variance of the data findable in literature but also by the deficiency in the chemicals´ purities. Another factor might be the loss of small amounts of chemicals during handling. In fact, inspecting the used materials (see figure 40 (annex A-14)) after the deconstruction of the set-up brought up doubts about the indicated purity of the salt. A description of similar problems and their solutions – namely the removal of organic contaminations from the salt by thermal decomposition and the relocation of the experimentation in vacuum – is described in Del Duca (1969).

Furthermore, a mass spectrometry of the LBE done by colleagues at SCK•CEN indicated an organic contamination of the provided LBE. To compound someone's own LBE with high purity chemicals completed by a purification process could put these things right.

In addition, evaporation deposits have been formed. To define their nature and influence on the measurements, and a way to avoid them should be part of future research.

Moreover, the use of chlorides as electrolyte became absurd in the nickel case, as lead shows a greater affinity to form a chloride compound than nickel. However, it seems to be a promising technology for iron and manganese detection and extraction (using $FeCl_2$ and $MnCl_2$ as electrolytes), especially as these two are corrosion products accruing in MYRRHA too.

9 Bibliography

Abderrahim, H. A.: Multi-purpose hYbrid Research Reactor for High-tech Applications a multipurpose fast spectrum research reactor, in Special Issue on Developments in Nuclear and Renewable Energy, in International Journal of Energy Research, by John Wiley & Sons Ltd., 2011.

Abderrahim, H. A.: Contribution of the European Comission to a European Strategy for HLW Management Through Partitioning & Transmutation – Presentation of MYRRHA and Its Role in the European P&T Strategy, in Nuclear Back-end and Transmutation Technology for Waste Disoposal, from Nakajima K., Springer, 2015, pp. 59-71

Barin I.: Thermochemical Data of Pure Substances, third edition, VCH Verlagsgesellschaft mbH, Weinheim, Germany, 1995,

De Duca, S.: Electrochemical Behavior of the Aluminum Electrode in Molten Salt Electrolytes, NASA Technical Note TN D-5503, Lewis Research Center, Cleveland, Ohio, 1969, http://ntrs.nasa.gov/archive/nasa/casi.ntrs.nasa.gov/19690030855.pdf, (27.07.2017), pp. 3-4

EIA: Glossary – nuclear, from Independent Statistics and Analysis – United States Energy Information Administration, 2016, https://www.eia.gov/tools/glossary/index.cfm?id=R#reason_assur_res, (27.07.2017)

Gokcen, N.A.: The Bi-Pb (Bismuth-lead) System, in Journal of Phase Equilibria, 13, 21, 1992

Gossé, S.: Thermodynamic assessment of solubility and activity of iron, chromium, and nickel in lead bismuth eutectic, in Journal of Nuclear Materials, Volume 449, Elsevier B.V., 2014, http://ac.els-cdn.com/S0022311514001202/1-s2.0-S0022311514001202-main.pdf?_tid=567300a4-2d54-11e6-a359-00000aacb360&acdnat=1465375273_dde66602d4eb1c63233bd9a21e9ff480, (27.07.2017), pp. 122-131)

IAEA: Classification of Radioactive Waste – General Safety Guide, in IAEA Safety Standard Series No. GSG-1, Vienna, STI/PUB/1419, International Atomic Energy Agency, 2009, http://www-pub.iaea.org/MTCD/publications/PDF/Pub1419_web.pdf, (27.07.2017), pp. 4-16

IEA: World Energy Outlook 2014, International Energy Agency, 2014, https://www.iea.org/topics/nuclear/, (27.07.2017)

IEA: Energy and Climate Change – World Energy Outlook Special Report, International Energy Agency, 2015, https://www.iea.org/publications/freepublications/publication/WEO2015SpecialReportonEnergyandClimateChange.pdf, (27.07.2017), p. 37

Kumar, M.R., Mohan, S. and Behera, C.K.: Measurement of Activity of Indium in Liquid BI-In-Sn Alloys by EMF Method, in Journal of Electronic Materials, Volume 45, Issue 8, from The Minerals, Metals and Materials Society, 2016, 4314-4323

Lecomte, M. & Bonin B.: Le traitement-recyclage du combustible usé : La séparation des actinides - Application à la gestion des déchets, CEA Saclay ; Groupe Moniteur, 2008, E-den, Une monographie de la Direction de l´énergie nucléaire, CEA, 9782281113761, Commissariat de l´énergie atomique et aux énergies alternatives, https://hal.archives-ouvertes.fr/cea-01153306/document, (27.07.2017), p. 153

Martinelli, L. et al.: Nickel solubility limit in liquid lead-bismuth eutectic, Journal of Nuclear Materials, Volume 400, Elsevier B.V., 2010, http://ac.els-cdn.com/S0022311510000930/1-s2.0-S0022311510000930-main.pdf?_tid=fa1f69ca-2d4c-11e6-8f40-00000aab0f02&acdnat=1465372111_131de9bc1238d217282120fb67a37308, (27.07.2017), pp. 232-239

Noggle, J. H.: Physical Chemistry, third edition, from HarperCollins Publishers Inc., 1996

OECD/IAEA and OECD/NEA: Uranium 2014: Resources, Production and Demand, in A Joint Report by the OECD Nuclear Energy Agency and the International Atomic Energy Agency, in NEA No. 7209, Organisation for Economic Co-operation and Development, 2014, https://www.oecd-nea.org/ndd/pubs/2014/7209-uranium-2014.pdf, (27.07.2017), pp. 107-132

OECD/IEA and OECD/NEA: Technology Roadmap – Nuclear Energy, in Energy Technology Perspectives, 2015 edition, https://www.iea.org/media/freepublications/technologyroadmaps/TechnologyRoadmapNuclearEnergy.pdf, (27.07.2017), p. 22

OECD/NEA: Plutonium Fuel – An Assessment – Report by an expert Group, in NEA No. 6519, Organisation for Economic Cooperation and Development, Paris 1989, https://www.oecd-nea.org/ndd/reports/1989/nea6519-plutonium-fuel.pdf, (27.07.2017), p. 22

OECD/NEA: Handbook on Lead-bismuth Alloy and Lead Properties, Materials Compatibility, Thermal-hydraulics and Technologies, in Nuclear Science, in NEA No. 7268, Organisation for Economic Co-operation and Development, 2015 edition, https://www.oecd-nea.org/science/pubs/2015/7268-lead-bismuth-2015.pdf, (27.07.2017), pp. 27-211

Okamoto H.J.: Phase Equilib. Diffus., Bi-Ni (Bismuth-Nickel), in Journal of Phase Equilibria and Diffusion Volume 33, Issue 6, Section III: Supplemental Literature Review, ASM International, 2012, out of Wang 2011, http://paperity.org/p/8528860/bi-ni-bismuth-nickel, (27.07.2017), p. 492

SCK•CEN[1]: The proton accelerator, in Proton accelerator, in Accelerator Driven System, in MYRRHA, in MYRRHA Home, Belgian Nuclear Research Centre (SCK•CEN), Mol, http://myrrha.sckcen.be/en/MYRRHA/ADS/Proton_accelerator, (30.05.2016)

SCK•CEN[2]: The Spallation Target, in Spallation target, in Accelerator Driven System, in MYRRHA, in MYRRHA Home, Belgian Nuclear Research Centre (SCK•CEN), Mol, http://myrrha.sckcen.be/en/MYRRHA/ADS/Spallation_target, (30.05.2016)

SCK•CEN[3]: MYRRHA: an Accelerator Driven System (ADS), in Accelerator Driven System, in MYRRHA, in MYRRHA home, Belgian Nuclear Research Centre (SCK•CEN), Mol, http://myrrha.sckcen.be/en/MYRRHA/ADS, (31.05.2016)

SCK•CEN[4]: The subcritical core, in Sub-critical core, in Accelerator Driven System, in MYRRHA, in MYRRHA home, Belgian Nuclear Research Centre (SCK•CEN), Mol, http://myrrha.sckcen.be/en/MYRRHA/ADS/Sub-critical_core, (31.05.2016)

SCK•CEN[5]: The MYRRHA fuel element and fuel assembly pre-design, in Fuel elements & assemblies, in Engineering, in MYRRHA home, Belgian Nuclear Research Centre (SCK•CEN), Mol, http://myrrha.sckcen.be/en/Engineering/Fuel, (31.05.2016)

Sobolev, V.: Database of Thermophysical Properties of Liquid Metal Coolants for GEN-IV, SCK•CEN report BLG-1069, Mol, Belgium, December 2010, (rev. December 2011)

UNSCEAR: Sources and Effects of Ionizing Radiation, United Nations Scientific Committee on the Effects of Atomic Radiation, UNSCEAR 2008 – Report to the General Assembly with Scientific Annexes, Volume I, United Nations Publication Sales No. E.10.XI.3, United Nations New York 2010, http://www.unscear.org/docs/reports/2008/09-86753_Report_2008_GA_Report_corr2.pdf, (27.07.2017), p. 4

Wang J., et al.: Thermodynamic optimization of Bi-Ni binary system, Transaction of Nonferrous Metals Society of China 21, Elsevier B.V., 2011, http://www.ysxbcn.com/down/upfile/soft/20110126/21-p0139-20595.pdf, (27.07.2017), pp. 139-145

Weeks, J.R.: Liquid Metal Compatibility of Structural Materials with Liquid Lead-bismuth and Mercury, 1997 TMS Annual Meeting, Orlando, FL, 9-13 February, M.S. Wechsler et al. (eds.), The Minerals, Metals & Materials Society (TMS), 1998

WNA[1]: Radioactive Waste Management, World Nuclear Association, Update October 2015, http://www.world-nuclear.org/information-library/nuclear-fuel-cycle/nuclear-wastes/radioactive-waste-management.aspx, (19.05.2016)

WNA[2]: Physics of Uranium and Nuclear Energy, World Nuclear Agency, Update September 2014, http://www.world-nuclear.org/information-library/nuclear-fuel-cycle/introduction/physics-of-nuclear-energy.aspx, (20.05.2016)

WNA[3]: Nuclear Radiation and Health Effects, World Nuclear Association, Update May 2016, http://www.world-nuclear.org/information-library/safety-and-security/radiation-and-health/nuclear-radiation-and-health-effects.aspx (20.05.2016), link under “Further Information – Notes – a.”, http://www.world-nuclear.org/uploadedImages/org/info/radioactive_decay_series.png, (20.05.2016)

10 Bibliography of Formulas

(3.1): OECD/NEA: Handbook on Lead-bismuth Alloy and Lead Properties, Materials Compatibility, Thermal-hydraulics and Technologies, in Nuclear Science, in NEA No. 7268, Organisation for Economic Co-operation and Development, 2015 edition, https://www.oecd-nea.org/science/pubs/2015/7268-lead-bismuth-2015.pdf, (27.07.2017), p. 43

(3.2): OECD/NEA: Handbook on Lead-bismuth Alloy and Lead Properties, Materials Compatibility, Thermal-hydraulics and Technologies, in Nuclear Science, in NEA No. 7268, Organisation for Economic Co-operation and Development, 2015 edition, https://www.oecd-nea.org/science/pubs/2015/7268-lead-bismuth-2015.pdf, (27.07.2017), p. 46

(3.3): OECD/NEA: Handbook on Lead-bismuth Alloy and Lead Properties, Materials Compatibility, Thermal-hydraulics and Technologies, in Nuclear Science, in NEA No. 7268, Organisation for Economic Co-operation and Development, 2015 edition, https://www.oecd-nea.org/science/pubs/2015/7268-lead-bismuth-2015.pdf, (27.07.2017), p. 77

(3.4): OECD/NEA: Handbook on Lead-bismuth Alloy and Lead Properties, Materials Compatibility, Thermal-hydraulics and Technologies, in Nuclear Science, in NEA No. 7268, Organisation for Economic Co-operation and Development, 2015 edition, https://www.oecd-nea.org/science/pubs/2015/7268-lead-bismuth-2015.pdf, (27.07.2017), p. 77

(3.5): OECD/NEA: Handbook on Lead-bismuth Alloy and Lead Properties, Materials Compatibility, Thermal-hydraulics and Technologies, in Nuclear Science, in NEA No. 7268, Organisation for Economic Co-operation and Development, 2015 edition, https://www.oecd-nea.org/science/pubs/2015/7268-lead-bismuth-2015.pdf, (27.07.2017), p. 118

(3.6): Sobolev, V.: Database of Thermophysical Properties of Liquid Metal Coolants for GEN-IV, SCK•CEN report BLG-1069, Mol, Belgium, December 2010 (rev. December 2011), in OECD/NEA: Handbook on Lead-bismuth Alloy and Lead Properties, Materials Compatibility, Thermal-hydraulics and Technologies, in Nuclear Science, in NEA No. 7268, Organisation for Economic Co-operation and Development, 2015 edition, https://www.oecd-nea.org/science/pubs/2015/7268-lead-bismuth-2015.pdf, (27.07.2017), p. 126

(3.7): OECD/NEA: Handbook on Lead-bismuth Alloy and Lead Properties, Materials Compatibility, Thermal-hydraulics and Technologies, in Nuclear Science, in NEA No. 7268, Organisation for Economic Co-operation and Development, 2015 edition, https://www.oecd-nea.org/science/pubs/2015/7268-lead-bismuth-2015.pdf, (27.07.2017), p. 128

(3.8): OECD/NEA: Handbook on Lead-bismuth Alloy and Lead Properties, Materials Compatibility, Thermal-hydraulics and Technologies, in Nuclear Science, in NEA No. 7268, Organisation for Economic Co-operation and Development, 2015 edition, https://www.oecd-nea.org/science/pubs/2015/7268-lead-bismuth-2015.pdf, (27.07.2017), p. 149

(4.1): Noggle, J. H.: Physical Chemistry, third edition, from HarperCollins Publishers Inc., 1996, p. 422
(4.2): Noggle, J. H.: Physical Chemistry, third edition, from HarperCollins Publishers Inc., 1996, pp. 348-352
(4.3): Noggle, J. H.: Physical Chemistry, third edition, from HarperCollins Publishers Inc., 1996, p. 422
(4.5): Ganesan, R. et al.: Diffusivity, activity and solubility of oxygen in liquid lead and lea-bismuth eutectic alloy by electrochemical methods, Journal of Nuclear Materials, Volume 349, Elsevier B.V., 2005, http://ac.els-cdn.com/S0022311505005003/1-s2.0-S0022311505005003-main.pdf?_tid=4eb15734-2d5f-11e6-ade4-00000aacb361&acdnat=1465379984_f26165cafd70c1b599dbfeb212d287cd, (27.07.2017), pp. 133-149
(4.10): Ganesan, R. et al.: Determination of standard molar Gibbs free energy of formation of Bi2O3 over a wide temperature range by EMF method, The Journal of Chemical Thermodynamics, Volume 35, Elsevier B.V., 2003, pp. 1703-1716
(4.12): Lim, J.: measured by Lim and given through internal communication
(4.14): Martinelli, L. et al.: Nickel solubility limit in liquid lead–bismuth eutectic, in Journal of Nuclear Materials, Volume 400, Elsevier B.V., 2010, pp. 232-239
(4.15): Martinelli, L. et al.: Nickel solubility limit in liquid lead–bismuth eutectic, in Journal of Nuclear Materials, Volume 400, Elsevier B.V., 2010, pp. 232-239
(6.1): OECD/NEA: Handbook on Lead-bismuth Alloy and Lead Properties, Materials Compatibility, Thermal-hydraulics and Technologies, in Nuclear Science, in NEA No. 7268, Organisation for Economic Co-operation and Development, 2015 edition, out of: Gossé, 2014 https://www.oecd-nea.org/science/pubs/2015/7268-lead-bismuth-2015.pdf, (27.07.2017), p. 151
(6.2): OECD/NEA: Handbook on Lead-bismuth Alloy and Lead Properties, Materials Compatibility, Thermal-hydraulics and Technologies, in Nuclear Science, in NEA No. 7268, Organisation for Economic Co-operation and Development, 2015 edition, out of: Gossé, 2014 https://www.oecd-nea.org/science/pubs/2015/7268-lead-bismuth-2015.pdf, (27.07.2017), p. 151
(6.3): OECD/NEA: Handbook on Lead-bismuth Alloy and Lead Properties, Materials Compatibility, Thermal-hydraulics and Technologies, in Nuclear Science, in NEA No. 7268, Organisation for Economic Co-operation and Development, 2015 edition, out of: Gossé, 2014 https://www.oecd-nea.org/science/pubs/2015/7268-lead-bismuth-2015.pdf, (27.07.2017), p. 151
(6.4): OECD/NEA: Handbook on Lead-bismuth Alloy and Lead Properties, Materials Compatibility, Thermal-hydraulics and Technologies, in Nuclear Science, in NEA No. 7268, Organisation for Economic Co-operation and Development, 2015 edition, out of: Weeks, 1998 https://www.oecd-nea.org/science/pubs/2015/7268-lead-bismuth-2015.pdf, (27.07.2017), p. 151

11 List of Figures

12 List of Tables

13 List of Abbreviations

A	ampere – (Amper)
ADS	accelerator driven system – (beschleunigerbetriebenes System)
Bi	bismuth – (Bismut)
Bq	Becquerel
C	concentration – (Konzentration)
Cu	copper – (Kupfer)
COP 21	21st Conferences of Parties
E	electric potential (elektrisches Potenzial)
E^0	standard electrode potential (Standardpotential)
E^{th}	thermoelectric potential (Thermospannung)
EIA	U.S. Energy Information Administration
emf	electromotive force (elektromotorische Kraft)
eV	electronvolt – (Elektronenvolt)
F	Faraday constant – (Faraday-Konstante)
FNR	fast neutron reactor (Schneller Brüter)
IAEA	International Atomic Energy Agency – (Internationale Atomenergiebehörde)
IEA	International Energy Agency – (Internationale Energiebehörde)
INDC	Intended Nationally Determined Contribution
INES	International Nuclear and Radiological Event Scale – (Internationale Bewertungsskala für nukleare Ereignisse)
K	Kelvin
LBE	lead-bismuth eutectic – (Blei-Bismut-Eutektikum)
m	meter – (Meter)
M_W	Moment magnitude scale – (Momenten-Magnituden-Skala)
MOX	mixed oxide (fuel) – (Mischoxid(-Brennelemente))
MYRRHA	Multi-purpose hYbrid Research Reactor for High-tech Applications
NEA	Nuclear Energy Agency – (Kernenergieagentur)
O	oxygen – (Sauerstoff)
OECD	Organisation for Economic Co-operation and Development – (Organisation für wirtschaftliche Zusammenarbeit und Entwicklung)
Pb	lead – (Blei)
ppm	parts per million
Pu	plutonium – (Plutonium)
R	universal gas constant (universelle Gaskonstante)
R^2	coefficient of determination – (Determinationskoeffizient)
RAR	reasonably assured resources
RF	radiofrequency – (Hochfrequenz)
S	solubility – (Löslichkeit)
Sv	Sievert
t	metric ton (metrische Tonnen)
T	temperature – (Temperatur)
UNSCEAR	United Nations Scientific Committee on the Effects of Atomic Radiation – (Wissenschaftliches Komitee der Vereinten Nationen zur Untersuchung der Auswirkungen atomarer Strahlung)
U	uranium – (Uran)
USD	United States (of America) Dollars – (US-Dollar)
W_e	watt (electrical) – (Watt, elektrisch)
WNA	World Nuclear Association – (Welt-Nuklear-Verband)
A	activity coefficient (Aktivitätskoeffizient)
K	equilibrium constant – (Gleichgewichtskonstante)
K_H	Henry's law volatility constant (Henry-Flüchtigkeitskonstanten)

ΔT	temperature difference – (Temperaturdifferenz)
°C	degree Celsius – (Grad Celsius)
at.%	atomic percentage (Atomprozent (At.-%))
mole%	mole fraction (Stoffmengenanteil (Mol-%))
wt.%	weight per cent – (Gewichtsprozent (Gew.-%))
a	activity (Aktivität)
σ	standard deviation (Standardabweichung)

Annex Table of Contents

Annex

A-1

(Millisieverts[a])

Source or mode	*Annual average dose (worldwide)*	*Typical range of individual doses*	*Comments*
Natural sources of exposure			
Inhalation (radon gas)	1.26	0.2–10	The dose is much higher in some dwellings.
External terrestrial	0.48	0.3–1	The dose is higher in some locations.
Ingestion	0.29	0.2–1	
Cosmic radiation	0.39	0.3–1	The dose increases with altitude.
Total natural	**2.4**	**1–13**	**Sizeable population groups receive 10-20 millisieverts (mSv).**
Artificial sources of exposure			
Medical diagnosis (not therapy)	0.6	0-several tens	The averages for different levels of health care range from 0.03 to 2.0 mSv; averages for some countries are higher than that due to natural sources; individual doses depend on specific examinations.
Atmospheric nuclear testing	0.005	Some higher doses around test sites still occur.	The average has fallen from a peak of 0.11 mSv in 1963.
Occupational exposure	0.005	~0–20	The average dose to all workers is 0.7 mSv. Most of the average dose and most high exposures are due to natural radiation (specifically radon in mines).
Chernobyl accident	0.002[b]	In 1986, the average dose to more than 300,000 recovery workers was nearly 150 mSv; and more than 350,000 other individuals received doses greater than 10 mSv.	The average in the northern hemisphere has decreased from a maximum of 0.04 mSv in 1986. Thyroid doses were much higher.
Nuclear fuel cycle (public exposure)	0.000 2[b]	Doses are up to 0.02 mSv for critical groups at 1 km from some nuclear reactor sites.	
Total artificial	**0.6**	**From essentially zero to several tens**	**Individual doses depend primarily on medical treatment, occupational exposure and proximity to test or accident sites.**

[a] Unit of measurement of effective dose.

[b] Globally dispersed radionuclides. The value for the nuclear fuel cycle represents the maximum per caput annual dose to the public in the future, assuming the practice continues for 100 years, and derives mainly from globally dispersed, long-lived radionuclides released during reprocessing of nuclear fuel and nuclear power plant operation.

Table 5: Annex A-1; Annual average doses and ranges of individual doses of ionizing radiation by source (UNSCEAR, 208, p. 4)

A-2

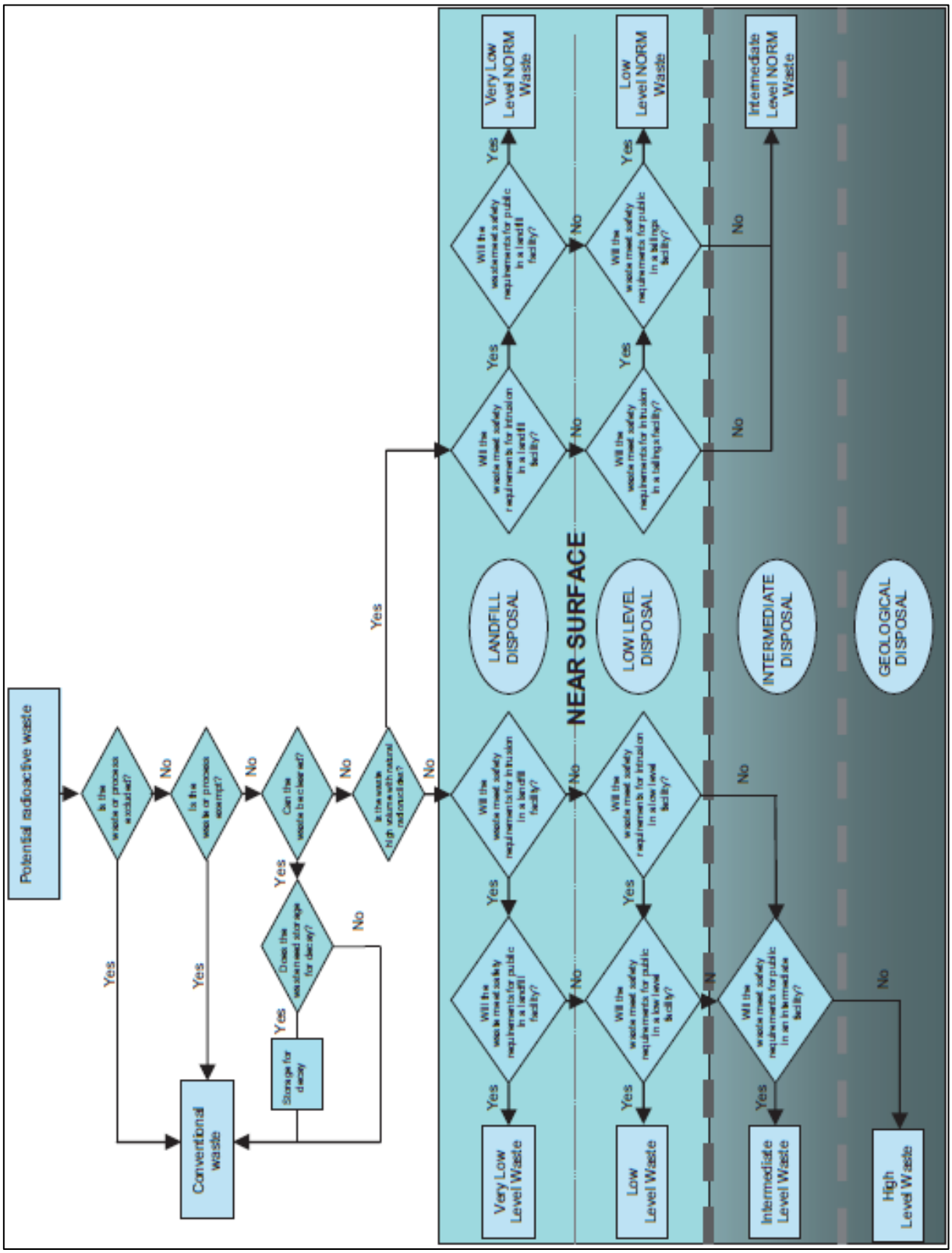

Figure 27: Annex A-2; An illustration of the use of the nuclear waste classification scheme (IAEA, 2009, p. 16)

A-3

Example in Fig. III–1	Half-life	Activity	Volume	Example
i	<100 d	100 MBq	Small	Y-90, Au-198 (brachytherapy)
ii	<100 d	5 TBq	Small	Ir-192 (brachytherapy)
iii	<15 a	<10 MBq	Small	Co-60, H-3 (tritium targets), Kr-85
iv	<15 a	<100 TBq	Small	Co-60 (irradiators)
v	<30 a	<1 MBq	Small	Cs-137 (brachytherapy, moisture density detectors)
vi	<30 a	<1 PBq	Small	Cs-137 (irradiators) Sr-90 (thickness gauges, radioisotope thermoelectric generators (RTGs))
vii	>30 a	<40 MBq	Small, but may be large numbers of sources (up to tens of thousands)	Pu, Am, Ra (static eliminators)
viii	>30 a	<10 GBq		Am-241, Ra-226 (gauges)

Table 6: Annex A-3; Disused sealed radioactive sources (IAEA, 2009, p. 41)

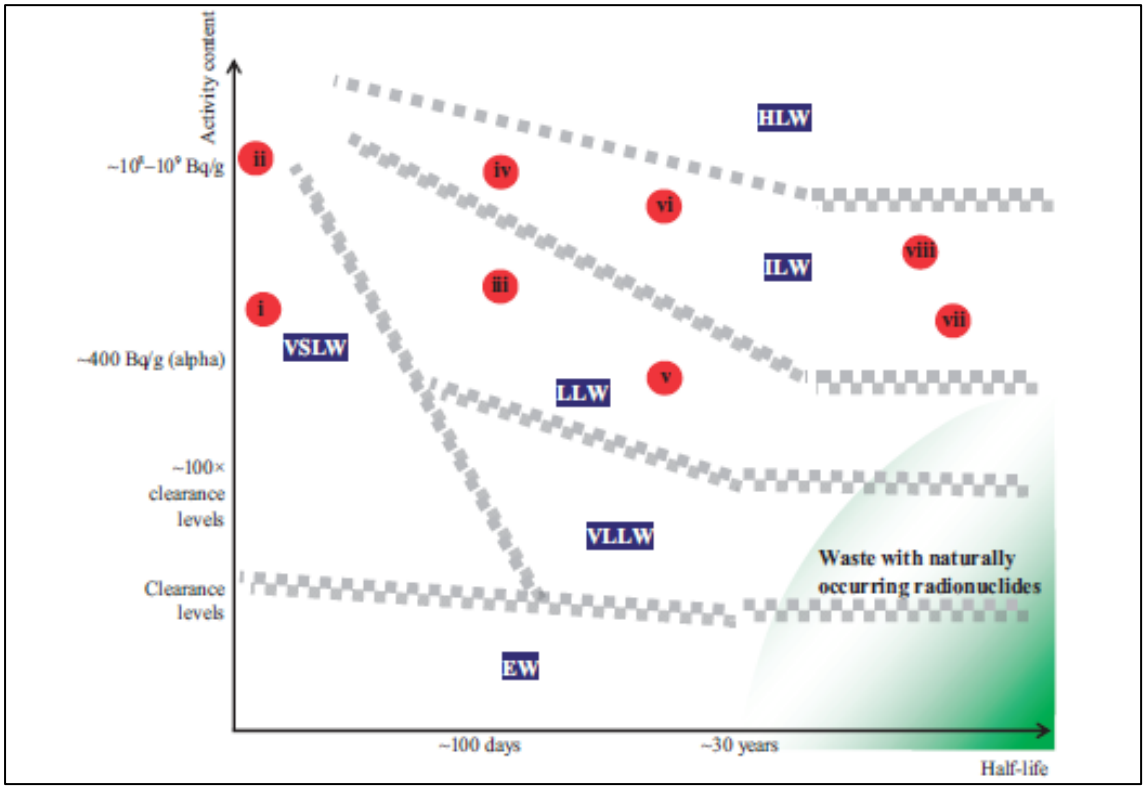

Figure 28: Annex A-3; Illustrative example of the application of the waste classification scheme (IAEA, 2009, p. 41)

NB: The numbers refer to examples of disused sealed sources set out in the table above.

A-4

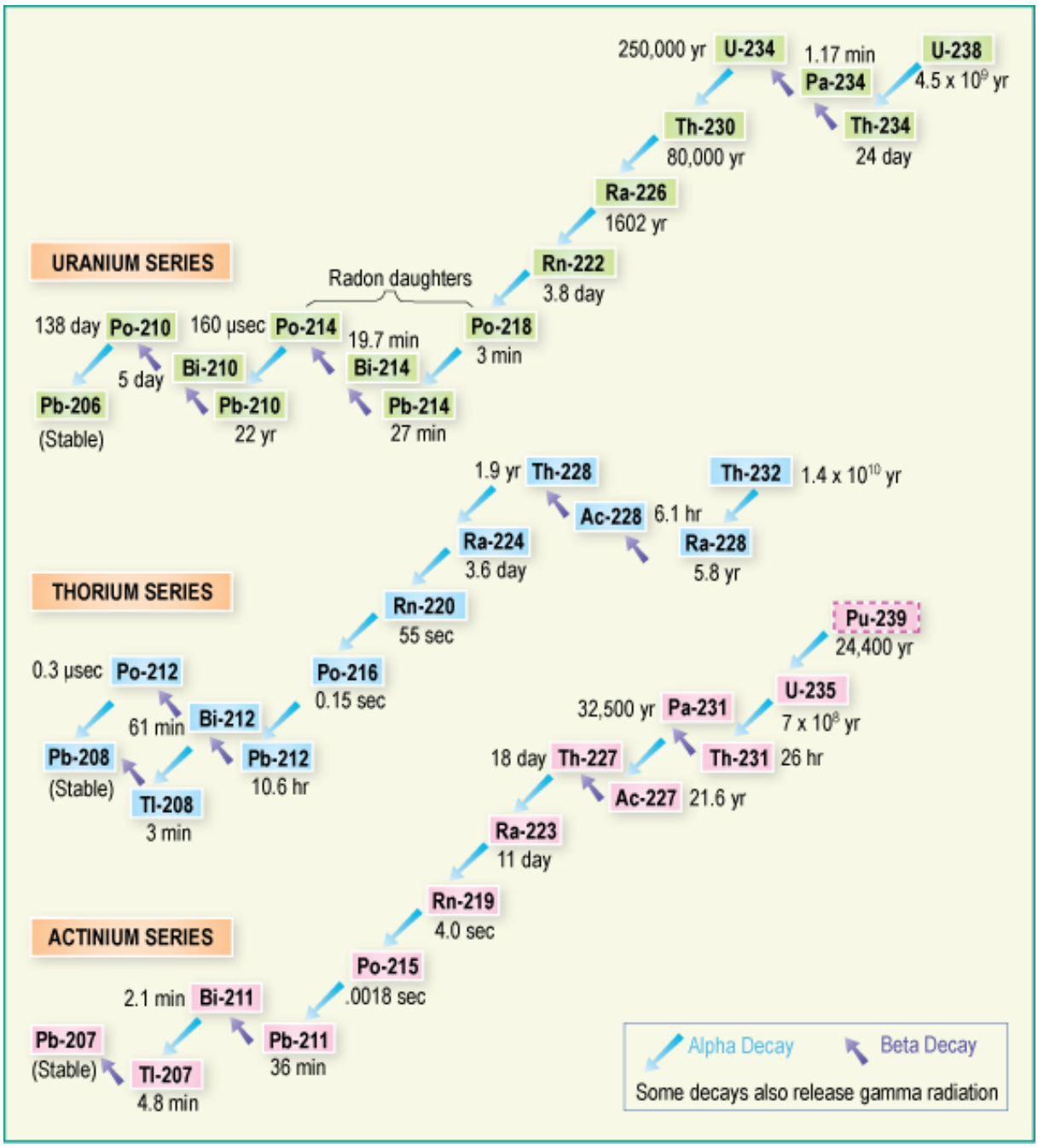

Figure 29: Annex 4-4; The three major radioactive decay series (WNA[3])

A-5

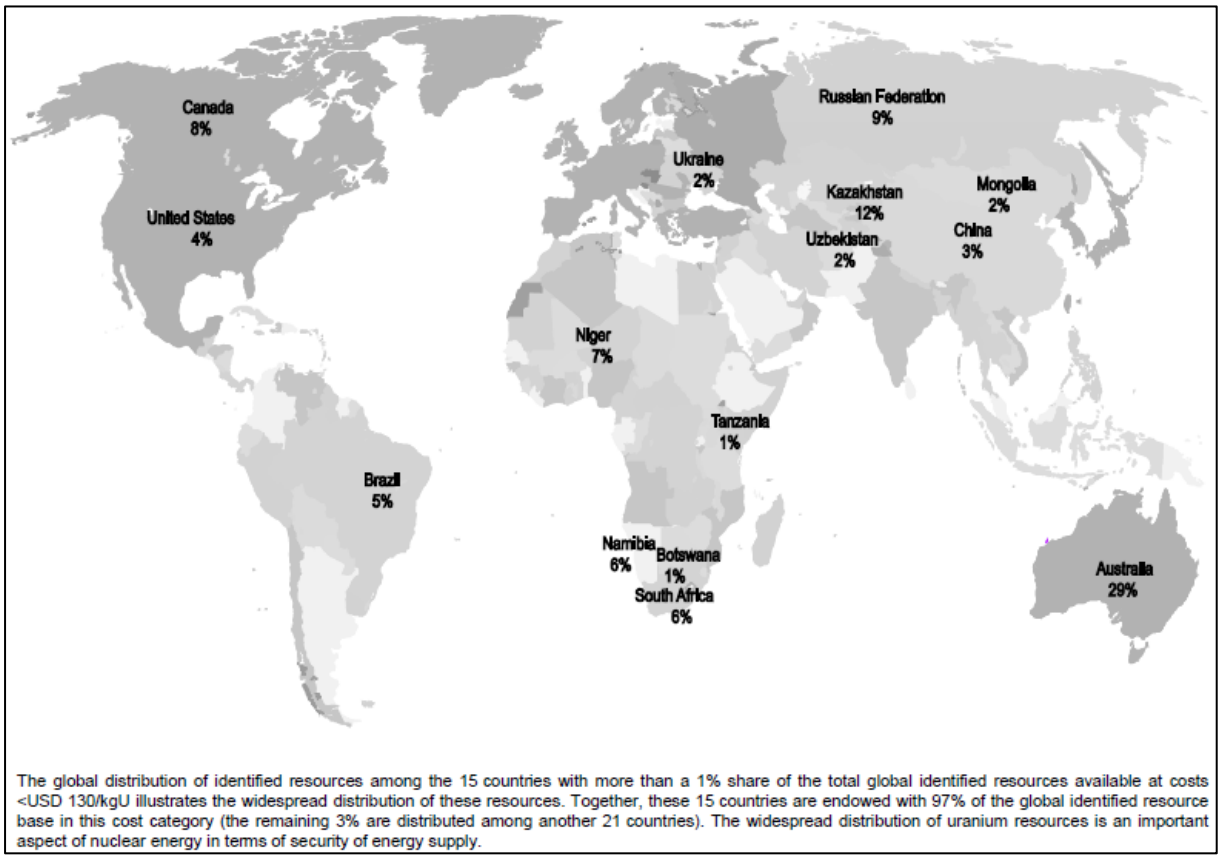

The global distribution of identified resources among the 15 countries with more than a 1% share of the total global identified resources available at costs <USD 130/kgU illustrates the widespread distribution of these resources. Together, these 15 countries are endowed with 97% of the global identified resource base in this cost category (the remaining 3% are distributed among another 21 countries). The widespread distribution of uranium resources is an important aspect of nuclear energy in terms of security of energy supply.

Figure 30: Annex A-5; Global distribution of identified resources (OECD/IAEA and OECD/NEA, 2014, p. 19)

A-6

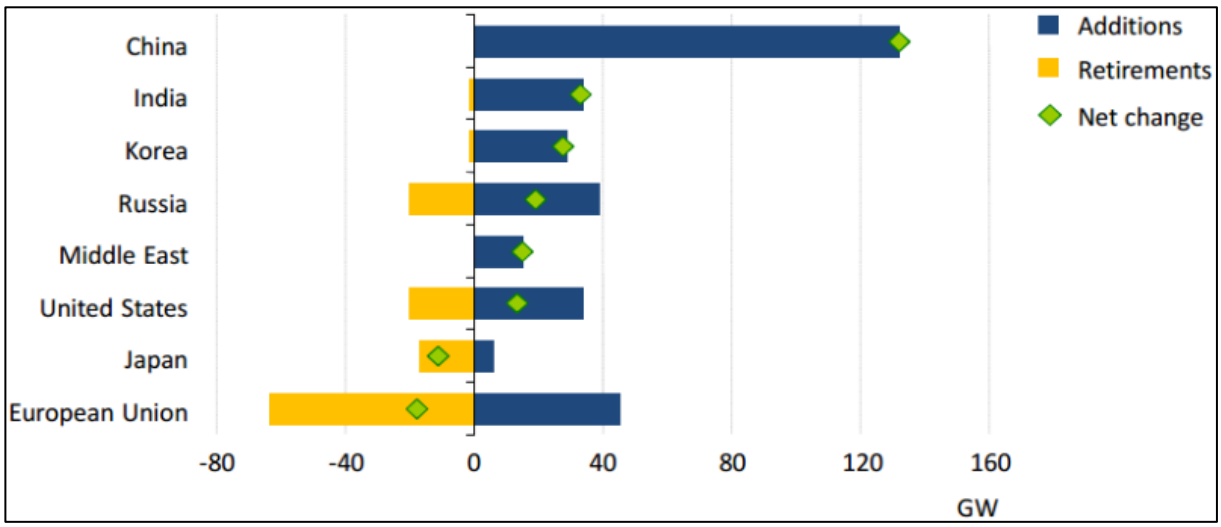

Figure 31: Annex A-6; Nuclear power capacity additions and retirements by key region in the New Policies Scenario, 2014-2020 (IEA, 2014, p. 388)

In this scenario, the capacity grows by 60 % to 624 GW in 2040.

A-7

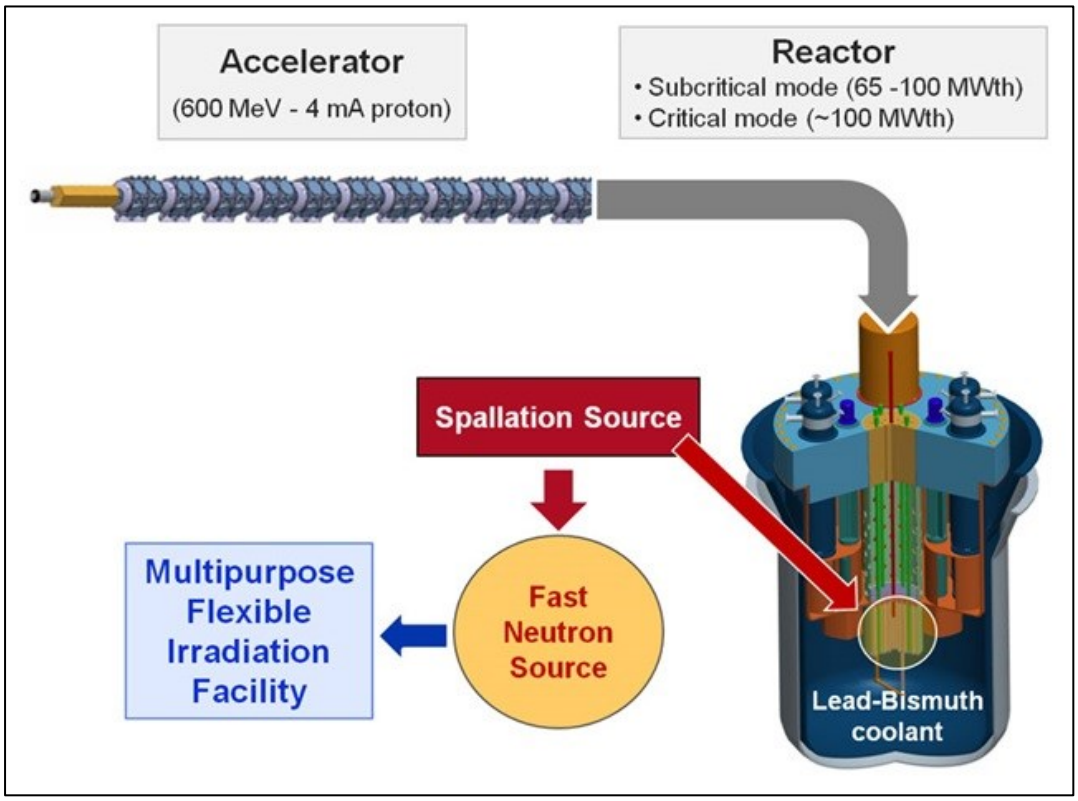

Figure 32: Annex A-7; ADS scheme (SCK•CEN[3])

A-8

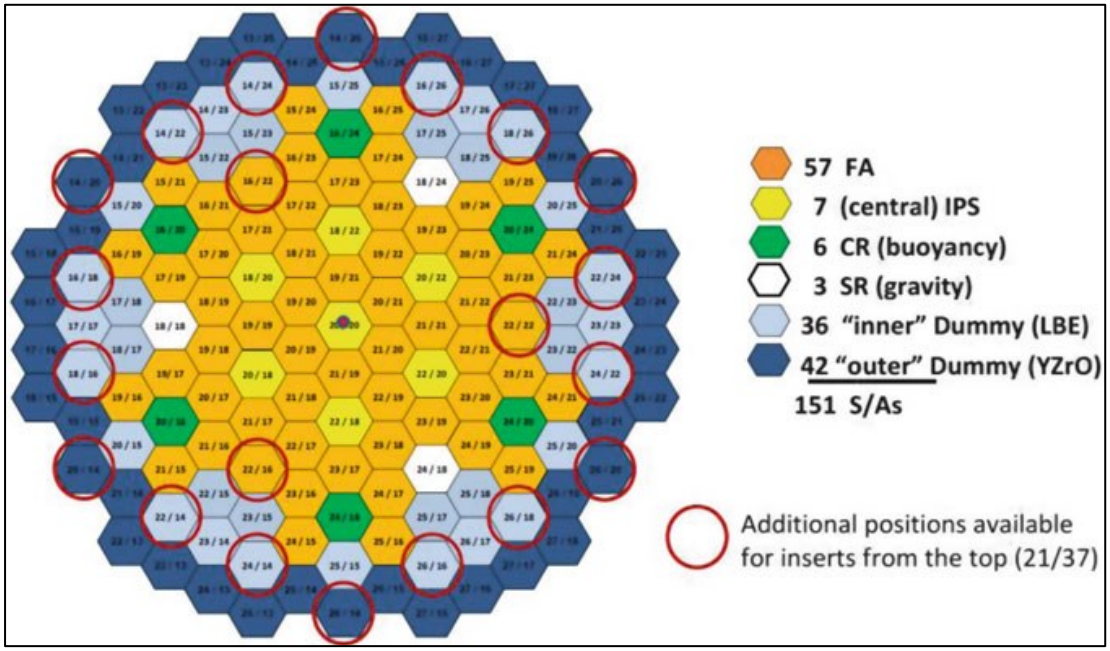

Figure 33: Annex A-8; Cut of the MYRRHA-FASTEF core showing the central target, the different types of fuel assemblies and the dummy components (Abderrahim, 2015, p. 66)

A-9

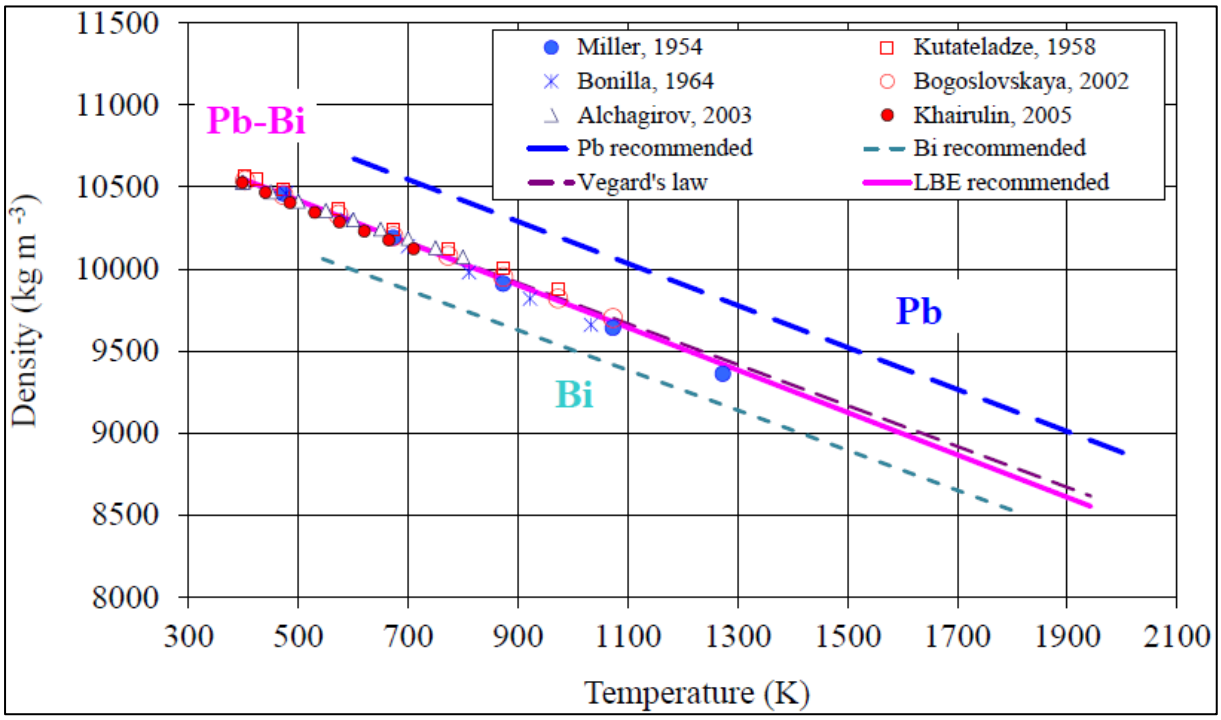

Figure 34: Annex A-9; Densities of lead, bismuth and LBE as a function of the temperature (OECD/NEA, 2015, p. 77, out of: Sobolev, 2011)

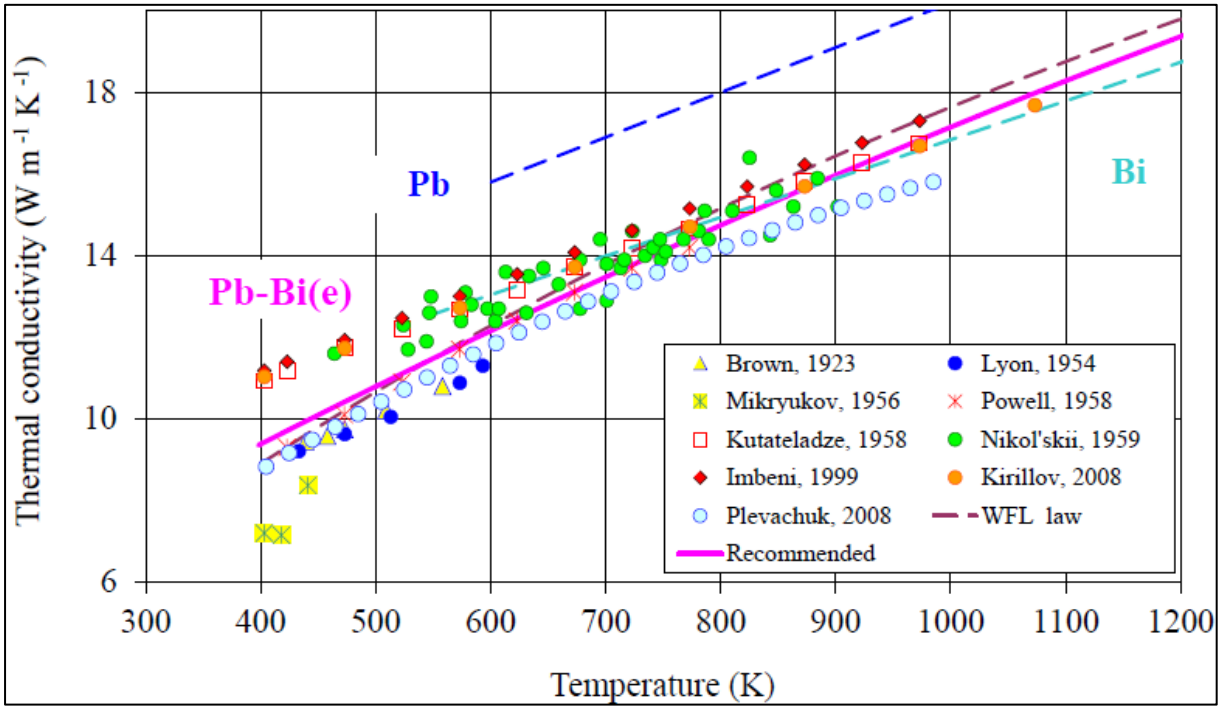

Figure 35: Annex A-9; Thermal conductivity of molten lead, bismuth and LBE as a function of temperature (OECD/NEA, 2015, p. 127, out of Sobolev, 2011)

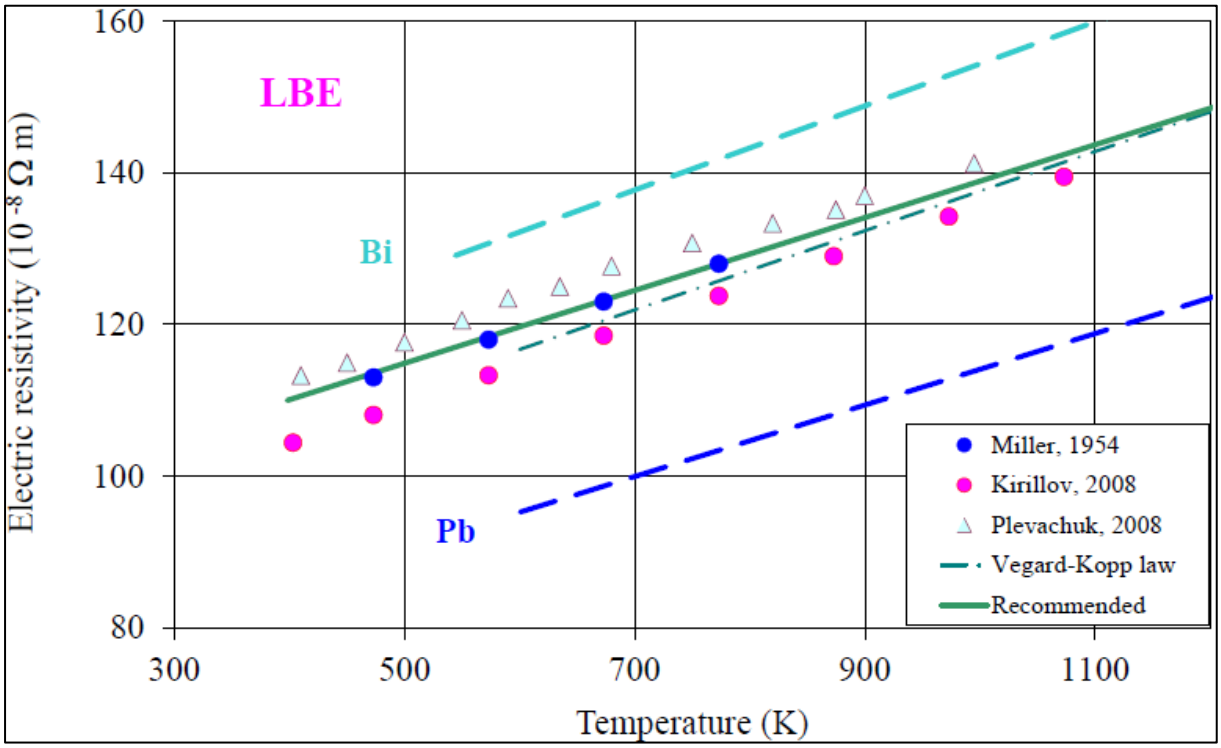

Figure 36: Annex A-9; Electric resistivity of molten lead, bismuth and LBE as a function of temperature at normal temperature (OECD/NEA, 2015, p. 117, out of: Sobolev, 2011)

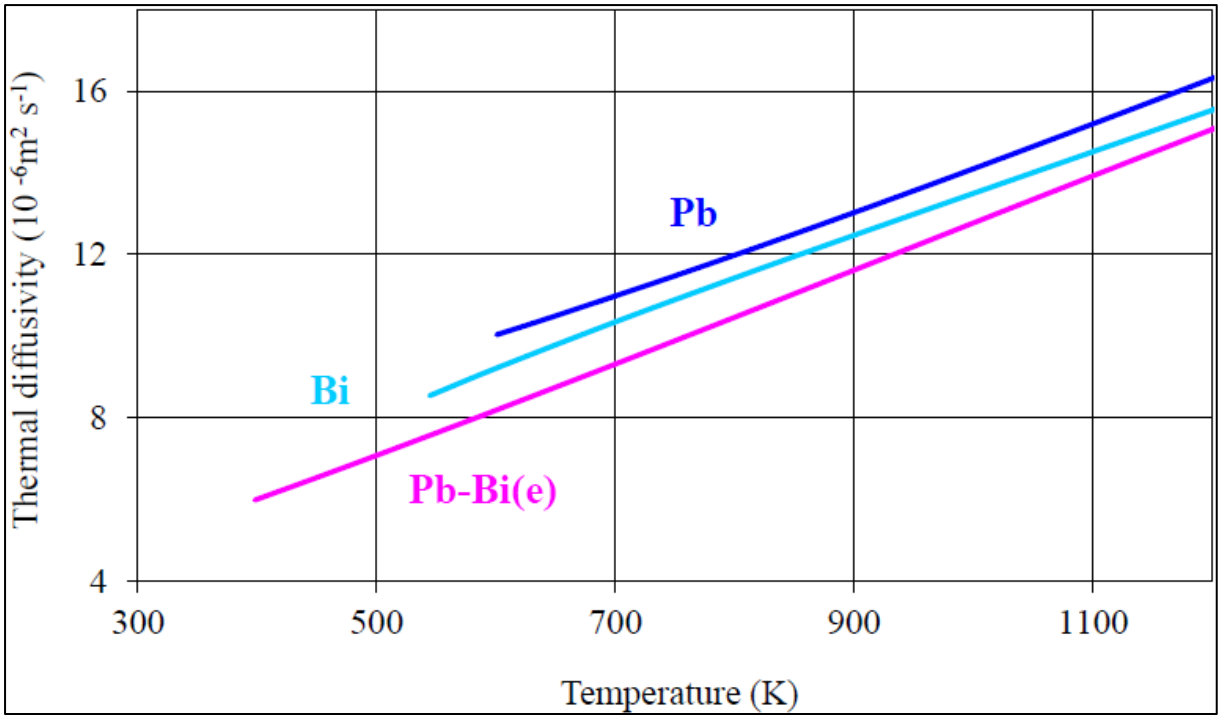

Figure 37: Annex A-9; Thermal diffusivity of molten lead, bismuth and LBE (OECD/NEA, 2015, p. 128, out of: Sobolev, 2011)

A-10

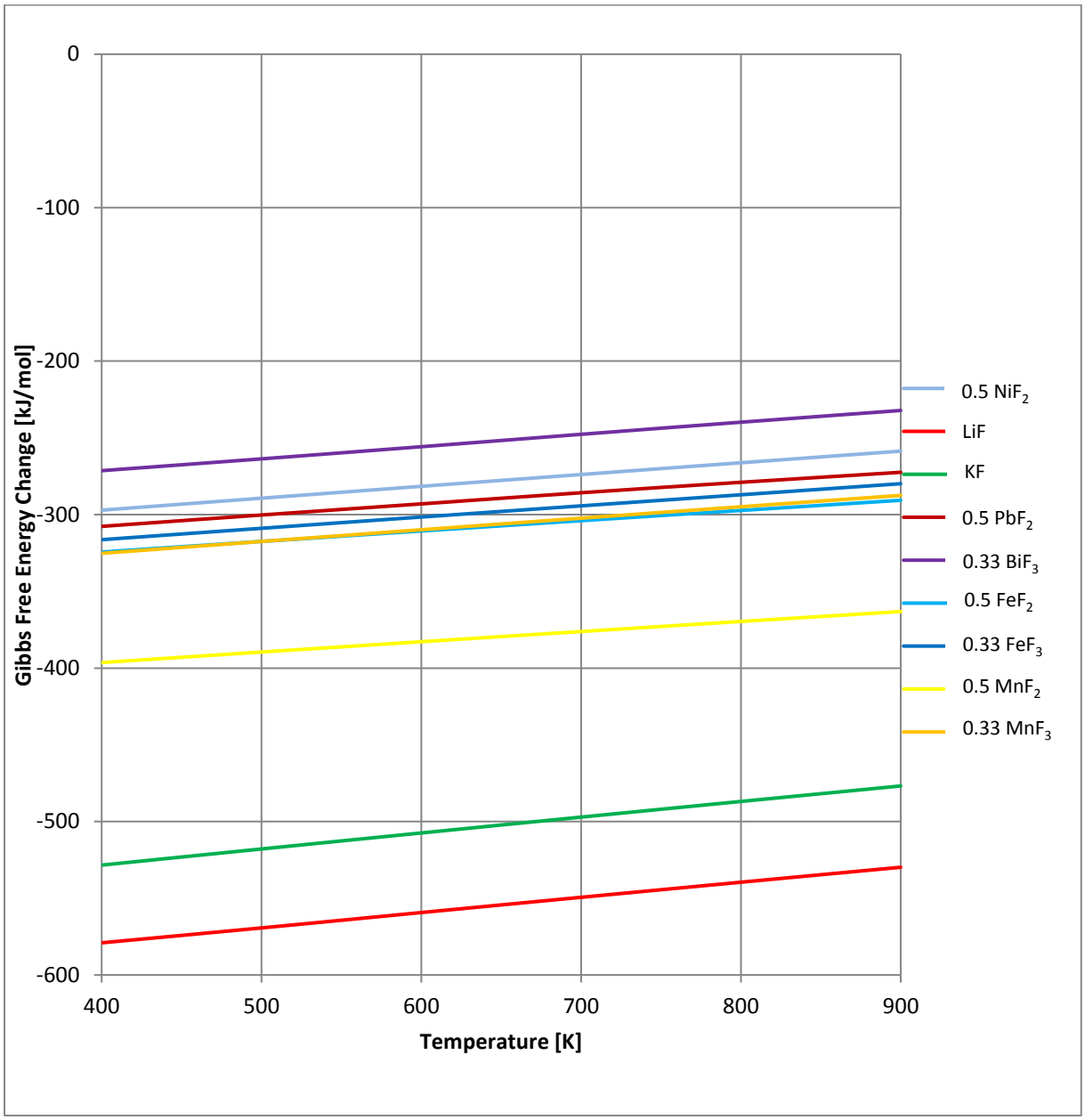

Figure 38: Annex A-10; Ellingham diagram of fluorides

A-11

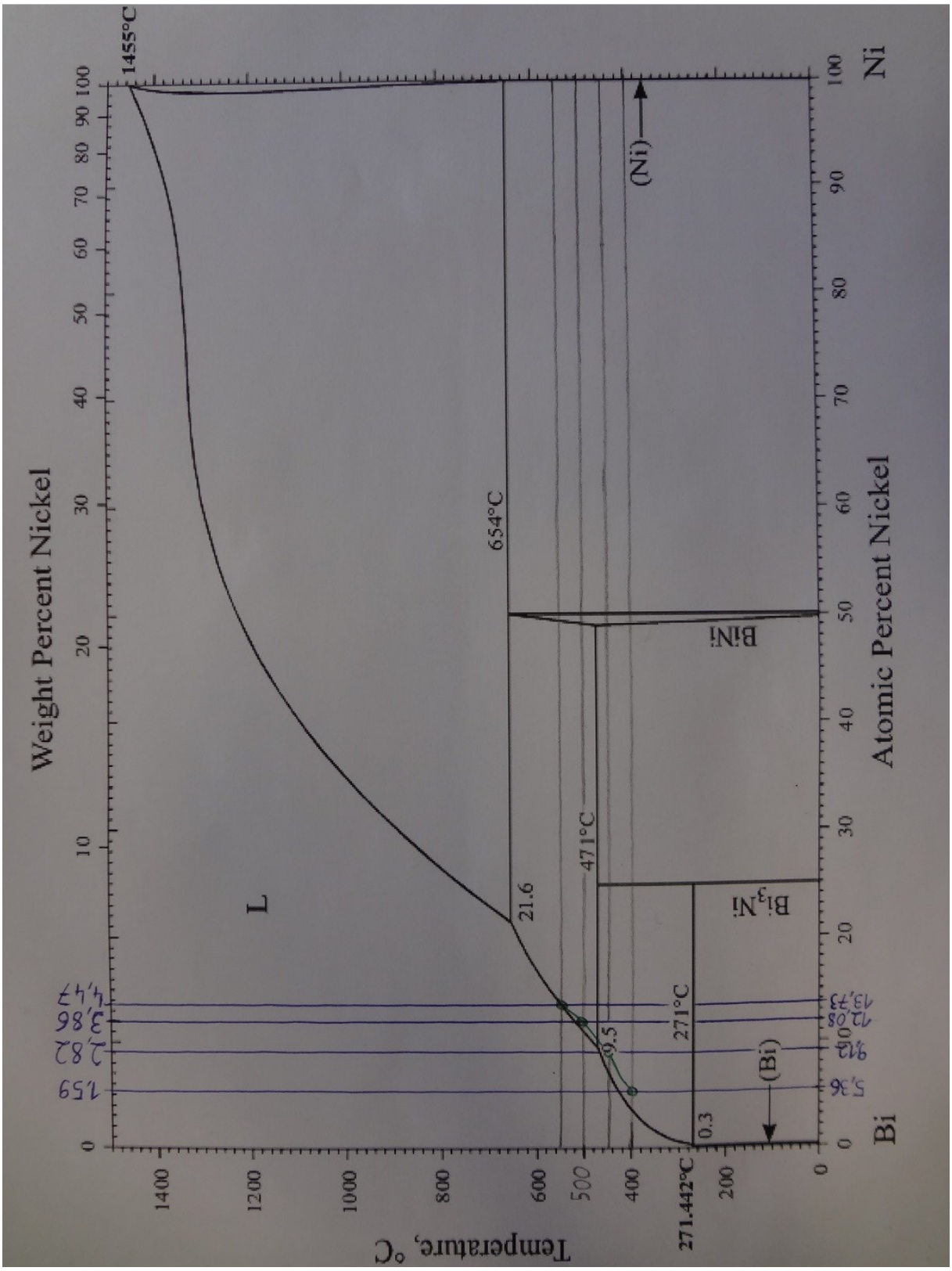

Figure 39: Annex A-11; Bi-Ni phase diagram (Okamoto, 2012, p. 492, out of: Wang, 2011) and personal supplements

A-12

Used chemicals:

- Bismuth: from Alpha Aesar – ThermoFisher (Kandel) GmbH, Germany
  Bismuth granules, 1-2 mm, packaged under argon
  Purity: 99,997%

- Copper: from Goodfellow Cambridge Lilited, England
  Copper wire, 1.0 mm diameter
  Purity: 99.98%

- Nickel: from Goodfellow Cambridge Limited, England
  Nickel wire, 1.0 mm diameter
  Purity: 99.98%

- Nickel chloride. from Alpha Aesar – ThermoFisher (Kandel) GmbH, Germany
  Nickel(II) chloride, ultra-dry, powder, ampouled under argon
  Purity: 99,9%

- Salt: from Alpha Aesar – ThermoFisher (Kandel) GmbH, Germany
  LiCl (59.5 mol.%)-KCl (40.5 mol.%), -10 Mesh, (hygroscopic), packed under argon, melting point: 357 °C
  Purity of LiCl used: 98% and purity of KCl used: 99.0%

Used equipment:

- Computer program: Agilent Technologies, USA
  Agilent BenchLink Data Logger 3
  Set configurations:

measuring range:	+/- 10 V
Resolution:	6.5 digits
Internal electrical resistance:	10 GΩ
Measurement every:	10 seconds

- Nickel wire: from Goodfellow Cambridge Limited
  Nickel wire, 1.0 mm diameter
  Purity: 99.98%

- Molybdenum wire: from Alpha Aesar – ThermoFisher (Kandel) GmbH, Germany
  Molybdenum wire, 0.5mm diameter
  Purity: 99.95%

- Multimeter: Agilent Technologies, USA
  Agilent 34972A – LXI Data Acquisition/Switch Unit

- Thermocouple: Thermocoax SAS, France
  K-type thermocouple, (NiCr [+] and NiAl [-])
  Mean sensitivity: 41 µV/°C

- Tube furnace: Carbolite Gero Limited, UK
  Universal tube furnace MTF
  Inner tube diameter: 15 mm, maximal temperature 1000 °C

A-13

- **Experiment 1**

Bismuth mass: 25.0781 g
Salt mass: 5.2257 g
Nickel chloride mass: 0.1621 g
(Copper Mass): 0.0258 g

Hour	Mass of Ni added	Total Ni-concentration	Temperature
0.00	0.0599 g	0.2386 wt.%	502 °C
4.10	0.0125 g	0.2884 wt.%	502 °C
6.50	0.1000 g	0.6856 wt.%	502 °C
23.57	0.1006 g	1.0851 wt.%	502 °C
48.20	0.1005 g	1.4842 wt.%	502 °C
72.13	X	1.4842 wt.%	452 °C
75.50	0.1009 g	1.8850 wt.%	452 °C
79.01	0.1000 g	2.2821 wt.%	452 °C
95.73	0.1008 g	2.6825 wt.%	452 °C

Table 7: Masses of nickel added and temperature changes of experiment 1

- **Experiment 2**

Bismuth mass: 25.0015 g
Salt mass: 5.3687 g
Nickel chloride mass: 0.1626 g

Hour	Mass of Ni added	Total Ni-concentration	Temperature
0.00	0.0018 g	0.0072 wt.%	406 °C
39.40	0.1000 g *	0.4055 wt.%	406 °C
135.98	x	0.4055 wt.%	504 °C
160.00	x	0.4055 wt.%	404 °C
168.00	0.0984 g	0.7944 wt.%	404 °C
233.20	0.1020 g	1.1943 wt.%	404 °C
261.58	0.0999 g	1.5828 wt.%	404 °C
287.16	0.0996 g	1.9672 wt.%	404 °C

Table 8: Masses of nickel added and temperature changes of experiment 2

*estimation, as the exact data got lost

A-14

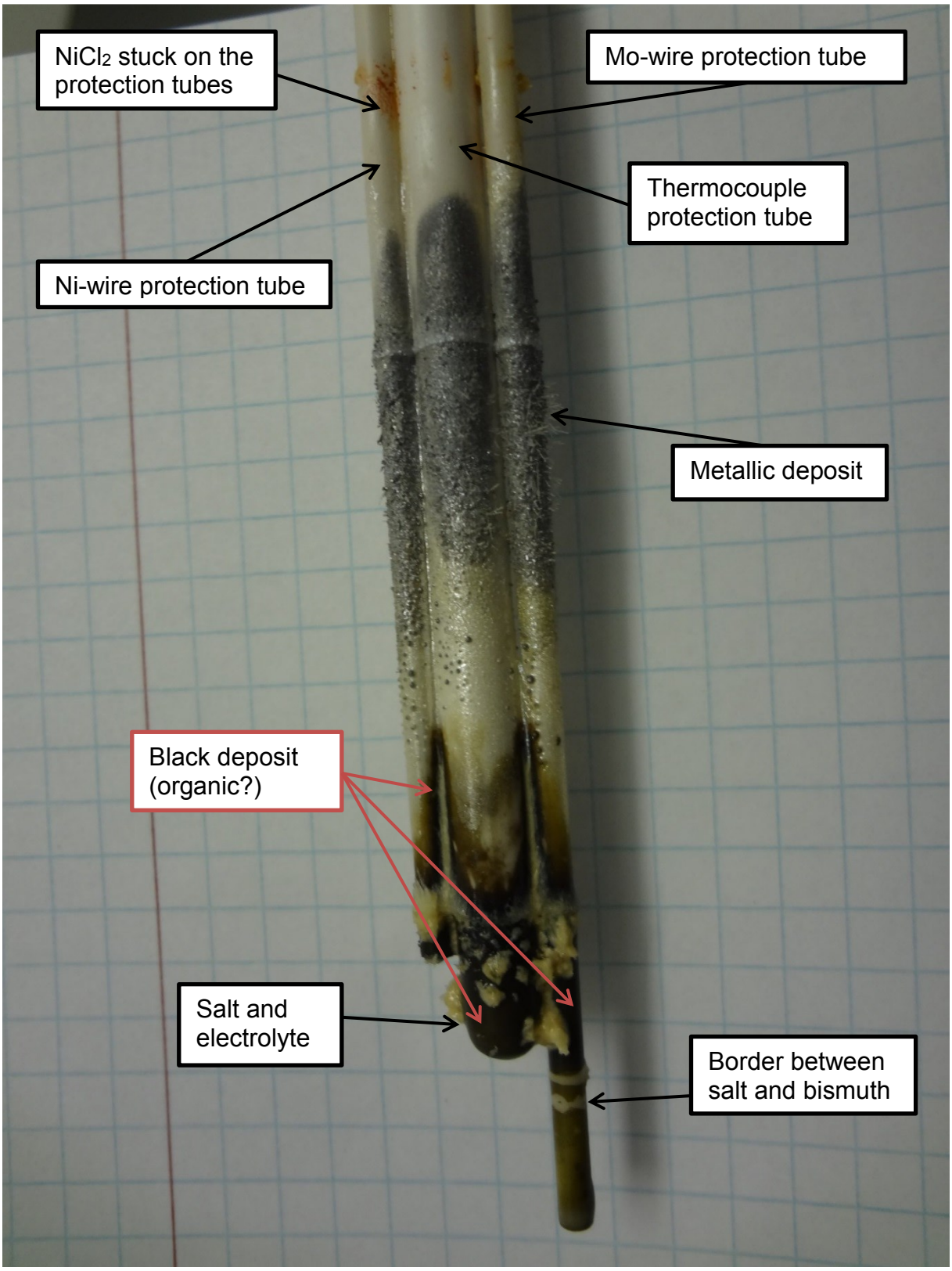

Figure 40: Annex A-14; Depositions on the protection tube of the wires and the thermocouple